Properties of Buried Heterostructure Single Quantum Well (Al,Ga)As Lasers

Thesis by

Pamela L. Derry

In Partial Fulfillment of the Requirements

for the Degree of

Doctor of Philosophy

California Institute of Technology

Pasadena, California

1989

(submitted June 8, 1988)

Acknowledgements

I would like to express my appreciation to my advisor, Professor Amnon Yariv, for his guidance and support.

I would like to thank Dr. T. R. Chen, Dr. Kerry Vahala, Yu-Hua Zhuang, Joel Paslaski, Michael Mittelstein, Dr. Kam Y. Lau, Dr. Nadav Bar-Chaim, Kevin Lee, and Jan Rosenberg who contributed to the work reported on in this thesis. I would also like to express my gratitude to Dr. Hadis Morkoç for his guidance and encouragement.

I would like to acknowledge Dr. Anders Larsson, whose work inspired the topic of this thesis. I would especially like to thank Dr. J. Steven Smith, who taught me the methods of MBE and with whom I collaborated on work not discussed in this thesis. Thanks are due to Dr. Christopher Lindsey, who introduced me to semiconductor processing techniques. I am grateful to Dr. Aharon Agranat for his help and expertise with temperature controlled systems. I would also like to acknowledge a valuable discussion on the properties of buried heterostructures with Dr. Dan Botez of TRW.

I am grateful to Jana Mercado for help in everyday matters and Desmond Armstrong and Ali Ghaffari for technical assistance.

I gratefully acknowledge financial support from the IBM Corporation, California Institute of Technology, the National Science Foundation, the Office of Naval Research, and the Air Force Office of Scientific Research.

Finally I would like to thank my husband, Lane Dailey, for his love, encouragement, and support. Lane also helped proofread the thesis.

Abstract

Unlike conventional semiconductor lasers, single quantum well (SQW) lasers with high reflectivity end facet coatings have dramatically reduced threshold currents as a result of the smaller volume of the (active) quantum well region. A cw threshold current of 0.55 mA was obtained for a buried graded-index separate-confinement heterostructure SQW laser with facet reflectivities of ~80%, a cavity length of 120 μm, and an active region stripe width of 1 μm. This is believed to be the lowest threshold current so far reported for any semiconductor laser at room temperature.

The submilliampere threshold currents of these lasers allow them to be modulated at high speed without any current prebias or feedback monitoring. The relaxation oscillation frequency for these lasers was also measured. Values of differential gain derived from these measurements demonstrated that the differential gain in the uncoated lasers is less than in the coated devices. This result was expected because of gain saturation.

As predicted, SQW lasers have substantially narrower spectral linewidths than bulk double heterostructure lasers. This result is attributed to lower internal loss, linewidth enhancement factor, and spontaneous emission factor. A further major reduction ($> 3\times$) in the linewidth of these SQW lasers was observed when the facet reflectivities were enhanced. This observation is explained theoretically on the basis of the very low losses in coated SQW lasers and the value of the spontaneous emssion factor.

Table of Contents

Acknowledgements ii

Abstract iii

Chapter 1: Introduction

1.1 Semiconductor Diode Lasers 1

1.2 Motivations for Investigation of Stripe Quantum Well Lasers 3

1.3 Outline 6

1.4 References 8

Chapter 2: Single Quantum Well: Laser Structure for Lower Threshold Current Density (Al,Ga)As Lasers

2.1 Introduction 10

2.2 Quantum Wells Versus Conventional Double Heterostructures 10

2.3 Single Quantum Wells Versus Multiquantum Wells 23

2.4 Graded-Index Separate-Confinement Heterostructure Quantum Wells 23

2.5 Optimal Single Quantum Well Thickness 28

2.6 Conclusion 30

2.7 References 31

Chapter 3: Molecular Beam Epitaxial Growth of (Al,Ga)As Lasers

3.1 Introduction 35

3.2 Principles of (Al,Ga)As Molecular Beam Epitaxy 36

3.3 Growth Conditions 38

3.4 Dopants 43

3.5 Substrate Preparation 45

3.6 Growth of an (Al,Ga)As Laser 49
3.7 Tilted Substrates 52
3.8 "Cracked" Arsenic 53
3.9 Conclusion 54
3.10 References 56

Chapter 4: Ultralow Threshold Buried Heterostructure Single Quantum Well (Al,Ga)As Lasers

4.1 Introduction 60
4.2 Planar GRIN SCH SQWs Grown by MBE 66
4.3 LPE Regrowth 69
4.4 Leakage Current 71
4.5 High Reflectivity End Facet Coatings 76
4.6 Threshold Current Results 82
4.7 Steps for Improvement 95
4.8 Conclusion 97
4.9 References 98

Chapter 5: Spectral Characterstics of Buried Heterostructure Single Quantum Well (Al,Ga)As Lasers

5.1 Introduction 102
5.2 Spectrum 102
5.3 Spectral Linewidth: Theory 114
5.4 Spectral Linewidth: Experiment 120
5.5 Steps for Improvement 129
5.6 Conclusion 130
5.7 References 131

Chapter 6: Dynamic Characteristics of Buried Heterostructure Single Quantum Well (Al,Ga)As Lasers

6.1 Introduction 134

6.2 Modulation Without Prebias 135

6.3 Relaxation Oscillation Frequency: Theory 140

6.4 Parasitics 147

6.5 Relaxation Oscillation Frequency: Experiment 148

6.6 Steps for Improvement 157

6.7 Conclusion 160

6.8 References 162

Chapter 1

Introduction

1.1 Semiconductor Laser Diodes

Lasing action from semiconductor GaAs and GaAsP p-n junctions was first observed in 1962 by four groups.[1,2,3,4] This development was made possible by the realization that lasing action in direct band gap semiconductor lasers was feasible,[5] and by the realization that mirrors for the lasing cavity could be formed from the ends of the semiconductor crystal. For these early lasers the mirrors were formed by polishing two parallel ends of the semiconductor chip. Later[6] it was demonstrated that mirrors could be formed more simply by orienting the laser cavity perpendicular to natural cleavage planes and cleaving along two of these planes.

The early homostructure semiconductor lasers were very inefficient since they did not contain a strong mechanism for confining radiative recombination to a thin layer or for guiding the light generated. They therefore had extremely high threshold currents, which made continuous operation at room temperature impossible. Semiconductor lasers were dramatically improved by the use of heterostructures.[7,8,9] In a typical conventional double heterostructure (DH) (Al,Ga)As semiconductor laser (illustrated in Figure 1.1), an undoped GaAs active region with a thickness on the order of 1000 Å is sandwiched between an N-AlGaAs cladding layer and a P-AlGaAs cladding layer. This structure has two important features: (1) recombination of electrons and holes producing light will occur efficiently in the GaAs active region, which has a smaller bandgap energy then the AlGaAs cladding layers; and (2) since GaAs has a larger refractive index than AlGaAs, the active region will act as a waveguide for the laser light produced in it.

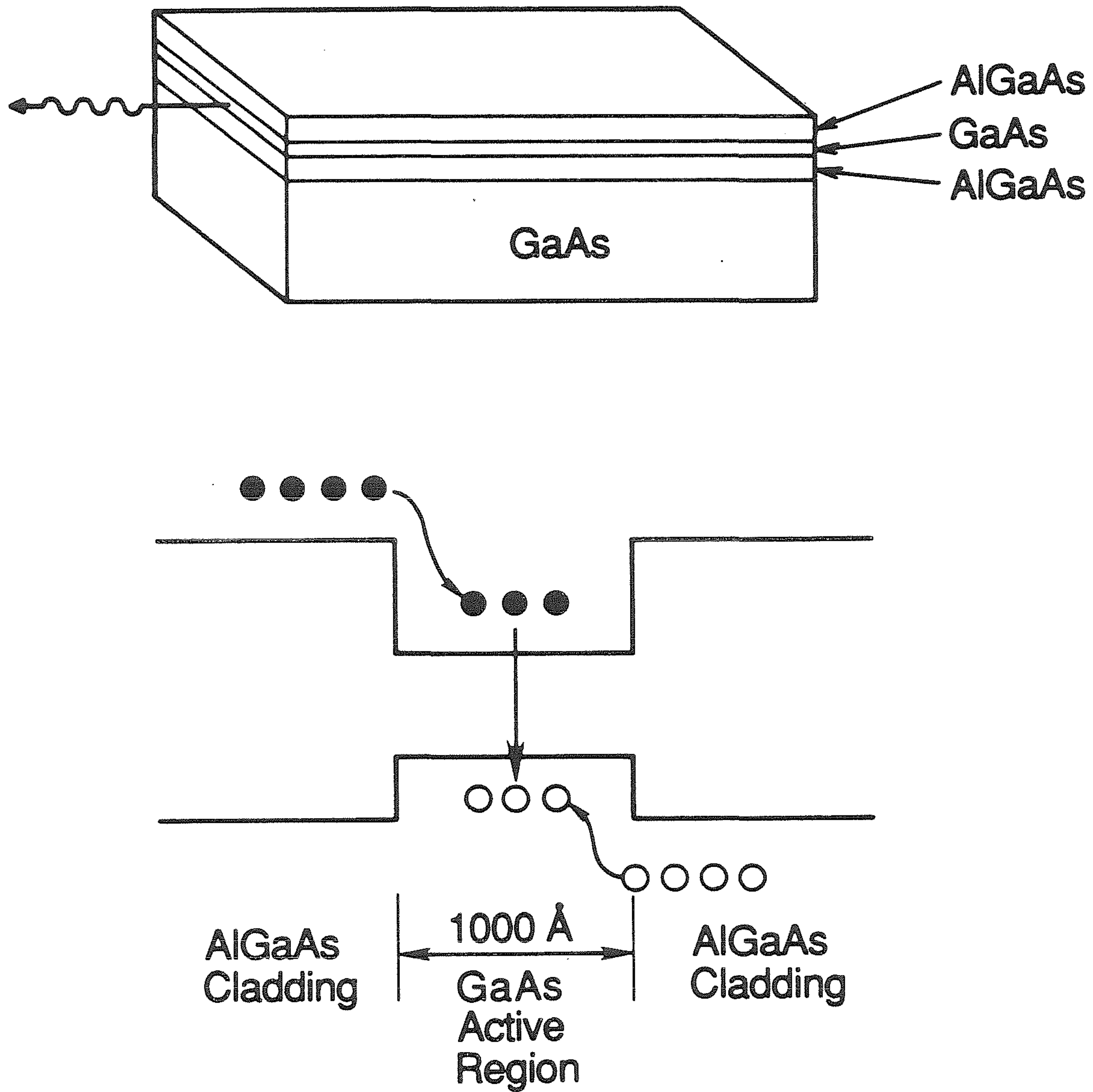

Figure 1.1: Schematic diagram of a conventional double heterostructure (Al,Ga)As semiconductor laser diode and the corresponding energy band diagram.

The development of DH lasers, along with the development of structures which provide confinement in the plane of the active region, have made semiconductor lasers useful for a variety of commercial applications. Some of the features which contribute to the commercial importance of semicondutor lasers are[10] their small physical size, the low electrical power required for their operation, their efficiency in converting electrical power into light, and their ability to be modulated at frequencies in the GHz range. In addition, semiconductor fabrication technology is well suited for mass production.

DH semiconductor lasers can be fabricated from a variety of semiconductor materials. The restrictions are: the materials must be lattice matched and the active region must have a direct band gap which is smaller than that of the cladding layers and its refractive index must be larger than that of the cladding layers. Within these constraints, the semiconductor alloy composition can be varied to tailor the lasing wavelength for specific applications. The two material systems[11,12] most frequently used are GaAs/AlGaAs, because of its mature technology and short lasing wavelenth (7000-9000 Å), and InP/InGaAsP because of its lasing wavelength range (11000-17000 Å), which includes the wavelengths at which optical fibers have the lowest loss and material dispersion.

1.2 Motivations for Investigation of Stripe Quantum Well Lasers

Future generations of supercomputers will rely on monolithic semiconductor lasers for their internal communication. The number of lasers involved is so large that a major premium is placed on a reduction of threshold current of such lasers. This application and others involve modulating the lasers to carry information.

It is desirable to amplitude modulate semiconductor lasers without current prebias or a feedback circuit. When a current pulse of amplitude I is applied to a

semiconductor laser, there is a time delay before lasing begins, because it takes time for a carrier population to build up. When the current pulse ends, it takes time for the carrier population to decay. Once a semiconductor laser reaches its threshold carrier density, the carrier density in the active region is clamped at approximately that value since additional injected carriers will recombine by induced transitions. The turn-on time τ_d is therefore longer than the turn-off time, which is just the time for the carrier density to drop below its threshold value. For a large current pulse τ_d is approximately proportional to I_{th}/I, where I_{th} is the threshold current. Therefore if I is much larger than I_{th}, τ_d may be sufficiently reduced to obviate the need for current prebias. Unfortunately the current pulse required with a normal I_{th} is too large to be practical. All of these problems are, however, obviated with lasers that have ultralow threshold currents, i.e., a submilliampere threshold current.[13,14]

In this thesis the fabrication and properties of quantum well (QW) (Al,Ga)As lasers, which meet this requirement, are described. In a typical bulk DH (Al,Ga)As semiconductor laser the GaAs active region thickness is on the order of 1000 Å. In a QW laser the active region is approximately reduced to $\leq$200 Å. (For a review of QWs see Dingle,[15], Holonyak et al.,[16], or Okamoto.[17]) QW lasers have inherently lower threshold currents than conventional DH lasers, because of their lower transparency currents, which result from the smaller volume of the (active) QW region.[6] Transparency is the point at which the gain in the semiconductor laser medium is zero. The threshold current of a semiconductor laser is the transparency current plus a term which is proportional to the internal and end losses of the laser. In a QW laser the low transparency current makes the losses a much more significant portion of the total threshold current than they are in a conventional DH laser.

The laser cavity of a simple semiconductor laser is formed by cleaving the ends of the structure. Lasers are fabricated with their lasing cavity oriented per-

pendicular to a cleavage plane. While forming the laser cavity in this manner is advantageous, since it is much simpler than using external mirrors, the reflectivity of the GaAs/air interface is only ~31% so the end losses are relatively large. The end losses can, however, be reduced significantly by applying high reflectivity coatings to the end facets. For a QW laser with a low transparency current, high reflectivity coatings cause a very significant reduction in threshold current. Although this effect had been appreciated theoretically[19], it was exploited here to produce ultralow threshold (<1 mA) lasers at room temperature for the first time.

Other properties of QW lasers are superior to those of bulk DH lasers, because of the low internal loss of QWs[20] and their gain characteristics.[21] Many applications of semiconductor lasers require phase coherence; for instance, modulation of phase rather than amplitude. The spectral linewidth of a semiconductor laser, which is the full width at half maximum of the lasing mode, is directly related to its phase coherence. The linewidth is primarily due to fluctuations in the phase of the optical field. A narrower linewidth, therefore, means a more coherent laser. It has been predicted that QW lasers have narrower linewidths than conventional DH lasers primarily because of a smaller linewidth enhancement factor.[21] The linewidth enhancement factor[22,23] enters into the linewidth because changes in carrier density cause changes in the refractive index of the lasing material and vice versa; in other words, because of a coupling between amplitude and phase fluctuations. The reduction in the linewidth of a distributed feedback laser by a multiquantum well (MQW) has been measured,[24] but the measurements of the linewidth of single quantum well (SQW) lasers described here are believed to be the first reported so far.

While much narrower linewidths were measured for SQWs without high reflectivity coatings than what is commonly measured for conventional DHs, the linewidth reduction with high reflectivity coatings is truly dramatic. This further reduction

is related to the very low losses in a SQW with high reflectivity coatings.[25]

1.3 Outline

The subject of this thesis is the fabrication and properties of buried heterostructure SQWs.

Chapter 2 discusses the basic differences between QWs and conventional DHs. The reasons why QW lasers have lower threshold currents than DH lasers are explained on the basis of theoretical calculations. The design of a QW for as low a threshold as possible is described.

Chapter 3 describes the growth of laser structures by molecular beam epitaxy (MBE). Optimization of growth conditions for high quality laser material is discussed.

In Chapter 4 the properties of the MBE SQW material grown and its fabrication into stripe buried heterostructure lasers are described. Application of high reflectivity coatings to the end facets of the stripe lasers is also described. Threshold results for stripe SQW lasers with and without high reflectivity coatings are given and modeled. The role of leakage current is considered.

Spectral characteristics of the stripe SQW lasers are described in Chapter 5. The effects of high reflectivity coatings, low internal loss, the spontaneous emission factor, and the linewidth enhancement factor on the spectral linewidth are considered theoretically and experimentally. In addition the effect of coatings on the spectrum is discussed.

Modulation characteristics of the stripe SQW lasers are described in Chapter 6. The relaxation oscillation frequency is considered both experimentally and theoretically. Steps to improve the measured values are described. The change in differential gain when high reflectivity coatings are applied is derived from the measurements of

relaxation oscillation frequency. The advantage of ultralow threshold current lasers for high frequency modulation without current prebias is also discussed.

Work presented here or strongly related to it is the subject of References 13, 14, 18, 25, and 26.

1.4 References

[1] R. N. Hall, G. E. Fenner, J. D. Kingsley, T. J. Soltys, and R. O. Carlson, *Phys. Rev. Lett.* **9**(9), pp. 366-368 (1962).

[2] M. I. Nathan, W. P. Dumke, G. Burns, F. H. Dill, Jr., and G. Lasher, *Appl. Phys. Lett.* **1**(3), pp. 62-64 (1962).

[3] N. Holonyak, Jr. and S. F. Bevacqua, *Appl. Phys. Lett.* **1**(4), pp. 82-83 (1962).

[4] T. M. Quist, R. H. Rediker, R. J. Keyes, W. E. Krag, B. Lax, A. L. McWhorter, and H. J. Zeigler, *Appl. Phys. Lett.* **1**(4), pp. 91-92 (1962).

[5] W. P. Dumke, *Phys. Rev.* **127**(5), pp. 1559-1563 (1962).

[6] W. L. Bond, B. G. Cohen, R. C. C. Leite, and A. Yariv, *Appl. Phys. Lett.* **2**(3), pp. 57-59 (1963).

[7] Zh. I. Alferov, V. M. Andreev, V. I. Korol'kov, E. L. Portnoi, and D. N. Tret'yakov, *Sov. Phys. Semicond.* **2**(7), pp. 843-844 (1969).

[8] H. Kressel, and H. Nelson, *RCA Rev.* **30**(1), pp. 106-113 (1969).

[9] I. Hayashi, M. B. Panish, and P. W. Foy, *IEEE J. Quantum Electron.* **QE-5**(4), pp. 211-212 (1969).

[10] A. Yariv, *Optical Electronics, 3rd Edition*, p. 467, Holt, Rinehart, and Winston, New York (1985).

[11] G. H. B. Thompson, *Physics of Semiconductor Laser Devices*, pp. 8-15, John Wiley & Sons, New York (1980).

[12] H. C. Casey, Jr. and M. B. Panish, *Heterostructure Lasers, Part B: Materials and Operating Characteristics*, pp. 1-6, Academic Press, Orlando (1978).

[13] K. Y. Lau, N. Bar-Chaim, P. L. Derry, and A. Yariv, *Appl. Phys. Lett.* **51**(2), pp. 69-71 (1987).

[14] P. L. Derry, H. Z. Chen, H. Morkoç, A. Yariv, K. Y. Lau, N. Bar-Chaim, K. Lee, and J. Rosenberg, *J. Vac. Sci. Technol.* **B6**(2), pp. 689-691 (1988).

[15] R. Dingle, in *Festkörper Probleme XV (Advances in Solid State Physics)*, edited by H. Queisser, pp. 21-48, Pergamon, New York (1975).

[16] N. Holonyak, Jr., R. M. Kolbas, R. D. Dupuis, R. D. Dupuis, and P. D Dapkus, *IEEE J. Quantum Electron.* **QE-16**(2), pp. 170-186 (1980).

[17] N. Okamoto, *Jpn. J. Appl. Phys.* **26**(3), pp. 315-330 (1987).

[18] P. L. Derry, A. Yariv, K. Y. Lau, N. Bar-Chaim, K. Lee, and J. Rosenberg, *Appl. Phys. Lett.* **50**(25), pp. 1773-1775 (1987).

[19] A. Sugimura, *IEEE J. Quantum Electron.* **QE-20**(4), pp. 336-343 (1984).

[20] M. Mittelstein, Y. Arakawa, A. Larsson, and A. Yariv, *Appl. Phys. Lett.* **49**(25), pp. 1689-1691 (1986).

[21] Y. Arakawa and A. Yariv, *IEEE J. Quantum Electron.* **QE-21**(10), pp. 1666-1674 (1985).

[22] K. Vahala and A. Yariv, *IEEE J. Quantum Electron.* **QE-19**(6), pp. 1096-1101 (1983).

[23] C. H. Henry, *IEEE J. Quantum Electron.* **QE-18**(2), pp. 259-264 (1982).

[24] S. Noda, K. Kojima, K. Kyuma, K. Hamanaka, and T. Nakayama, *Appl. Phys. Lett.* **50**(14), pp. 863-865 (1987).

[25] P. L. Derry, T. R. Chen, Y. H. Zhuang, J. Paslaski, M. Mittelstein, K. Vahala, and A. Yariv, (to be published in *Appl. Phys. Lett.*).

[26] K. Y. Lau, P. L. Derry, and A. Yariv, *Appl. Phys. Lett.* **52**(2), pp. 88-90 (1988).

Chapter 2

Single Quantum Well: Laser Structure for Lowest Threshold Current Density (Al,Ga)As Lasers

2.1 Introduction

Stripe semiconductor lasers with ultralow absolute threshold currents are of great interest for applications such as computer optical interconnects. It is highly desirable to have a laser which is compatible with standard logic level voltages. Envisioning future generations of optical supercomputers utilizing a great many semiconductor lasers suggests that ultralow threshold current lasers will become a necessity, since limiting power consumption will become a significant factor when a large number of lasers are used.

The first step in achieving an ultralow threshold stripe laser is fabricating high quality low threshold current density semiconductor material which can be processed into stripe lasers. In this chapter it is shown that QW lasers have inherently lower threshold current densities than bulk DH lasers. The specifications for a specific (Al,Ga)As QW laser structure for lowest threshold current density are described.

2.2 Quantum Wells Versus Conventional Double Heterostructures

The active region in a conventional DH semiconductor laser (see Figure 1.1 for a schematic illustration) is wide enough that it acts as bulk material and no quantum effects are apparent. In such a laser the conduction band and valence band are continuous (Figure 2.1a). In bulk material the density of states for a transition energy E per unit volume per unit energy is:[1]

$$\mathcal{D}(E) = \frac{m_r}{\pi^2 \hbar^3} \sqrt{2 m_r (E - E_g)}, \quad E > E_g \tag{2.1}$$

where E_g is the band gap energy and m_r is the effective mass which is defined as:

$$\frac{1}{m_r} = \frac{1}{m_c} + \frac{1}{m_v} \tag{2.2}$$

where m_c is the conduction band mass and m_v is the valence band mass.

If the active region of a semiconductor laser is very thin (on the order of the DeBroglie wavelength of an electron) quantum effects become important. When the active region is this narrow (less than ~200 Å) the structure is called a quantum well. For a review of QWs see Dingle[2], Holonyak et al.[3], or Okamoto.[4] Since the quantum effects in a QW are occurring in only one dimension they can be described by the elementary quantum mechanical problem of a particle in a one dimensional quantum box.[5]

In such a well, solution of Schrodinger's equation shows that a series of discrete energy levels (Figure 2.1b) are formed instead of the continuous energy bands of the bulk material. With the approximation that the well is infinitely deep the allowed energy levels are given by:

$$E_n = \frac{(n\pi\hbar)^2}{2mL_z^2} \tag{2.3}$$

where $n = 1, 2, 3, \ldots$, m is the effective mass of the particle in the well, and L_z is the quantum well thickness. Setting the energy at the top of the valence band equal to zero, the allowed energies for an electron in the conduction band of a semiconductor QW become

$$E = E_g + E_n^c \tag{2.4}$$

where E_n^c is E_n with m equal to m_c . The allowed energies for a hole in the valence band are then

$$E = -E_n^v \tag{2.5}$$

where E_n^v is E_n with m equal to m_v.

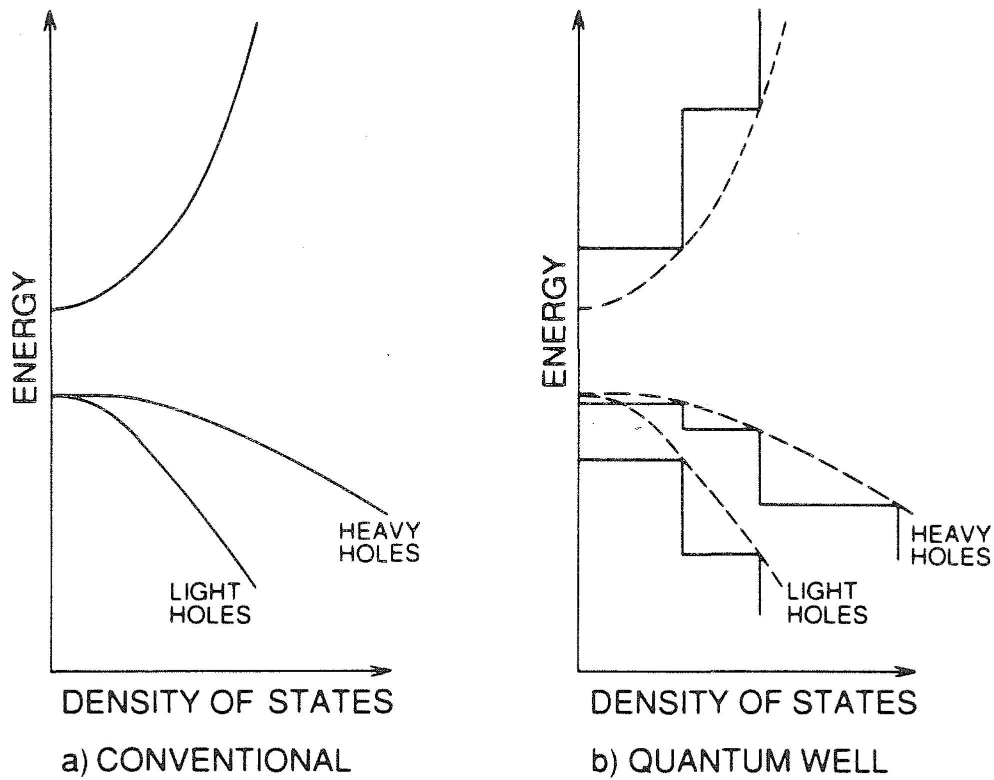

Figure 2.1: Schematic diagram of the density of states for (a) a conventional double heterostructure and (b) a quantum well.

This quantization of energy levels will, of course, change the density of states. For a transition energy E, the possible energies are limited to:

$$E = E_g + E_n^c + E_n^v + \frac{\hbar^2 k^2}{2m_r} \tag{2.6}$$

where k is the wavevector, rigorous k-selection is assumed, and transitions are limited to those with $\Delta n = 0$. For allowed energies, $\mathcal{D}(E)$ per unit volume is equal to $(1/L^2 L_z)dN/dE$ where N is the number of states with wavevector less than k and the unquantized dimensions of the QW are equal to L. Since the particles are confined in one dimension, k can only change in two dimensions. There is one allowed value of k per area $(2\pi/L)^2$ in k space, therefore

$$N = 2\left(\frac{L}{2\pi}\right)^2 \pi k^2 \tag{2.7}$$

where the factor of 2 accounts for two particles per value of k due to spin and πk^2 is the area of a circle of radius k.

$$\frac{dN}{dE} = \frac{L^2}{\pi} k \frac{dk}{dE} \tag{2.8}$$

and from Equation (2.6), $dk/dE = m_r/\hbar^2 k$ for each quantized level. Substituting into Equation (2.8) each quantized level contributes $m_r/L_z\pi\hbar^2$ to $\mathcal{D}(E)$ (which is per unit volume) at allowed energies. In GaAs there are two hole bands: the heavy hole band, which is the more significant of the two for the calculations here, and the light hole band, which should also be summed over. There are also indirect conduction bands but their contributions are negligible at room temperature and can be neglected.[6] The restrictions on energy can be incorporated into the formula for $\mathcal{D}(E)$ by using the Heavyside function, $H(E - E_g - E_n^c - E_n^v)$ giving the final result:

$$\mathcal{D}(E) = \sum_{i=l,h} \sum_{n=1}^{\infty} \frac{m_r^i}{L_z \pi \hbar^2} H(E - E_g - E_n^c - E_{n,i}^v) \tag{2.9}$$

where l and h refer to light and heavy holes.

The modal gain in a semiconductor laser is proportional to the stimulated emission rate[7] and with rigorous k-selection can be described as:[8]

$$g(E_L,N) = \Gamma \int \frac{C(E_L)\mathcal{D}(E)\big(f_c(E,N) - f_v(E,N)\big)\hbar\gamma}{(E-E_L)^2 + (\hbar\gamma)^2}\, dE \qquad (2.10)$$

where Γ is the optical confinement factor, $C(E_L)$ is a term which is proportional to the transition probability, E_L is the transition energy at which g is evaluated at (the lasing energy), N is the carrier density of either electrons or holes (the active region is undoped so they have equal densities), γ is the inverse of the intraband relaxation time τ_{in}, and $f_c(E,N)$ and $f_v(E,N)$ are the Fermi occupation factors for the conduction and valence bands.

The Lorentzian factor is included to account for broadening due to carrier-carrier and carrier-phonon interactions. It should be noted that this is an approximation and may not be the most accurate way of accounting for broadening. On one hand the Lorentzian lineshape maybe too broad and may cause too wide a range of energy transitions to significantly contribute to the gain.[9] It is possible that other broadening factors such as a Gaussian lineshape might fit better. To further complicate matters, the value of τ_{in} is not known very exactly. The value of τ_{in} is estimated to be in the range $\sim$0.07 to $\sim$ 0.2 psec in undoped GaAs.[10,11,12] In this thesis a value of 0.2 psec is used for τ_{in}. Additional error may be introduced by taking τ_{in} as a constant as it depends on carrier concentration.[8]

The optical confinement factor, Γ, is defined as the ratio of the light intensity of the lasing mode within the active region to the total intensity over all space. Since a QW is very thin, Γ_{QW} will be much smaller than Γ_{DH}. Γ_{DH} is typically around 0.5 whereas Γ_{QW} is approximately an order of magnitude smaller.

The Fermi occupation functions are given by:

$$f_c(E_c, N) = \frac{1}{1 + exp((E_g + E_c - F_c)/kT)} \tag{2.11}$$

and

$$f_v(E_v, N) = \frac{1}{1 + exp(-(E_v + F_v)/kT)} \tag{2.12}$$

where k is the Boltzmann constant, T is temperature, E_c is the energy level of the electron in the conduction band (relative to the bottom of the band), E_v is the absolute value of the energy level of the hole in a valence band, and F_c and F_v are the quasi-Fermi levels in the conduction and valence bands. Note that E_c and E_v are dependent on the transition energy so f_c and f_v are functions of the transition energy.

f_c and f_v are also functions of N through F_c and F_v. F_c and F_v are obtained by evaluating the expressions for the electron and hole densities. The total carrier density is obtained by integrating the distribution of occupied states over the allowed energy ranges:[13]

$$N = \int \mathcal{D}_c(E_c) f_c(E_c)\, dE_c \tag{2.13}$$

and

$$N = \int \mathcal{D}_v(E_v) f_v(E_v)\, dE_v \tag{2.14}$$

where $\mathcal{D}_c(E_c)$ and $\mathcal{D}_v(E_v)$ are the densities of states for the conduction and valence bands and follow the same form as $\mathcal{D}(E)$ for a transition.

The transition probability term

$$C(E_L) = \frac{e^2 \hbar}{n_r m_o^2 c \epsilon_o E_L} |M(E_L)|^2 \tag{2.15}$$

where e is the charge of an electron, n_r is the refractive index of GaAs, m_o is the mass of an electron, ϵ_o is the dielectric constant of free space, and $|M(E_L)|$ is the

average matrix element of the transition. Using the $\mathbf{k} \cdot \mathbf{p}$ method of Kane[14] for a DH laser, $|M_{DH}|^2$ can be determined to be approximately equal to $1.33 m_o E_g$ and is independent of the transition energy. For a QW, $|M_{QW}(E_L)|^2$ will depend on the transition energy and also on the polarization of the lasing mode.[15] Asada et al. have shown that $|M_{QW}(E_L)|^2$ for TE polarization is approximately given by:

$$|M_{QW}(E_L)|^2 = |M_{DH}|^2 \frac{3}{4} \left(1 + \frac{E_n^c + E_{n,i}^v}{E_L - E_g} \right) \tag{2.16}$$

for the nth quantized level.

In Figure 2.2, the results of evaluating Equation (2.10) numerically as a function of carrier density are plotted for a DH laser with an active region thickness of 1000 Å and for 70 Å and 100 Å QWs. The values of gain plotted are the maximum values at particular carrier densities. The lasing energy for a quantum well increases slightly with the threshold carrier density, because of the increasing contribution of the second quantized state.[16] The gain curves for the QWs are very nonlinear because of saturation of the first quantized state as the carrier density increases. The transparency carrier density N_o is the carrier density at which the gain is zero. From Figure 2.2 it is clear that the transparency carrier densities for QW and DH lasers are very similar and are on the order of 2×10^{18} cm.$^{-3}$

The advantage of a QW over a DH laser is not immediately apparent. Consider, however, the transparency current density J_o. At transparency

$$J_o = \frac{N_o L_z e}{\tau_s} \tag{2.17}$$

where L_z is the active layer thickness and τ_s is the effective recombination time near transparency. τ_s is aproximately 2 to 4 ns for either a QW or a DH laser. Since N_o is about the same for either structure, any difference in J_o will be directly proportional to d. But L_z is approximately ten times smaller for a QW; therefore, J_o will be

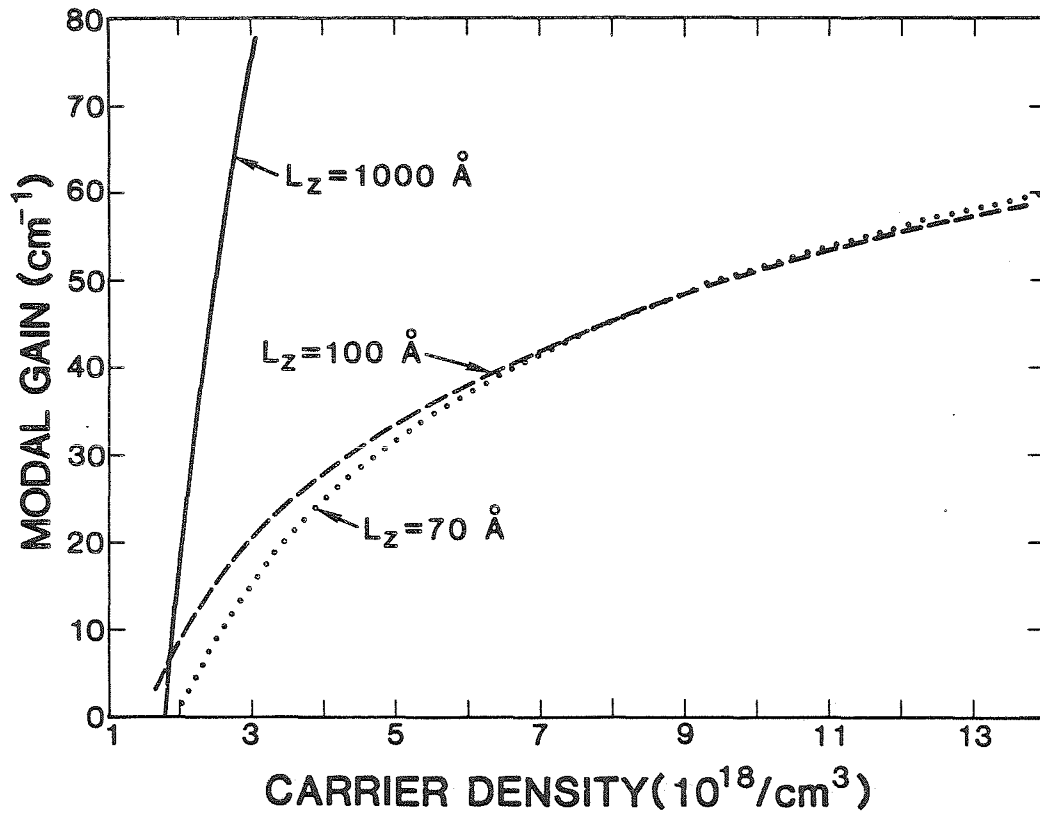

Figure 2.2: Modal gain as a function of carrier density for a conventional double heterostructure with an active region thickness of 1000 Å and for 70 Å and 100 Å single quantum wells.

approximately ten times lower for a QW than for a conventional DH laser. (A lower J_o will result in a lower threshold current density since the threshold current density is equal to J_o plus a term proportional to the threshold gain.) Note that this result is not determined by the quantization of energy levels; it occurs because fewer carriers are needed to reach the same carrier density in a QW as in a DH laser. In other words, this result is achieved because the QW is thin!

To consider the dependence of the modal gain on the current density more rigorously, the current density must be calculated as a function of the carrier density. The current density, $J(N)$, is proportional to the integral of the rate of spontaneous emission, $r_{spont}(E)$ over transition energy:[18]

$$J(N) = \frac{eL_z}{\eta_i} \int r_{spont}(E)\, dE \tag{2.18}$$

where η_i is the internal quantum efficiency, defined as the ratio of the rate of photon creation inside the lasing cavity to the number of carriers injected. Using the Lorentzian lineshape:

$$J(N) = \frac{n_r e L_z}{\eta_i \hbar^3 \pi^2 c^2} \int E_L C(E_L) \int \mathcal{D}(E) \frac{f_c(E,N)\big(1 - f_v(E,N)\big)\hbar\gamma}{(E - E_L)^2 + (\hbar\gamma)^2}\, dE\, dE_L \tag{2.19}$$

The only factor appearing in this formula which has not yet been discussed is η_i. η_i is defined by:[19]

$$P_{stim} = \frac{(I - I_{th})\eta_i E_L}{e} \tag{2.20}$$

where I is current, I_{th} is threshold current, and P_{stim} is the total stimulated power inside the laser. To relate η_i to a quantity which can be measured, consider the external differential quantum efficiency, η_{ext} defined as the ratio of increase in photons output to the increase in injection rate of carriers:

$$\eta_{ext} = \frac{d\big((P_1 + P_2)/E_L\big)}{d\big((I - I_{th})/e\big)} \tag{2.21}$$

where P_1 and P_2 are respectively the output power at the facet of the laser with reflectivity R_1 and that of the facet with reflectivity R_2. $P_1 + P_2$ is the portion of P_{stim} which is transmitted outside the laser:

$$P_1 + P_2 = \frac{(1/2L)ln(1/R_1R_2)}{\alpha_i + (1/2L)ln(1/R_1R_2)} P_{stim} \tag{2.22}$$

where L is the cavity length, R_1 and R_2 are the end facet reflectivities, α_i is all internal loss, $(1/2L)ln(1/R_1R_2)$ is the end loss and the denominator is the total loss. Combining Equation (2.19) and Equation (2.21):

$$P_1 + P_2 = \frac{(1/2L)ln(1/R_1R_2)}{\alpha_i + (1/2L)ln(1/R_1R_2)} \frac{(I - I_{th})\eta_i E_L}{e} \tag{2.23}$$

Substituting Equation (2.23) into Equation (2.21) and solving for η_i:

$$\eta_i = \frac{\alpha_i + (1/2L)ln(1/R_1R_2)}{(1/2L)ln(1/R_1R_2)} \eta_{ext} \tag{2.24}$$

In a typical high quality single QW (SQW), η_{ext} is measured to be as high as 79%.[20] With typical internal losses, end reflectivities, and cavity lengths, η_i approaches unity. In calculations it can, therefore, be approximated as one. In a conventional DH laser, however, η_{ext} is much lower. Typically this will result in values of η_i (≤ 0.7)[21] which cannot be neglected.

Setting $\eta_i = 0.6$ for a DH laser and calculating $J(N)$ from Equation (2.18) numerically on a computer, the gain versus current relationships shown in Figure 2.3 are obtained for a DH laser with an active region thickness of 1000 Å and for 70 Å and 100 Å QWs. The potential for lower threshold current densities for QW lasers is clear for threshold gains less than that where the curve for the DH laser intercepts those of the QWs. The threshold condition is reached when the gain is equal to the losses (both internal and external):

$$g_{th} = \alpha_i + \frac{1}{2L} ln \frac{1}{R_1R_2} \tag{2.25}$$

With low losses, the threshold current of a QW laser will be substantially lower than that of a DH laser, since the threshold gain will be below the interception point.

To see how the internal loss in a QW should compare to that in a DH laser, consider the contributions to α_i:[22]

$$\alpha_i = \Gamma\alpha_{fc} + \alpha_w + (1-\Gamma)\alpha_c \tag{2.26}$$

where α_{fc} is loss in the active region, mostly due to free carrier absorption, α_w is scattering loss due to waveguide imperfections and irregularities at the heterostructure interfaces, and α_c is loss in the cladding region primarily due to free carrier absorption. The most dominant of these losses is α_{fc} but its contribution is limited by Γ. Since Γ is much smaller for a QW, α_i should be lower for a QW than for a DH laser. This is in fact what is observed experimentally; α_i has been measured to be ≤ 2 cm^{-1} for high quality QW lasers,[16] while in a DH laser α_i is around 15 cm^{-1}.[23]

To get an appreciation for how the threshold current density of a QW will compare to that of a DH laser consider that near transparency, the modal gain is approximately linearly dependent on the current density:

$$g(J) = A(J - J_o) \tag{2.27}$$

where A is a constant which should have a similar value for either a QW or a DH laser (this can be seen visually on Figure 2.3). Taking Equation (2.27) at threshold we can equate it to Equation (2.25):

$$A(J_{th} - J_o) = \alpha_i + \frac{1}{2L} ln \frac{1}{R_1 R_2} \tag{2.28}$$

where J_{th} is the threshold current density. Solving for J_{th}:

$$J_{th} = J_o + \frac{\alpha_i}{A} + \frac{1}{2LA} ln \frac{1}{R_1 R_2} \tag{2.29}$$

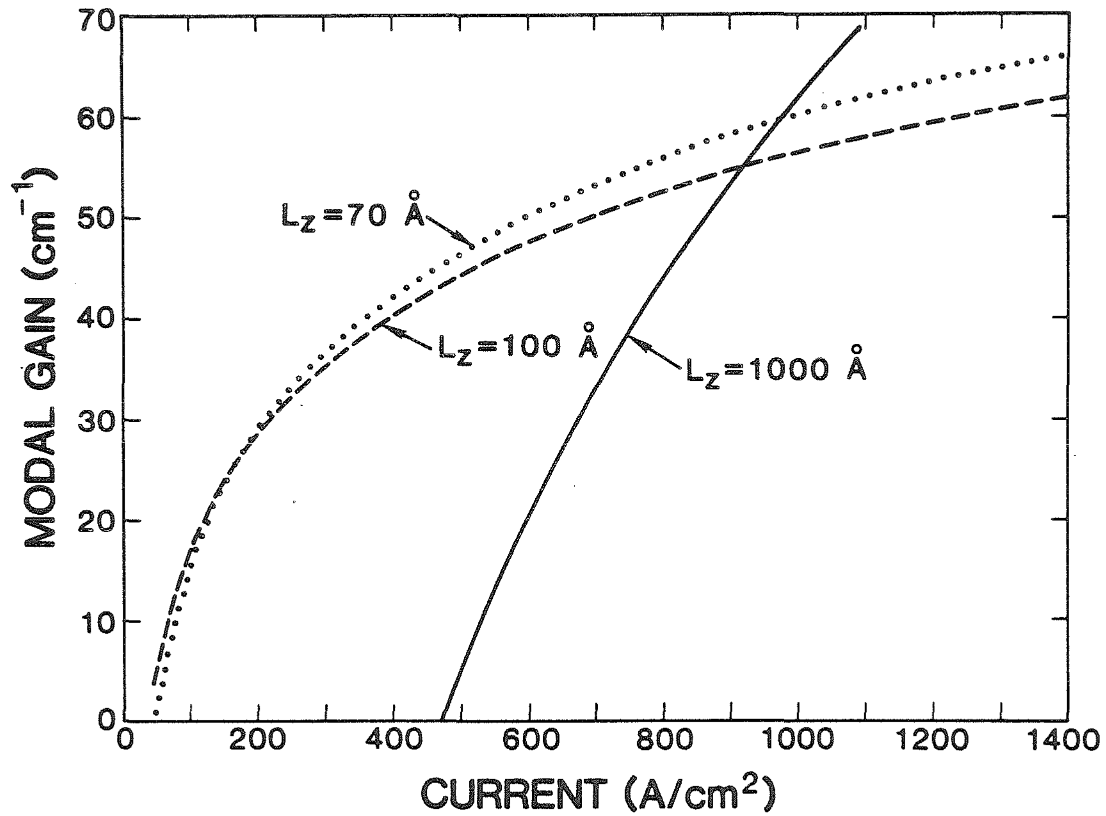

Figure 2.3: Modal gain as a function of current density for a conventional double heterostructure with an active region thickness of 1000 Å and for 70 Å and 100 Å single quantum wells.

Now substitute in the numbers in order to get an idea for the difference between a QW and a DH laser. Reasonable values are:[24] $A_{QW} \sim 0.7$ A^{-1}cm, $A_{DH} \sim 0.4$ A^{-1}cm, $J_o^{QW} \sim 50$ A/cm^2, $J_o^{DH} \sim 500$ A/cm^2, $\alpha_i^{QW} \sim 2$ cm^{-1}, $\alpha_i^{DH} \sim 15$ cm^{-1}, $L \sim 250$ μm, and for uncoated facets $R_1 = R_2 = 0.31$. Substituting in we get:

$$J_{th}^{QW} = 50 \text{ A/cm}^2 + 2.9 \text{ A/cm}^2 + 66.9 \text{ A/cm}^2 \tag{2.30}$$

$$J_{th}^{DH} = 500 \text{ A/cm}^2 + 3.8 \text{ A/cm}^2 + 117.1 \text{ A/cm}^2 \tag{2.31}$$

$$J_{th}^{QW} = 120 \text{ A/cm}^2 \tag{2.32}$$

$$J_{th}^{DH} = 621 \text{ A/cm}^2 \tag{2.33}$$

It is clear that changes in the losses will have a more noticeable effect on threshold current for a QW than for a DH laser since losses are responsible for a more significant portion of the threshold current of a QW laser. The gain curve of a QW laser saturates due to the filling of the first quantized energy level, so operating with low losses is even more important for a QW than is illustrated by the above calculation. When the gain saturates, the simple approximation of Equation (2.27) is invalid. Operating with low end losses is also important for a QW, since they are a large fraction of the total losses. This explains why threshold current density results for QW lasers are typically quoted for laser cavity lengths on the order of 400-500 μm, while DH lasers are normally cleaved to lengths on the order of 250 μm. High quality broad area SQW lasers have threshold current densities lower than 200 A/cm^2 (threshold current densities as low as 93 A/cm^2 have been achieved[25,26]) while the very best DH lasers have threshold current densities as low as 600 A/cm^2.[27]

2.3 Single Quantum Wells Versus Multiquantum Wells

In the discussion so far we have only considered SQWs. Structures in which several quantum wells are separated by thin AlGaAs barriers are called multiquantum wells (MQWs)and also have useful properties. For a given carrier density, a MQW with N QWs of equal thickness L_z has gain which is approximately N times the gain for a SQW of the same thickness L_z, but the current density is also approximately increased by a factor of N.[28] The transparency current density will be larger for the MQW than for the SQW since the total active region thickness is larger. Figure 2.4 shows that as a function of current density, the gain in the SQW will start out higher than that in the MQW because of the lower transparency current but the gain in the MQW increases more quickly so the MQW gain curve crosses that of the SQW at some point.

Which QW structure has a lower threshold current will depend on how large the losses are for a particular device structure and on where the gain curves cross. While theoretical calculations sometimes indicate that MQWs will have lower threshold currents for normal device conditions,[28,29] experimental results disagree. All the record low threshold currents have been achieved with SQWs.[20,25,26,30,31,32,33] This seems to indicate that the gain curves cross at higher gains than have been calculated. The best structure for low threshold current is normally a SQW, but for some applications involving very large losses and requiring high gain a MQW is superior. For applications in which high output power is more important than low current a MQW is appropiate.

2.4 Graded-Index Separate-Confinement Heterostructure Single Quantum Wells

It is clear that a low threshold (Al,Ga)As laser should be a SQW, but the

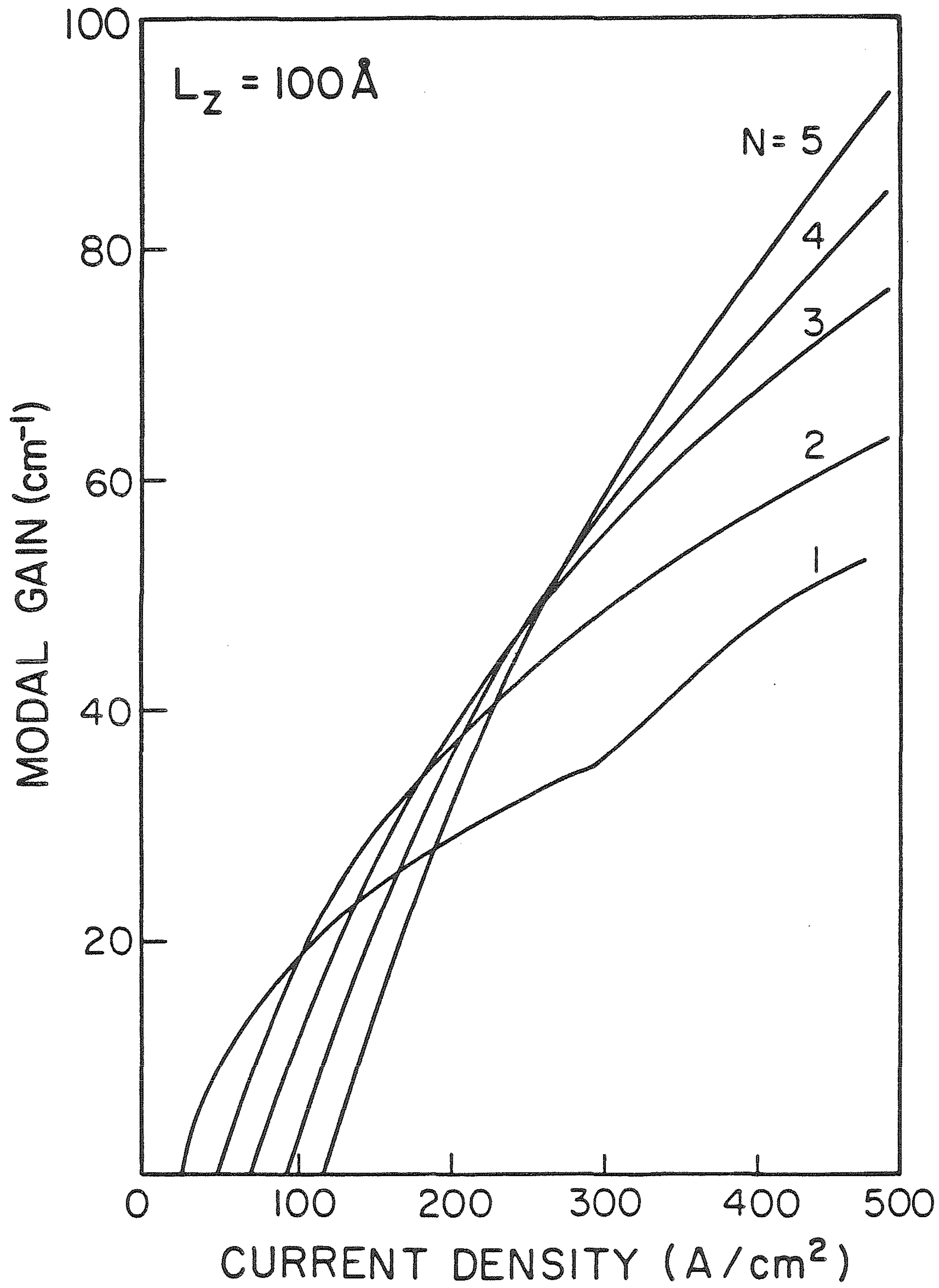

Figure 2.4: Modal gain as a function of current density for a SQW and MQWs with 2, 3, 4, and 5 QWs. Each QW has a thickness of 100 Å. (From Reference 28)

SQW structure for optimized performance needs to be considered. A disadvantage of QW lasers compared to DH lasers is the loss of optical confinement. One of the advantages of a DH laser is that the active region acts as a waveguide, but in a QW the active region is too thin to make a reasonable waveguide. Guiding layers are needed between the QW and the (Al,Ga)As cladding layers. The band structure of the simplest structure which accomplishes this is illustrated in Figure 2.5a. A layer of intermediate aluminum content and thickness on the order of 2000 Å is inserted between the QW and each cladding layer. The advantage of this structure is separate optical and electrical confinement and it is called a separate confinement heterostructure[33] (SCH) SQW. The carriers are confined in the QW, but the optical mode is confined in the surrounding layers. Experimentally it has been found that the optimum AlAs mole fraction, x, for layers around a QW is approximately[34] 0.2. In order to confine the optical mode well the cladding layers need a low index refraction compared to that of an $x = 0.2$ layer. In a simple DH laser, the cladding layers typically have x between 0.3 and 0.4, but for good confinement in an $x = 0.2$ layer more aluminum should be incorporated into the cladding layers; x should be between 0.5 and 0.7.

A better SQW structure based on the same principle as the SCH SQW is the graded-index separate-confinement heterostructure (GRIN SCH) SQW. This structure, which was introduced by Tsang[30,35] is illustrated in Figure 2.5b. The GRIN SCH SQW structure has produced all of the record low threshold current densities.[20,25,26,30,31,32,33] In a GRIN SCH SQW the intermediate low Al content layer of the SCH structure is replaced by a graded region which has high aluminum mole fraction ($0.5 \leq x \leq 0.7$) at the cladding layer and grades down to $x = 0.2$ at the QW. Typically the thickness of each graded layer (on either side of the QW) is between 1500 to 2000 Å. The grading is usually done at a rate which gives a

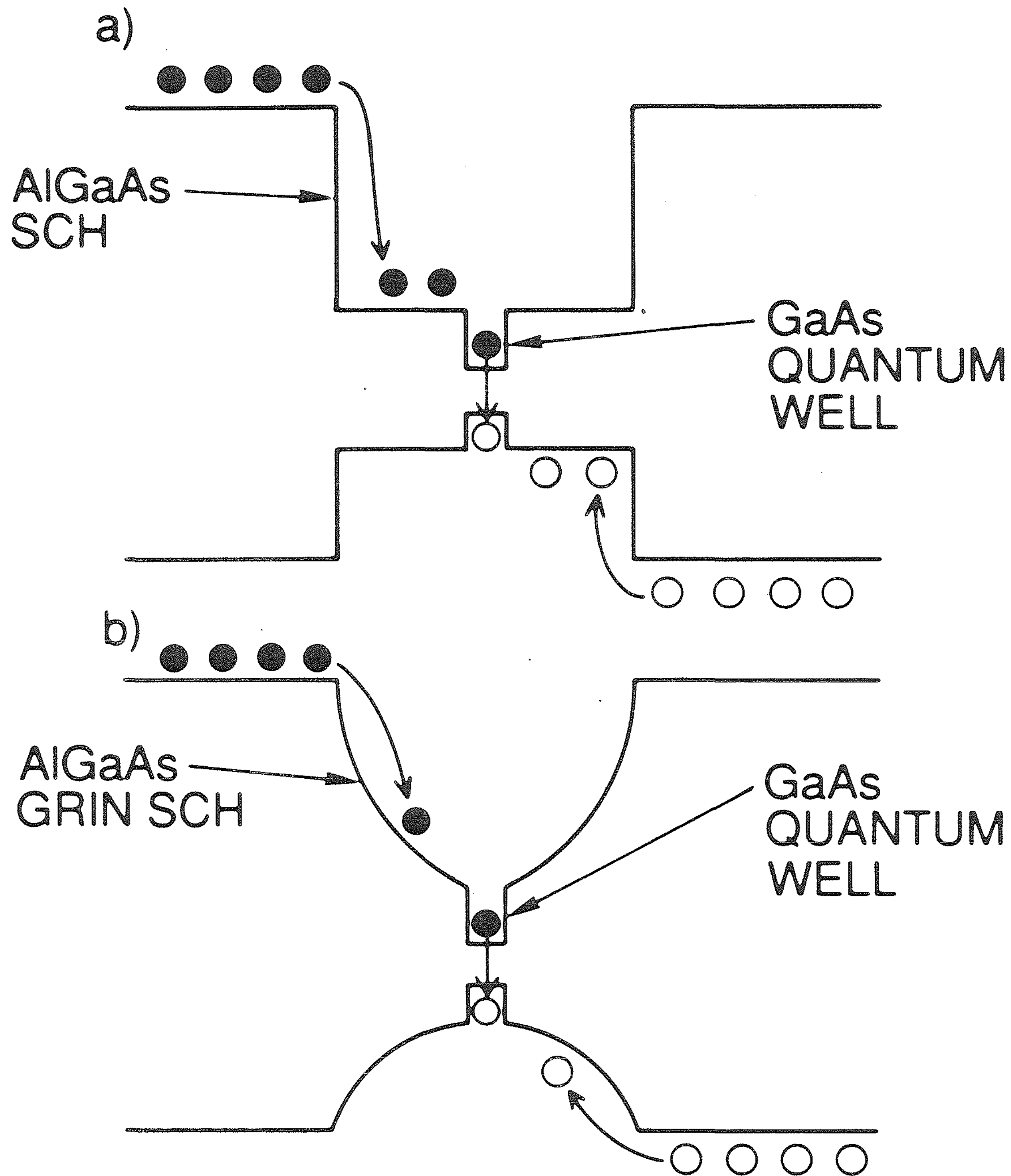

Figure 2.5: Schematic energy band diagram for (a) a SCH SQW and (b) a GRIN SCH SQW.

parabolic refractive index profile.

The optical mode supported by a GRIN SCH SQW with a parabolic refractive index profile is the lowest order Hermite-Gaussian.[33] Higher order modes are cut off. A Hermite-Gaussian mode decays as $e^{-(z/w_o)^2}$, where z is the distance from the center of the waveguide and w_o is the beam waist. The fundamental mode supported by a rectangular SCH structure will have a cosinusoidal decay inside the SCH structure. (For a discussion of waveguides see, for example, Reference 36.) The GRIN SCH structure is a better waveguide since the mode it supports is more tightly confined than that in a rectangular SCH structure of the same thickness. The optical confinement factor in the SQW will still be very small in the GRIN SCH SQW although it is a little larger than that in the SCH SQW.[37]

Another reason why the GRIN SCH SQW is superior is its density of states.[38,39] Since a real QW is not infinitely deep, confined states with energies in the parabolic band edge of Figure 2.5 can be occupied. In the SCH SQW the density of states in the rectangular SCH structure will be that of 3-dimensional bulk material. In the GRIN SCH SQW quantized energy levels will exist at the bottom of the GRIN SCH. It will take fewer carriers to fill these states than those in the rectangular SCH. In other words, the bottom of the GRIN SCH is narrower than that of the rectangular SCH so it takes less current to pump it (as it takes less current to pump a SQW than to pump a conventional DH).

It has been suggested that there is enhanced carrier confinement in the GRIN SCH due to an electron "funneling" effect in the GRIN SCH,[40] however, calculations show that differences in the electron capture times of the two structures are negligible.[41] Recent experimental results[42] agree that the capture time is not significantly affected by the confinement structure, but indicate that trapping efficiency is improved for the GRIN SCH. This result is consistent with the very

high quantum efficiencies obtained for GRIN SCH SQWs.[20] The lower trapping efficiency in the SCH SQW is attributed to radiative and nonradiative recombination in the confinement layers.[42] It is observed experimentally that structures with doping in the confinement heterostructure have lower threshold currents than those without, due to more efficient carrier injection into the SQW.

Another advantage of the GRIN SCH SQW is related to the growth mechanisms. When AlGaAs/GaAs heterostructures are grown by molecular beam epitaxy (MBE) it is well established that an interface of GaAs grown after AlGaAs (called an "inverted" interface) is inferior to one of AlGaAs grown on top of GaAs.[43,44,45] This problem has been attributed to various mechanisms such as interface roughness,[44] impurity build up,[45] and strain.[46] The interfaces are of course very important for a SQW since it is so thin. QWs with a graded interface have been shown to have higher photoluminescence intensity than those without.[47,48] (Strong photoluminescence intensity is a good indication of quality laser material.) In one study[49] DH lasers with a graded buffer layer before the lower AlGaAs cladding layer were shown to have lower threshold currents than those without. The improvement is attributed to a better "inverted" interface due to smoothing or strain reduction. It is therefore possible that the grading in the half of the GRIN SCH grown before the SQW improves the "inverted" interface of the SQW, which would lead to lower threshold currents.

2.5 Optimal Single Quantum Well Thickness

We have established that the structure for low threshold current (Al,Ga)As laser diodes is the GRIN SCH SQW. The question that remains is how narrow a SQW should be used. In the limit of very thin QWs (less than 20 Å) higher threshold currents are expected due to loss of carrier confinement and interface problems. In

the limit of very wide QWs (greater than 200 Å) higher threshold currents are also expected due to the onset of 3-dimensional density of states.[26,50] Theoretical calculations such as those derived here and those in Reference 39 suggest very little change in threshold current for some intermediate range of QW thicknesses (50-100 Å). This result is not surprising if one considers Equation (2.10) in which dependence of the modal gain on quantum well thickness enters through Γ and $\mathcal{D}(E)$. Γ is approximately proportional to L_z while $\mathcal{D}(E)$ is inversely proportional to L_z. Equation (2.10) therefore suggests that as a function of carrier density the modal gain shows little dependence on L_z for intermediate values of L_z. Considering Equation (2.19) it is clear that the carrier density will also show little dependence on L_z. L_z appears explicitly in Equation (2.19) but $J(N)$ also depends on $\mathcal{D}(E)$, so dependence on L_z again cancels out.

Some experimental work[32] has, however, shown a strong threshold current dependence on QW thickness. More recent work[26,50] suggests, however, that this result is due to experimental error. The threshold current of an (Al,Ga)As laser grown by MBE is very sensitive to growth conditions. If the MBE growth conditions were not optimized, it could have a large effect on the results. Variations in cavity length could also effect the results, since the end loss is significant for normal cavity lengths. In the more recent work[26] the threshold current densities reported were less than half those in the earlier work, suggesting that the growth conditions were more optimal. For comparison of different QW widths, very long cavity lengths ($\sim$3 mm) were used to minimize the effect of end loss on the results. Under these conditions, no threshold current dependence existed for QW thickness in the range of 65-165 Å. Therefore, the more recent experimental work agrees with the theoretical results[39] suggesting no significant threshold dependence on QW thickness for QWs of intermediate thicknesses.

2.6 Conclusion

On the basis of the discussion in this chapter we can conclude that the best (Al,Ga)As diode laser structure for achieving low threshold current is a SQW. This is true because a SQW laser has a lower transparency current than other semiconductor laser structures. The transparency current is lower because it takes fewer carriers to reach the transparency carrier density in a SQW. It takes fewer carriers because the volume of the active region (the SQW) is smaller than that of other lasers. Primarily because of the low optical confinement in a QW, the SQW should be surrounded by a GRIN SCH. On the basis of calculations and the most recent experimental work it appears that the exact width of the QW within a range of ~65-165 Å does not matter. In the next chapter, a method for epitaxial growth of QW lasers is described.

2.7 References

[1] See for example: G. H. B. Thompson, *Physics of Semiconductor Laser Devices*, pp. 45-46, John Wiley & Sons, New York (1980).

[2] R. Dingle, in *Festkörper Probleme XV (Advances in Solid State Physics)*, edited by H. Queisser, pp. 21-48, Pergamon, New York (1975).

[3] N. Holonyak, Jr., R. M. Kolbas, R. D. Dupuis, R. D. Dupuis, and P. D Dapkus, *IEEE J. Quantum Electron.* **QE-16**(2), pp. 170-186 (1980).

[4] N. Okamoto, *Jpn. J. Appl. Phys.* **26**(3), pp. 315-330 (1987).

[5] See for example: C. Cohen-Tannoudji, B. Diu, and F. Lalöe, *Quantum Mechanics, Volume One*, pp. 74-78, John Wiley & Sons, New York (1977).

[6] H. C. Casey, Jr. and M. B. Panish, *Heterostructure Lasers, Part A: Fundamental Principles*, p. 203, Academic Press, Orlando (1978).

[7] H. C. Casey, Jr. and M. B. Panish, Ibid., p. 165.

[8] Y. Nishimura, *Jpn. J. Appl. Phys.* **13**(1), pp. 109-117 (1974).

[9] M. Yamanishi and Y. Lee, *IEEE J. Quantum Electron.* **QE-23**(4), pp. 367-370 (1987).

[10] M. Yamada and Y. Suematsu, *J. Appl. Phys.* **52**(4), pp. 2653-2664 (1981).

[11] M. Yamada, H. Ishiguro, and H. Nagato, *Jpn. J. Appl. Phys.* **19**(1), pp. 135-142 (1980).

[12] E. H. Stevens and S. S. Yee, *J. Appl. Phys.* **44**(2), pp. 715-722 (1973).

[13] See for example: H. C. Casey, Jr. and M. B. Panish, Ibid., p. 197.

[14] E. O. Kane, *J. Phys. Chem. Solids* **1**, pp. 249-261 (1957).

[15] M. Asada, A. Kameyama, and Y. Suematsu, *IEEE J. Quantum Electron.* **QE-20**(7), pp. 745-753 (1984).

[16] M. Mittelstein, Y. Arakawa, A. Larsson, and A. Yariv, *Appl. Phys. Lett.* **49**(25), pp. 1689-1691 (1986).

[17] H. Kressel and J. K. Butler, *Semiconductor Lasers and Heterojunction LEDs*, p. 556, Academic Press, New York (1977).

[18] H. C. Casey, Jr. and M. B. Panish, Ibid., pp. 168-181.

[19] A. Yariv, *Quantum Electronics*, 2nd Edition, p. 237, John Wiley & Sons, New York (1975).

[20] A. Larsson, M. Mittelstein, Y. Arakawa, and A. Yariv, *Electron. Lett.* **22**(2), pp. 79-81 (1986).

[21] H. C. Casey, Jr. and M. B. Panish, *Heterostructure Lasers, Part B: Materials and Operating Characteristics*, p. 176, Academic Press, Orlando (1978).

[22] H. C. Casey, Jr. and M. B. Panish, Ibid., Part A, pp. 174-176.

[23] H. Kressel and J. K. Butler, Ibid., p.263.

[24] P. L. Derry, A. Yariv, K. Y. Lau, N. Bar-Chaim, K. Lee, and J. Rosenberg, *Appl. Phys. Lett.* **50**(25), pp. 1773-1775 (1987).

[25] H. Z. Chen, A. Ghaffari, H. Morkoç, and A. Yariv, *Appl. Phys. Lett.* **51**(25), pp. 2094-2096 (1987).

[26] H. Chen, A. Ghaffari, H. Morkoç, and A. Yariv, *Electron. Lett.* **23**(25), pp. 1334-1335 (1987).

[27] R. Fischer, J. Klem, T. J. Drummond, W. Kopp, H. Morkoç, E. Anderson, and M. Pion, *Appl. Phys. Lett.* **44**(1), pp. 1-3 (1984).

[28] Y. Arakawa and A. Yariv, *IEEE J. Quantum Electron.* **QE-21**(10), pp. 1666-1674 (1985).

[29] P. W. A. McIlroy, A. Kurobe, and Y. Uematsu, *IEEE J. Quantum Electron.* **QE-21**(12), pp. 1958-1963 (1985).

[30] W. T. Tsang, *Appl. Phys. Lett.* **40**(3), pp. 217-219 (1982).

[31] S. D. Hersee, M. Baldy, P. Assenat, B. de Cremoux, and J. P. Duchemin, *Electron. Lett.* **18**(20), pp. 870-871 (1982).

[32] T. Fujii, S. Hiyamizu, S. Yamakoshi, and T. Ishikawa, *J. Vac. Sci. Technol.* **B3**(2), pp. 776-778 (1985).

[33] W. T. Tsang, *Electron. Lett.* **16**(25), pp. 939-941 (1980).

[34] W. T. Tsang, *Appl. Phys. Lett.* **39**(10), pp. 786-788 (1981).

[35] W. T. Tsang, *Appl. Phys. Lett.* **39**(2), pp. 134-137 (1981).

[36] M. J. Adams, *An Introduction to Optical Waveguides*, John Wiley & Sons, New York (1981).

[37] D. Kasemset, C. S. Hong, N. B. Patel, and P. D. Dapkus, *Appl. Phys. Lett.* **41**(10), pp. 912-915 (1982).

[38] J. Nagle, S. Hersee, M. Krakowski, T. Weil, and C. Weisbuch, *Appl. Phys. Lett.* **49**(20), pp. 1325-1327 (1986).

[39] J. Nagle and C. Weisbuch, *Technical Digest 13th European Conference on Optical Communication (ECOC)*, Helsinki, Finland (Sept. 1987).

[40] S. D. Hersee, B. de Cremoux, and J. P. Duchemin, *Appl. Phys. Lett.* **44**(5), pp. 476-478 (1984).

[41] J. A. Brum, T. Weil, J. Nagle, and B. Vinter, *Phys. Rev.* **B34**(40), pp. 2381-2384 (1986).

[42] J. Feldman, G. Peter, E. O. Göbel, K. Leo, H.-J. Polland, K. Ploog, K. Fujiwara, and T. Nakayama, *Appl. Phys. Lett.* **51**(4), pp. 226-228 (1987).

[43] R. Fischer, W. T. Masselink, Y. L. Sun, T. J. Drummond, Y. C. Chang, M. V. Klein, and H. Morkoç, *J. Vac. Sci. Technol.* **B2**(2), pp. 170-174 (1984).

[44] H. Morkoç, T. J. Drummond, and R. Fischer, *J. Appl. Phys.* **53**(2), pp. 1030-1033 (1982).

[45] R. C. Miller, W. T. Tsang, and O. Munteanu, *Appl. Phys. Lett.* **41**(4), pp. 374-376 (1982).

[46] T. J. Drummond, J. Klem, D. Arnold, R. Fischer, R. E. Thorne, W. G. Lyons, and H. Morkoç, *Appl. Phys. Lett.* **42**(7), pp. 615-617 (1983).

[47] W. T. Màsselink, M. V. Klein, Y. L. Sun, Y. C. Chang, R. Fischer, T. J. Drummond, and H. Morkoç, *Appl. Phys. Lett.* **44**(4), pp. 435-437 (1984).

[48] R. Fischer, W. T. Masselink, Y. L. Sun, T. J. Drummond, Y. C. Chang, M. V. Klein, and H. Morkoç, *J. Vac. Sci. Technol.* **B2**(2), pp. 170-174 (1984).

[49] T. Hayakawa, T. Suyama, M. Kondo, K. Takahashi, S. Yamamoto, and T. Hijikata, *Appl. Phys. Lett.* **49**(4), pp. 191-193 (1986).

[50] P. L. Derry, H. Z. Chen, H. Morkoç, A. Yariv, K. Y. Lau, N. Bar-Chaim, K. Lee, and J. Rosenberg, *J. Vac. Sci. Technol.* **B6**(2), pp. 689-691 (1988).

Chapter 3

Molecular Beam Epitaxial Growth of (Al,Ga)As Lasers

3.1 Introduction

In Chapter 2 it was established that the optimal (Al,Ga)As laser structure for low threshold current is the GRIN SCH SQW with a QW thickness between ~65-165 Å. In the current chapter a method for growing this structure is described.

Many of the laser diode structures which have been developed are usually grown by liquid phase epitaxy[1] (LPE). In LPE, epitaxial layers are formed by precipitation of constituent atoms onto a single crystal substrate from a saturated liquid solution. Although some QW structures have been grown by LPE,[2] it is not well suited for growing thin structures because of lack of control and uniformity.[3] Better methods for growing thin (Al,Ga)As structures are molecular beam epitaxy[4] (MBE), which in the simplest terms is a complicated form of vacuum evaporation, and metalorganic chemical vapor deposition[5,6] (MO-CVD), which is a specialized form of chemical vapor deposition. In MO-CVD gases reacting over the surface of the substrate form epitaxial layers; some of the gases are metalorganics. Many QW structures were first developed with MBE although MO-CVD is capable of reproducing them. MBE is a very valuable tool in research environment, but MO-CVD is better suited to production since it is more efficient and less expensive. Both techniques involving working with hazardous materials like arsenic, but this problem is worse with MO-CVD since it requires hazardous gases. The QW structures described in this thesis were grown by MBE, so that is the method which is discussed here.

3.2 Principles of (Al,Ga)As Molecular Beam Epitaxy

MBE (which has been described in several reviews[4,7,8,9]) can be defined as an epitaxial growth process for growing high quality epitaxial layers lattice matched to a single crystal substrate through the thermal reaction of thermal beams of atoms and molecules with the substrate, which is held at an appropiate temperature in an ultrahigh vacuum. MBE is different from simple vacuum evaporation for several reasons: the growth is single crystalline, the growth is much more controlled and the vacuum system, evaporation materials, and substrate are cleaner. MBE growth of an alloy like (Al,Ga)As requires that the thermal beams be carefully controlled to achieve the correct ratios of constitutive elements in the epitaxial layers. MBE is a slow growth process (on the order of 1-2 μm per hour) which allows it to have the control needed to grow high quality thin structures like QWs. This slowness, however, makes MBE very sensitive to the build up of impurities on the surface of the substrate and on the epitaxial layers during growth. For this reason MBE growth must take place in an ultrahigh vacuum. Care must be taken that all components of the chamber are made of materials which will not contaminate the growth.

Figure 3.1 is a schematic diagram of an MBE growth chamber. To remove impurities such as water vapor after the growth chamber has been exposed to air it is baked at ~150-200°C for several days. To further remove contaminants from the growth environment the walls of the growth chamber are cooled with liquid nitrogen during growth; this causes contaminants to stick to the walls. To avoid a time consuming bake out every time a substrate wafer is loaded into the chamber, MBE systems have multiple vacuum chambers, which are separated by ultrahigh vacuum valves. The wafers are loaded into one of the other chambers without exposing the growth chamber to air. After the loading chamber has been pumped down,

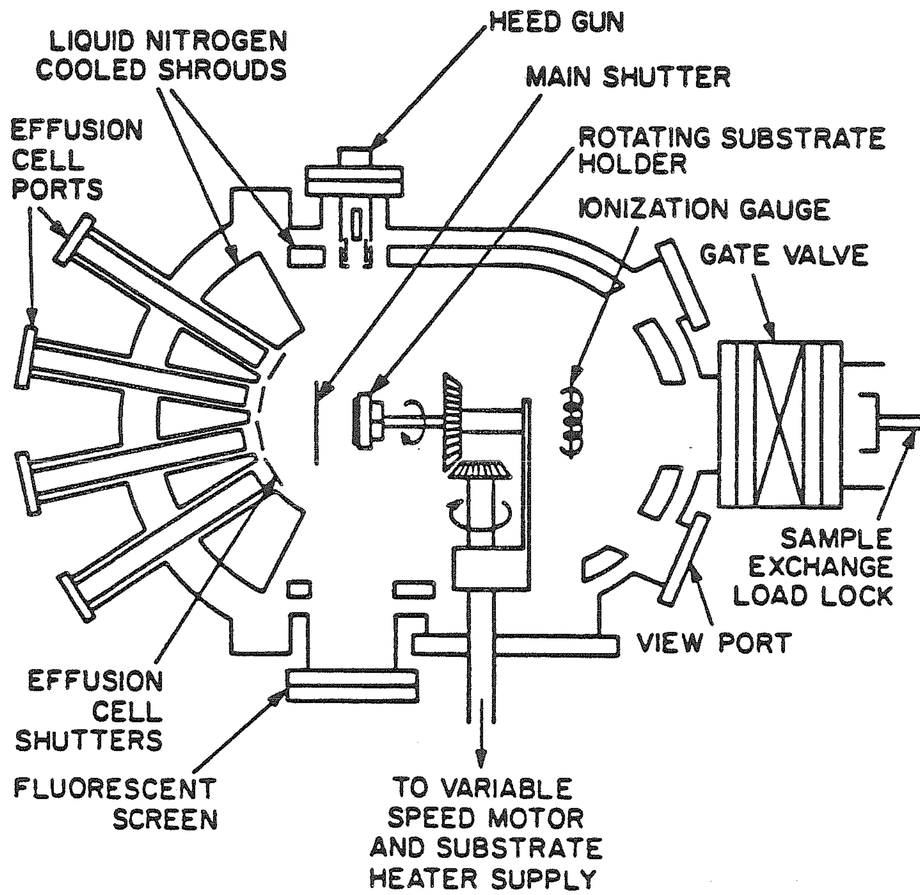

Figure 3.1: Schematic diagram of an MBE growth chamber.

the substrates can be transfered to the growth chamber as needed. MBE systems contain mechanical transfer mechanisms for this purpose. The growth chamber is then only exposed to air when repairs are required or when evaporation materials (As, Ga, Al, and dopants) need replenishing.

The evaporation materials are loaded in crucibles which are held in Knudsen effusion cells which are used to heat them. The effusion cells are oriented so that thermal beams from them will impinge on the substrate. For uniform flux coverage across the surface of the substate, which is necessary to achieve uniform growth, the substrate is rotated during growth. The crucibles are normally made of pyrolitic boron nitride, which has been found to be less of a contaminant than other possible materials such as graphite. Each effusion cell is individually heated and monitored with a thermocouple for precise control of each individual evaporation material. Unfortunately, the geometry of an effusion cell allows only a small area of contact between the thermocouple and the crucible, and the contact can vary each time a crucible is loaded into the effusion cell. The reading of the thermocouple is very sensitive to the contact with the crucible, so each time a crucible is loaded the temperature reading may be changed. Since the temperature to produce a desired flux from a particular cell will depend on the geometry of the system and how full the crucible is, the temperature necessary for that material must be individually calibrated for each MBE system and recalibrated whenever the material is replenished.

3.3 Growth Conditions

The sticking coefficients of aluminum and gallium on a GaAs substrate at a temperature of less than $\sim 640°C$ are close to one[10], but the sticking coefficient for arsenic is low. Elemental arsenic evaporates as As_4 unless it is "cracked" into As_2

by high temperature dissociation. For As_4 the reaction for forming GaAs involves pairwise dissociation of As_4 adsorbed on adjacent Ga atoms. For any two As_4 molecules four As atoms are incorporated into the epitaxial layer and four desorb as an As_4 molecule.[9] The sticking coefficient of As_4 is therefore less than 0.5 and for quality layers the flux ratio of As:Ga must be at least 2:1. A rough calibration of the fluxes for the As, Ga, and Al sources can be made by rotating an ionization gauge into the growth position of the substrate. The accuracy of this measurement will depend on the sticking coefficients of the materials. This is a reasonable technique for adjusting Al and Ga fluxes, since their sticking coefficients on a gauge are high, but As has a very low sticking coefficient on an ionization gauge, so its flux cannot be accurately determined with this method, although changes in As flux can be detected. Final determination of the appropiate temperatures for fluxes desired must be made by growing calibration layers.

Generally the gallium temperature is adjusted to achieve a desired growth rate for GaAs (for example, 1 μm/hour). The appropiate aluminum temperatures for various Al concentrations, x and the growth rate for those alloys $Al_xGa_{1-x}As$ must then be calibrated. When the sticking coefficients for Ga and Al are equal, x in a $Al_xGa_{1-x}As$ layer may be found by simply comparing its growth rate with that of a GaAs layer[7] grown at the same substrate temperature.

$$x = \frac{G(Al_xGa_{1-x}As) - G(GaAs)}{G(Al_xGa_{1-x}As)} \tag{3.1}$$

where $G(Al_xGa_{1-x}As)$ and $G(GaAs)$ are the growth rates for $Al_xGa_{1-x}As$ and GaAs. The growth rate is determined by measuring the thickness of a layer for which the growth time is known. A thick layer can be examined with an optical microscope although measurement with a scanning electron microscope (SEM) is more accurate. When examining layers with an SEM thin AlAs layers can be used as markers without any sample preparation. If AlAs markers are not used,

GaAs/$Al_xGa_{1-x}As$ interfaces can be stained to be visible for examination in either an optical microscope or an SEM. A solution of hydrogen peroxide with aluminum hydroxide added to achieve a pH of ~7.04 can be used as a stain. This solution works by etching GaAs much faster than $Al_xGa_{1-x}As$. An etch time of only 15-30 seconds is sufficient to stain a sample.

For more accurate determination of x, room temperature photoluminescence or X-ray diffraction can be used. For strong photoluminescence the sample must have a direct band gap ($x \leq 0.45$). In a photoluminescence measurement the sample is optically pumped (with a laser) and the energy of the photoluminescence excited is measured to determine the band gap of the material. From the band gap the aluminum concentration is known. X-ray diffraction measures x by determining the lattice constant of the crystal, which depends on the alloy composition. When photoluminescence or X-ray diffraction is used to measure x, the growth rate must of course still be measured to calibrate the MBE system for growing device structures.

An arsenic temperature high enough to produce sufficient As_4 flux can be determined by raising the arsenic temperature high enough that smooth GaAs layers are grown. The best arsenic temperature is, however, determined by examining GaAs layers while they are growing. The quality of a GaAs layer in progress can be determined by examining its high energy electron diffraction (HEED) pattern. As diagrammed in Figure 3.1, the HEED gun in an MBE growth chamber is situated so that the monoenergetic electron beam it produces will be incident on the substrate at a grazing angle. The reflected electrons are detected on a fluorescent screen on the opposite side of the growth chamber. The interpretation of HEED patterns is a complicated subject (see for example Reference 4). Streaked HEED patterns are an indication of a well defined single crystal surface. Spots indicate a rougher surface. MBE of (Al,Ga)As is usually performed on GaAs substrates with a (100)

crystal surface. The various HEED patterns on the (100) surface have been studied and related to specific arrangements of the outermost atoms on the surface. To determine the appropriate As_4 flux the arsenic temperature is raised high enough to obtain the HEED pattern associated with quality growth with an overpressure of arsenic. The arsenic temperature can then be lowered until this pattern is lost. The As:Ga flux ratio at the As temperature at which the pattern is lost should be close to 2:1. The best growths will be obtained with the As_4 flux slightly higher than at this point, but carefully maintained so that it does not dip below this point. The minimum As pressure that can be used is the best for two reasons: (1) high As_4 flux creates Ga vacancies which are electron traps;[11,12] and (2) if minimal arsenic is used the MBE system will not have to be opened as often to replenish the arsenic. The minimum As_4 flux which can be used will depend on the substrate temperature and on the growth rate. The As_4 flux has to be raised slightly, when Al is added to the growth, especially when a high substrate temperature is used. When the substrate temperature is high (higher than $\sim$640°C) the sticking coefficients of As and Ga decrease while the Al sticking coeffiecient does not.[10] At high temperatures, the Ga sticking coefficient increases when Al is present, and Equation (3.1) is invalid.

Much difficulty is associated with measuring the substrate temperature. The substrate is normally mounted on a molybdenum block which is heated resistively from the back and rotates for uniform growth. The temperature is measured with a thermocouple which contacts the back of the molybdenum block but does not rotate with it. There are two problems with this setup: (1) the thermocouple measures the temperature of the block and not the substrate; and (2) the contact of the thermocouple with the block may not be very good and can vary. For these reasons, temperature measurement with the thermocouple is very inaccurate and temperature readings in two different MBEs cannot be easily compared.

Another instrument for measuring substrate temperature is an optical pyrometer, which is mounted on the outside of the growth chamber and focused on the substrate through a viewport. This measurement is much more accurate than that of the thermocouple, but there are still problems associated with it: it can only be relied upon when growing GaAs since reflections from the aluminum cell can influence it; it depends on knowing the emissivity of the growing layers; the molybdenum block behind the substrate can influence the readings; and it depends on the viewport being unobstructed. The last restriction is the most serious since the viewport will be coated with GaAs during growths. When a temperature measurement is not being made the viewport is shuttered to prevent the accumulation of GaAs, but after months of MBE growth it will still be significantly coated. When the MBE machine is opened the viewport can be cleaned with a bromine/methanol solution, which etches away the GaAs.

Due to all the problems with temperature measurement, the optimum substrate temperature must be calibrated for each individual MBE machine and may need recalibrating periodically. It should be noted that the optimum temperature will depend on the As_4 flux and the layer composition. After the optimum temperature has been found, the best way to reproduce it is to reproduce the power which was used to maintain the substrate at that temperature.[13] The optimum temperature can be determined by examining the quality of layers at various temperatures. Strong photoluminescence intensity has been found to be a good indication of material which will make low threshold current lasers.[4,14] The best quality GaAs is grown at low substrate temperatures, ~580-620°C. This is the region in which As_4 has a high sticking coefficient. The photoluminescence from $Al_xGa_{1-x}As$ layers increases with increasing substrate temperature, but the morphology is degraded in an intermediate temperature range:[15] ~630-690°C. The morphology in this tem-

perature range can be improved somewhat by increasing the As_4 flux, but the best $Al_xGa_{1-x}As$ is grown at higher temperatures: ~700-720°C. This can be attributed to improved surface mobility of atoms at high temperatures and more efficient dissociation of As_4.[16] Another possible explanation is that the high temperature reduces the probability that impurities are incorporated in the layer; aluminum is more reactive with impurities like oxygen than gallium or arsenic.

The best test of optimum growth temperature for laser structures is to grow lasers at various temperatures and find the temperature which results in the lowest threshold current density.

3.4 Dopants

In order to grow a laser structure with MBE, doped material must of course be grown. Many of the dopants used for other types of (Al,Ga)As epitaxial growth cannot be used for MBE growth. Possible p-type dopants for III-V compounds are Zn, Cd, Be, Mg, Ge, and Mn; n-type dopants are Si, Ge, Sn, Te, and Se.[4,8] In order for an element to be used as a dopant for MBE it must have a reasonable sticking coefficient and surface lifetime and it must be possible to achieve an appropriate flux of the element on the substrate. If a dopant can be incorporated into (Al,Ga)As MBE layers, it should also be electrically active and incorporate evenly into the growth, i.e., not accumulate at the surface of the layer.

Zn and Cd have low sticking coefficients so they cannot be used as p-type MBE dopants.[4] Mg and Mn have a low degree of electrical activity in MBE layers so they are also inappropriate. Ge can act as a p-dopant but it is amphoteric: which type of dopant it acts as depends strongly on the growth conditions. This leaves Be, which is the best p-dopant for (Al,Ga)As MBE growth.[17] Be is not amphoteric, has a high sticking coeficient, and is electrically active in GaAs. High mobility

GaAs with carrier concentrations of up to 5×10^{19} cm^{-3} can be grown with Be doping. While higher carrier concentrations can be obtained, the quality of the layers, as measured by photoluminescence intensity, is reduced. This problem is attributed to interstitial Be, which acts as nonradiative centers.[18] $Al_xGa_{1-x}As$ is not doped as highly as GaAs by the same concentration of Be, due to a higher degree of compensation.[4,17] For this reason a p^+-GaAs contact layer is normally grown on top of the p-$Al_xGa_{1-x}As$ cladding layer of a semiconductor laser. If device constraints do not permit a p^+-GaAs layer, Zn can be diffused into the top of the p-$Al_xGa_{1-x}As$ cladding layer after growth to facilitate formation of an ohmic contact.

Although Be is the best p-type dopant for (Al,Ga)As MBE and has been used extensively, it has some drawbacks. High purity Be is difficult to obtain commercially because of its extreme toxicity, which makes companies reluctant to work with it extensively in order to purify it. Another drawback is that Be diffuses significantly at temperatures higher than ~700°C.[17,19] Since MBE growth of (Al,Ga)As is not done at temperatures much higher than 700°C, Be diffusion during growth is usually not a major problem, but it can be a very significant problem if device processing after growth requires high temperatures.

Of the possible n-type dopants Ge, is a poor choice for MBE because of its amphoteric nature. Te is difficult to control because it accumulates on the surface and displaces As atoms.[4,8,20] Se has a very high vapor pressure, which is unsuitable for MBE, although is has been used as an n-dopant in specialized circumstances.[21,22]

Sn was used extensively as an n-dopant in the early days of (Al,Ga)As MBE,[20] but is tends to accumulate on the surface during growth.[23,24] Si is amphoteric, but under typical MBE growth conditions it is an n-type dopant. Si does not accumulate on the surface as Sn does, so sharper doping profiles can be obtained

with it.[25] This is especially important for structures involving very thin layers like QWs. Si is now normally used as the n-dopant in MBE (Al,Ga)As laser structures. Si has one drawback; due to its amphoteric nature, very high doping levels cannot be obtained, since the doping is limited by compensation. Si n-doping in GaAs is limited to $\sim 1 \times 10^{19}$ cm^{-3} and this value can only be obtained at low growth rates.[26] If very high n-doping is required Sn must be used. This is especially true for $Al_xGa_{1-x}As$, since the doping obtained is significantly less than that in GaAs due to larger donor activation energy in $Al_xGa_{1-x}As$.[27] Generally, the n-doping in $Al_xGa_{1-x}As$ for a particular Si effusion cell temperature is approximately an order of magnitude less than that obtained for a GaAs layer when the Ga temperature is the same for both layers. Some of this difference is, of course, due to the faster growth rate of $Al_xGa_{1-x}As$.

3.5 Substrate Preparation

Since MBE is extremely sensitive to impurities, removing any surface contamination on the substrate wafer prior to growth is very important. Typically high quality commercially grown and polished substrates are purchased and chemically cleaned to remove surface contamination. During the course of the work described in this thesis two different cleaning procedures were used. Method 1 is modeled after that of Cho.[7,28] Method 2 is based on that of Morkoç.[13] For both procedures all glassware and tweezers used must be very clean, a clean deionized water supply is required, and the work must be done in a clean hood. It is very important to avoid contaminating the substrate with organics, so the person performing the cleaning must wear gloves at all times.

Method 1 is:

1. Degrease the substrate in trichloroethylene (TCE) heated to near boiling.

2. Remove TCE by rinsing twice in acetone, twice in methanol, and ten times in deionized water.
3. Soak in hydrochloric acid (HCL) for at least two minutes or longer (up to a several hours). HCL removes the native oxide and some organic contaminants.
4. Rinse ten times in deionized water.
5. Rinse at least twice in methanol to remove the water.
6. Polish by hand on lens paper soaked in a dilute bromine/methanol solution. Since bromine reacts with water, it is important that no water come in contact with the wafer during this step. It is also important that the bromine concentration be very dilute, or the wafer will be etched in an uneven pattern. This step is for polishing and removing surface contaminants, not for deep etching. Only about a micron of etching should occur. After this step the wafer can be held in a glass basket, which makes handling easier.
7. Rinse at least twice in methanol to remove all bromine. Then rinse ten times in deionized water.
8. Etch five minutes in 4:1:1 (4 parts sulfuric acid, 1 part water, and 1 part hydrogen peroxide), which has been cooled in a water bath. In this step a significant amount of etching occurs (on the order of fifty microns).
9. Rinse in deionized water ten times.
10. Soak in HCL for two minutes to remove any oxide and organic material.
11. Soak in deionized water for $\sim$1 minute to grow a passivating oxide which will protect the surface of the wafer until epitaxial layers are grown on it.
12. Rinse ten times in deionized water to remove HCL.
13. Dry with nitrogen gas.

Cleaning method 2 is:

1. & 2. Same as steps 1 & 2 of method 1.

3. Dip substrate into room temperature sulfuric acid momentarily before soaking in heated (~60°C) sulfuric acid for five minutes. The dip is for removing water that will react with the sulfuric acid. The soak in hot sulfuric acid is for removing organic contaminants.
4. Dip in room temperature sulfuric acid to remove hot sulfuric acid and rinse in deionized water ten times.
5. Etch in 4:1:1 (see step 8 of method 1).
6. Quench etch in room temperature sulfuric acid for less than one minute.
7. Finish the same as method 1, steps 9-13.

Method 2 is simpler and less time consuming since it does not include a bromine/methanol polish, which is difficult to perform. The reason for including the bromine/methanol polish is to try to reduce the oval defect density. Oval defects are isolated defects (with an oval shape) which occur on otherwise hiqh quality MBE layers. Mechanisms believed to cause oval defects are inadequate polishing, surface contamination,[29,30,31,32] Ga "spitting",[33] and gallium oxide in the Ga source.[34,35] Ga "spitting" occurs during MBE growth when Ga condensed at the opening of the Ga crucible falls back into the melted Ga inside the crucible, causing Ga droplets and possibly absorbed gases to splash out of the crucible, some of which would reach the growing epitaxial surface. Most of the possible mechanisms for oval defect formation involve an impurity on the surface, about which a defect grows. It is likely that more than one of the possible mechanisms contributes to oval defect formation.

A bromine/methanol polish is intended to insure a smooth surface and reduce surface contamination, which could lead to oval defects. In the MBE growth done for this thesis, however, it was not clear that method 1 resulted in fewer oval defects. Both cleaning methods appeared to work equally well. Since the oval defect density

also depends on effects inside the growth chamber, the comparison is not clear cut, but method 2 appears to be preferable, since it is less time consuming, caused no obvious increase in defects, and is also safer for the person performing the cleaning since bromine is a health hazard.

After cleaning, the wafer is mounted on a molybdenum block. To avoid stress on the substrate, which can affect the growth, the wafer is normally soldered to the block with melted indium instead of holding it mechanically with metal clips. After growth, the wafer can easily be removed by heating the block until the In melts and the wafer slides off the block. A molybdenum block can be used many times, but the In from the previous use must be etched off with HCL. If desired (Al,Ga)As can be etched off with a bromine/methanol solution, although it is alright to allow it to accumulate. If further cleaning is needed, the block can be dipped in a 50% nitric acid/50% HCL solution which etches molybdenum. After cleaning, the block should be placed in acetone before drying with nitrogen gas. It is important that the last cleaning solution is not water, since water promotes the growth of oxide on the surface of the block.

To solder the substrate to the block, the block is heated on a hot plate, which has been preheated to somewhere between ~240-330°C. The exact temperature needed depends on the soldering technique. Indium melts at 160°C. The soldering is difficult and requires practice since reproducibility is required. Differences in the contact of the wafer with the block can affect the heating of the substrate during the growth. The soldering technique involves heating the block, spreading a thin layer of In on it as the In melts, and placing the substrate wafer on the melted In. If the block is too cold, the indium will not spread well, producing gaps in the solder which will cause nonuniform heating of the wafer. If the block is too hot, inferior mounting will also result since the In will oxidize.

A drawback of mounting by In soldering is that some In evaporates from the block during growth. Having In as an impurity in the MBE system is not a problem of consequence. However, the change in the contact of the substrate wafer with the the block due to In evaporation is a problem. Since the wafer is heated through the block, to maintain a constant substrate temperature as In evaporates the heating current must be increased. As discussed in Section 3.3, the substrate temperature is critical for the quality of epitaxial layers. The thermocouple, which measures the temperature from the back of the block, will not detect the change in temperature at the substrate so adjusting the power to compensate for In evaporation can be tricky.

Since In soldering can cause problems in substrate temperature reproducibility, there is great interest in alternative mounting techniques. In the last few years progress has been made on holding the substrate mechanically without producing a great amount of strain on the wafer.[36,37]

After the substrate is mounted, it is loaded into the MBE system. After the loading chamber has pumped down to the 10^{-7} torr range, the substrate is briefly heated to ~250-300°C to desorb water vapor without removing the protective oxide, which desorbs at ~580°C.

3.6 Growth of an (Al,Ga)As Laser

In preparation for an MBE growth, the growth chamber is cooled with liquid nitrogen and the evaporation materials are preheated and degassed. For a laser structure the substrate is usually (100) GaAs n^+-doped with Si. To start the growth the substrate is gradually heated over a period of ~15 minutes until the oxide desorbs. The desorption of the oxide can be monitored by examining the HEED pattern produced by the substrate. The oxide produces a hazy semicircular

pattern; when it is removed the pattern changes to that of the GaAs surface. When the oxide desorbs it is important to place the substrate under As flux to replenish As which is desorbing from the heated surface. Under As flux, the substrate can be heated higher to degas it before the growth begins. No matter what structure will be grown, it is always desirable to begin the growth with a GaAs buffer layer (generally at least 0.5 μm thick and n^+-doped with Si for a laser structure). As discussed in Section 3.3, the best GaAs is grown at ~580-620°C. The buffer layer is included to allow the growth to stabilize and smooth out. It is not desirable to start a device structure at the substrate/layer interface, since this interface has relatively high resistivity due to carrier compensating centers which are probably caused by impurities.[38]

After the buffer layer, the laser structure can be grown. A typical laser structure is a 1.5 μm n-$Al_xGa_{1-x}As$ cladding layer, followed by an undoped active region (surrounded by a GRIN SCH structure in the case of a QW) and a 1.5 μm p-$Al_xGa_{1-x}As$ cladding layer. The structure is usually topped with a p^+-GaAs contact layer on the order of ~0.2 μm thick. As discussed in Section 3.3 the $Al_xGa_{1-x}As$ cladding layers should be grown at high substrate temperatures ~700-720°C. Since the GaAs active region is thin, there is not enough time to lower the substrate temperature for it, so it is grown at the same temperature as the cladding layers. For a contact layer, the substrate temperature should be lowered back to ~580-620°C.

It has been found experimentally that the lowest threshold semiconductor lasers are produced with the cladding layers and active region grown at high temperatures.[14] The higher photoluminescence intensity of $Al_xGa_{1-x}As$ grown at high substrate temperatures is of course a major reason for this result. The quality of the interface of GaAs grown on $Al_xGa_{1-x}As$ (which is called an "inverted" inter-

face) will also contribute.[39] As mentioned in Section 2.4, it is well known that this interface is inferior to that of $Al_xGa_{1-x}As$ grown on top of GaAs. The poor quality of the "inverted" interface is generally attributed to roughness of the $Al_xGa_{1-x}As$ layer, impurities such as carbon which accumulate on the $Al_xGa_{1-x}As$ layer due to the high reactivity of Al, or impurity trapping due to strain. At high substrate temperatures the interface appears to be smoother, probably due to increased surface mobility of the atoms on the epitaxial surface and possibly due to reduced absorption of impurities.

Some work has been done on growing smoother interfaces at lower growth temperatures by interrupting the growth at the interface to allow migration of Al and Ga to smooth the $Al_xGa_{1-x}As$ surface layer before growing GaAs.[40,41] A typical growth interruption is on the order of one minute at a substrate temperature of $\sim$580°C. There are several problems with this technique. During growth interruption, impurities can pile up on the surface and As desorbs from the substrate. The substrate is kept under As flux during the interruption to replenish the desorbing As, but at high substrate temperatures As desorbs quickly, which is why growth interruption is done at low substrate temperatures. Due to these problems, growth interruption is not promising for device fabrication, although it is of interest for studying the mechanisms of MBE growth.

The other approach to improving the "inverted" interface is to change the device structure. It was discovered that a superlattice just before the "inverted" interface improved the interface.[42,43,44,45,46] This improvement is generally attributed to trapping of impurities from the substrate and the $Al_xGa_{1-x}As$ layer, reducing strain at the heterointerface and smoothing the growth. The improvement was established by observing increased photoluminescence and decreased threshold current density when a superlattice was present. In later work, when a superlattice

in a GRIN SCH SQW laser was placed after the GaAs buffer layer before the N-$Al_xGa_{1-x}As$ cladding layer, an improvement was still observed.[47] This implies that the superlattice smooths the growth and getters impurities from the substrate.

Grading the heterointerface of a QW was also shown to increase photoluminescence intensity, but not by as much as a superlattice.[44,45] A graded region before the N-$Al_xGa_{1-x}As$ cladding layer of a DH laser[48] improved the threshold current and differential quantum efficiency by a factor of ~ 2.

Despite the observed improvements with superlattice or graded buffer layers it is difficult to separate their effect from that of growth conditions, which have a much larger effect. Superlattice buffer layers have more effect at low substrate temperatures.[45] This implies that if the growth conditions are truely optimized, these special buffer layers could be unnecessary. For QW lasers grown by MO-CVD, introducing a superlattice or graded buffer layer has little effect,[49] which supports the conclusion that with the correct growth conditions their effect should be negligible. However, achieving and maintaining optimized MBE growth conditions is difficult, so it is generally a good idea to include a special buffer layer in an MBE laser structure. To get the maximum effect, it is best to put any special buffer layer as close to the active region as possible. In fact, the lowest threshold current GRIN SCH SQW lasers which have been grown to this date were grown by MBE and included a superlattice buffer layer in the half of the GRIN SCH grown before the SQW.[50]

3.7 Tilted Substrates

In the discussion so far it has been assumed that the substrate has a (100) surface. It is, however, possible to grow MBE layers on other surfaces. Of the possible orientations, the ones which have been shown to be most interesting for growth of

low threshold lasers are misoriented or tilted substrates. Tsui et al.[51] discovered that AlGaAs layers grown at a substrate temperature of ~675°C on substrates misoriented by ~ 3° from (100) towards (111)A had much better surface morphologies than those grown on a (100) substrate. Photoluminescence from (Al,Ga)As QWs was also improved by use of this substrate orientation.[52] The improvement has been attributed to minimization of energetic instabilities at the growing surface.[53] Another mechanism for improvement is that tilted (100) substrates have steps ending with Ga, leaving more bonding sites for As, which should increase the sticking coefficient of As.[54]

Chen et al.[54] have used misoriented (100) substrates to produce extremely low threshold current density GRIN SCH SQWs. They fabricated a 520 μm long laser with a 125 Å QW thickness, which had a threshold current density of only 93 A/cm^2. This is significantly less than previous record low threshold current densities. All of the lasers described in this thesis were grown on the (100) surface, so the threshold currents reported in Chapter 4 could possibly be improved upon by the use of misoriented substrates.

3.8 "Cracked" Arsenic

The discussion in this chapter has been limited to (Al,Ga)As MBE with an As_4 source, because that is what was used for the work described in this thesis. It is possible and desirable to "crack" As_4 into As_2 by high temperature dissociation. An As "cracker" cell is a Knudsen cell which has a second section at high temperature. As_4 from the basic Knudsen cell enters this second section on the way to the substrate and is "cracked" into As_2.

The advantage of As_2 is that it has a higher sticking coefficient than As_4. As_2 is incorporated into the epitaxial layer by simple dissociative chemsorption.[4,8,9] Unlike

As_4, As_2 has a measurable surface lifetime even without free surface Ga adatoms although it will not permanently condense unless it bonds with Ga. Some of the As_2 will desorb as As_4, so an excess of As is still required for quality growth, but not as large an excess as is required with As_4. Requiring less As is a considerable advantage of "cracked" arsenic, since with As_4 the arsenic needs replenishing more frequently than the other evaporation materials. Opening an MBE system as infrequently as possible is important for efficiency, since each time it is opened a considerable amount of time and effort is required to return it to operating condition.

As_2 also has advantages for the quality of growth. Ga and As vacancies are sources of electron traps. As_2 (compared to As_4) has been shown to reduce the density of electron traps at lower substrate temperatures.[55] When the electron trap density is reduced, doping efficiency is increased. As discussed in Section 3.3, AlGaAs grown with As_4 at substrate temperatures of ~630-690°C has poor surface morphology. When As_2 is used, the surface morphology of AlGaAs at these substrate temperatures is improved.[16] While it is still desirable to grow AlGaAs at high substrate temperatures, with an As_2 source a small change in temperature will not have as much effect as it would with an As_4 source. The use of As_2 will therefore make it easier to maintain optimized growth conditions. Since it is difficult to measure substrate temperature accurately, this is an important advantage.

3.9 Conclusion

MBE is well suited for growing (Al,Ga)As QW lasers since it has the control necessary to grow thin layers. High quality laser structures can be grown with MBE, if the growth conditions are optimized, i.e., substrate temperature and As:Ga flux. Since both the As flux and substrate temperature are difficult to measure accurately, achieving and maintaining the correct growth conditions can be difficult.

Growing a SQW structure is the first step in fabricating stripe SQW lasers. In Chapter 4, SQW lasers grown by MBE and their fabrication into stripe lasers with ultralow threshold currents are described.

3.10 References

[1] M. B. Panish, J. Sumski, and I. Hayashi, *Met. Trans.* **2**, pp. 795-801 (1971).

[2] E. A. Rezek, R. Chin, N. Holonyak, Jr., S. W. Kirchoefer, and R. M. Kolbas, *J. Electron. Mat.* **9**(1), pp. 1-27 (1980).

[3] G. H. B. Thompson, *Physics of Semiconductor Laser Devices,* p. 16, John Wiley & Sons, New York (1980).

[4] W. T. Tsang, *Semiconductors and Semimetals Vol. 22*, Part A, pp. 95-207 (1971).

[5] R. D. Dupuis, and P. D. Dapkus, *IEEE J. Quantum Electron.* **QE-15**(3), pp. 128-135 (1979).

[6] R. D. Burnham, W. Streifer, T. L. Paoli, and N. Holonyak, Jr., *J. Cryst. Growth* **68**, pp. 370-382 (1984).

[7] A. Y. Cho, *Thin Solid Films* **100**, pp. 291-317 (1983).

[8] K. Ploog, *Crystal Growth, Properties and Applications, Vol. 3,* edited by H. C. Freyhardt, pp. 73-162, Springer, Berlin (1980).

[9] B. A. Joyce, *Rep. Prog. Phys.* **48**, pp. 1637-1697 (1985).

[10] R. Fischer, J. Klem, T. J. Drummond, R. E. Thorne, W. Kopp, H. Morkoç, and A. Y. Cho, *J. Appl. Phys.* **54**(5), pp. 2508-2510 (1983).

[11] R. A. Stall, C. E. C. Wood, P. D. Kirchner, and L. F. Eastman, *Electron. Lett.* **16**(5), pp. 171-172 (1980).

[12] J. P. Saleno, E. S. Koteles, J. V. Gormley, B. J. Sowell, E. M. Brody, J. Y Chi, and R. P. Holmstrom, *J. Vac. Sci. Technol.* **B3**(2), pp. 618-621 (1985).

[13] H. Morkoç, private communication.

[14] W. T. Tsang, F. K. Reinhart, and J. A. Ditzenberger, *Appl. Phys. Lett.* **36**(2), pp. 118-120 (1980).

[15] H. Morkoç, T. J. Drummond, W. Kopp, and R. Fischer, *J. Electrochem. Soc.* **129**(?), pp. 824-826 (1982).

[16] L. P. Erickson, T. J. Mattord, P. W. Palmberg, R. Fischer, and H. Morkoç, *Electron. Lett.* **19**(16), pp. 632-633 (1983).

[17] M. Ilegems, *J. Appl. Phys.* **48**(3), pp. 1278-1287 (1977).

[18] P. Enquist, L. M. Lunardi, G. W. Wicks, L. F. Eastman, and C. Hitzman, *J. Vac. Sci. Technol.* **B3**(2), pp. 634-635 (1985).

[19] J. N. Miller, D. M. Collins, and N. J. Moll, *Appl. Phys. Lett.* **46**(10), pp. 960-962 (1985).

[20] A. Y. Cho and J. R. Arthur, *Prog. Solid State Chem.* **10**(3), pp. 157-191 (1975).

[21] C. E. C. Wood, *Appl. Phys. Lett.* **33**(8), pp. 770-772 (1978).

[22] D. A. Andrews, M. Y. Kong, R. Heckingbottom, and G. J. Davies, *J. Appl. Phys.* **55**(4), pp. 841-845 (1984).

[23] K. Ploog and A. Fischer, *J. Vac. Sci. Technol.* **15**(2), pp. 255-259 (1978).

[24] C. E. C. Wood and B. A. Joyce, *J. Appl. Phys.* **49**(9), pp. 4854-4861 (1978).

[25] T. Shimanoe, T. Murotani, M. Nakatani, M. Otsubo, and S. Mitsui, *Surf. Sci.* **86**, pp. 126-136 (1979).

[26] R. Sacks and H. Shen, *Appl. Phys. Lett.* **47**(4), pp. 374-376 (1985).

[27] L. G. Salmon and I. J. D'Haenens, *J. Vac. Sci. Technol.* **B2**(2), pp. 197-200 (1984).

[28] J. S. Smith, thesis, *III-V Molecular Beam Epitaxy Structures for Electronic and Optoelectronic Applications*, California Institute of Technology, Pasadena (1986).

[29] Y. Nishikawa, K. Kanamoto, Y. Tokuda, K. Fujiwara, and T. Nakayama, *Jpn. J. Appl. Phys.* **25**(6), pp. 908-909 (1986).

[30] Y. G. Chai, Y.-C. Pao, and T. Hierl, *Appl. Phys. Lett.* **47**(12), pp. 1327-1329 (1985).

[31] S.-L. Weng, C. Webb, Y. G. Chai, and S. G. Bandy, *Appl. Phys. Lett.* **47**(4), pp. 391-393 (1985).

[32] Y. H. Wang, W. C. Liu, S. A. Liao, K. Y. Cheng, and C. Y. Chang, *Jpn. J. Appl. Phys.* **24**(5), pp. 628-629 (1985).

[33] G. D. Pettit, J. M. Woodall, S. L. Wright, P. D. Kirchner, and J. L. Freeouf, *J. Vac. Sci. Technol.* **B2**(2), pp. 241-242 (1984).

[34] Y. G. Chai and R. Chow, *Appl. Phys. Lett.* **38**(10), pp. 796-798 (1981).

[35] S.-L. Weng, *Appl. Phys. Lett.* **49**(6), pp. 345-347 (1986).

[36] L. P. Erickson, G. L. Carpenter, D. D. Seibel, and P. W. Palmberg, *J. Vac. Sci. Technol.* **B3**(2), pp. 536-537 (1985).

[37] D. E. Mars and J. N. Miller, *J. Vac. Sci. Technol.* **B4**(2), pp. 571-573 (1986).

[38] N. J. Kawai, C. E. C. Wood, and L. F. Eastman, *Jpn. J. Appl. Phys.* **53**(9), pp. 6208-6213 (1982).

[39] H. Morkoç, T. J. Drummond, and R. Fischer, *J. Appl. Phys.* **53**(2), pp. 1030-1033 (1982).

[40] H. Sakaki, M. Tanaka, and J. Yoshino, *Jpn. J. Appl. Phys.* **24**(6), pp. L417-L420 (1985).

[41] M. Tanaka, H. Sakaki, and J. Yoshino, *Jpn. J. Appl. Phys.* **25**(2), pp. L155-L158 (1986).

[42] T. J. Drummond, J. Klem, D. Arnold, R. Fischer, R. E. Thorne, W. G. Lyons, and H. Morkoç, *Appl. Phys. Lett.* **42**(7), pp. 615-617 (1983).

[43] R. Fischer, J. Klem, T. J. Drummond, W. Kopp, H. Morkoç, E. Anderson, and M. Pion, *Appl. Phys. Lett.* **44**(1), pp. 1-3 (1984).

[44] W. T. Masselink, M. V. Klein, Y. L. Sun, Y. C. Chang, R. Fischer, T. J. Drummond, and H. Morkoç, *Appl. Phys. Lett.* **44**(4), pp. 435-437 (1984).

[45] R. Fischer, W. T. Masselink, Y. L. Sun, T. J. Drummond, Y. C. Chang, M. V. Klein, and H. Morkoç, *J. Vac. Sci. Technol.* **B2**(2), pp. 170-174 (1984).

[46] P. M. Petroff, R. C. Miller, A. C. Gossard, and W. Wiegmann, *Appl. Phys. Lett.* **44**(2), pp. 217-219 (1984).

[47] T. Fujii, S. Hiyamizu, S. Yamakoshi, and T. Ishikawa, *J. Vac. Sci. Technol.* **B3**(2), pp. 776-778 (1985).

[48] T. Hayakawa, T. Suyama, M. Kondo, K. Takahashi, S. Yamamoto, and T. Hijikata, *Appl. Phys. Lett.* **49**(4), pp. 191-193 (1986).

[49] M. E. Givens, L. J. Mawst, C. A. Zmudzinski, M. A. Emanuel, J. J. Coleman, *Appl. Phys. Lett.* **50**(6), pp. 301-303 (1987).

[50] H. Z. Chen, A. Ghaffari, H. Morkoc, and A. Yariv, *Electron. Lett.* **23**(25), pp. 1334-1335 (1987).

[51] R. K. Tsui, J. A. Curless, G. D. Kramer, M. S. Peffley, and D. L. Rode, *J. Appl. Phys.* **58**(7), pp. 2570-2572 (1985).

[52] R. K. Tsui, G. D. Kramer, J. A. Curless, and M. S. Peffley, *Appl. Phys. Lett.* **48**(14), pp. 940-942 (1986).

[53] D. L. Rode, W. R. Wagner, and N. E. Schumaker, *Appl. Phys. Lett.* **30**(2), pp. 75-78 (1977).

[54] H. Z. Chen, A. Ghaffari, H. Morkoc, and A. Yariv, *Appl. Phys. Lett.* **51**(25), pp. 2094-2096 (1987).

[55] R. T. Chen, N. H. Sheng, and D. L. Miller, *J. Vac. Sci. Technol.* **B3**(2), p. 652 (1985).

Chapter 4

Ultralow Threshold Buried Heterostructure Single Quantum Well (Al,Ga)As Lasers

4.1 Introduction

In this chapter the fabrication and threshold properties of buried heterostructure SQW (Al,Ga)As lasers are discussed. In Chapter 2 it was shown that the optimal structure for low threshold current is a GRIN SCH SQW. To fabricate an ultralow threshold current (< 1 mA) SQW laser at room temperature, low losses (both internal and external) are necessary. As discussed in Section 2.2, reducing the losses has a much greater effect on the threshold current of a QW laser than of a bulk DH laser because of the much lower transparency current in the QW.

In a SQW laser the internal loss is low,[1] so for normal cavity lengths the largest portion of the loss is the end loss. The reflectivity of the GaAs/air interface is only ~31% so the end loss can be reduced significantly by evaporating high reflectivity coatings on the end facets of an (Al,Ga)As laser. For a QW laser a reduction in end loss obtained in this manner will result in a dramatic reduction in threshold current. This point has been appreciated previously theoretically[2] and high reflectivity coatings have been applied to some QW lasers,[3,4,5] but it has not been utilized previously with a SQW laser stripe structure appropiate for achieving an ultralow threshold current.

To achieve an ultralow threshold semiconductor laser, the stripe width must be narrow (on the order of < 2 μm). For a laser stripe of this dimension, optical and current confinement become major considerations. The metallic contact on the n-doped side of a semiconductor laser is normally applied with no definition for current confinement; current confinement is introduced on the p-side of the device.

For a wide stripe laser, a dielectric coating (usually SiO_2 or Si_3N_4) is evaporated on the p-side of the laser. Contact openings in the dielectric are made through photolithography combined with chemical etching of the dielectric. The p-metallic contact is then applied across the whole device, but makes electrical contact only at the dielectric openings. This structure is called a contact stripe or an oxide stripe. Normally openings (through photolithography and chemical etching) in the metal are also made to separate adjacent lasers on a wafer. This step is required for all semiconductor laser single stripe structures unless adjacent lasers are separated by cleaving. A contact stripe works very well for wide stripes, but in narrow stripes current spreading is a very significant drawback, because there is no mechanism to prevent current spreading after the current is injected. Also since the GaAs active region extends outside of the stripe, there is no mechanism to prevent optical leakage in a contact stripe laser.

A more complicated stripe structure with electrical and optical confinement is required for an efficient narrow stripe laser. A number of structures which accomplish the necessary confinement have been developed. For some of these the active region is grown by LPE over a patterned substrate. Since LPE is not well suited for growth of QW lasers because of its lack of control, the structures with LPE grown active regions are not good choices for a SQW stripe laser. The most probable structures for efficient SQW stripe lasers are lasers on patterned substrates grown by MBE[6,7,8,9] or MO-CVD,[10] lasers with stripes formed by disordering,[11,12,13,14] and buried heterostructure lasers.[15,16]

A patterned substrate is one on which stripe channels are etched before any growth, exposing crystral planes other than that of the flat substrate. When MBE or MO-CVD layers are grown on top of the patterned substrate, the growth rate will be different on the side of a channel or mesa compared to a flat surface. Figure

4.1 schematically illustrates the laser structure formed by MBE epitaxial growth on a (100) GaAs surface with mesas in the $[0\bar{1}\bar{1}]$ direction. In this situation the growth rate is enhanced on the sides of the mesa.[7] A lasing mode will be confined in the region with a wider active region because of total internal reflection; in other words, because of a larger effective index of refraction. This structure provides the optical confinement lacking in a contact stripe laser.

Growth on a patterned substrate, however, provides no mechanism for current confinement so processing after growth for current confinement is required. The simplest method for current confinement on a patterned substrate laser is to apply a contact stripe as illustrated in Figure 4.1, however, this will not prevent current spreading. Therefore it is preferable to make the material outside the stripe highly resistive by damaging it, for instance by proton implantation of the p-AlGaAs cladding layer. Proton implantation produces lattice defects which cause high resistivity in the implanted area.[17] Proton implantation causes optical damage,[18] so implantation should not be heavy enough to reach the active region.

Growth of a laser on a patterned substrate by MBE is not trivial because of MBE's sensitivity to impurities. In the normal MBE cleaning (described in Section 3.5) a significant amount of substrate material (on the order of $\sim$50 μm) is etched away to provide a clean surface. On a patterned substrate the cleaning etch must be significantly reduced or the pattern will be etched away. Of course, with less etching, impurities on the surface are more likely.

Formation of a QW stripe laser by disordering takes advantage of the fact that diffusion of an impurity such as Si, Ge, or Zn mixes the Al and Ga in the cladding regions with that in the QW. After disordering, no QW exists; an AlGaAs alloy of averaged composition has been formed. For the simplest form of QW stripe laser with disordering, a planar QW laser structure is grown. The lasing stripe is

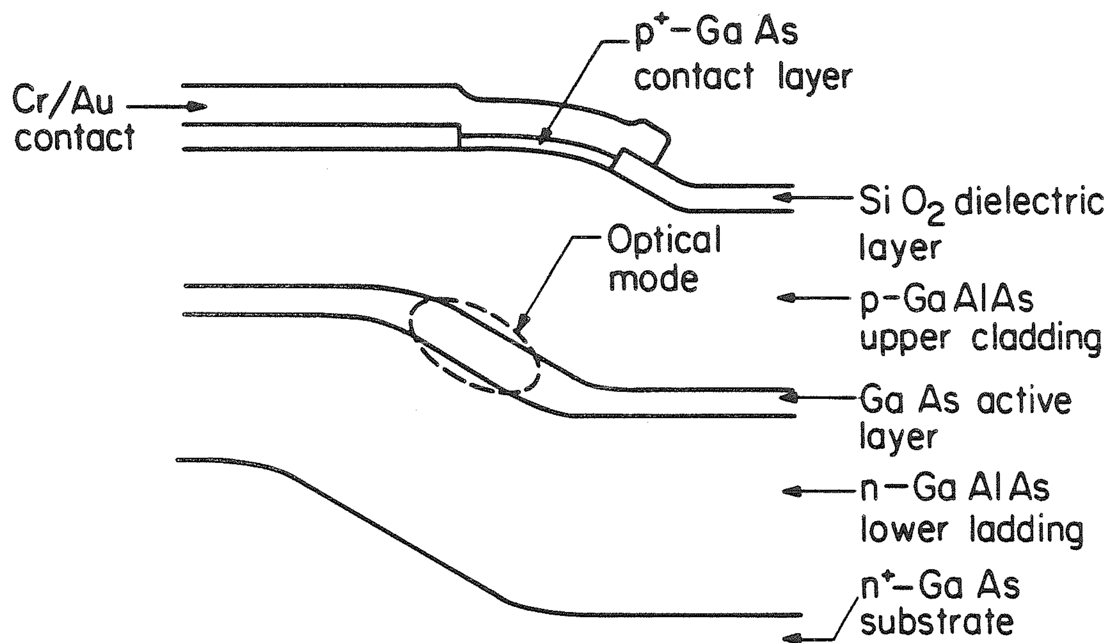

Figure 4.1: Schematic diagram of a stripe laser formed by MBE growth on a patterned substrate with mesa stripes oriented along the [011] direction.

masked and impurity disordering is performed on either side of it. After disordering the stripe has good optical confinement since the QW is completely surrounded by AlGaAs (which has a lower index of refraction). The impurities used are dopants for (Al,Ga)As and diffusing one of them does not destroy the electrical quality of the layers around the stripe, so additional processing for current confinement is required. (More complicated structures which involve regrowth and utilize impurity disordering provide current confinement.[19])

The buried heterostructure laser was first developed by Tsukada.[15] To form a BH stripe, a planar laser structure is first grown. Stripe mesas of the laser structure are formed by photolithography combined with wet chemical etching. AlGaAs is then regrown around the lasing stripe by LPE. Figure 4.2 is a schematic diagram of a buried heterostructure with a GRIN SCH SQW active layer. The etching around the mesa must reach GaAs, since LPE regrowth cannot be performed on AlGaAs because of aluminum oxide (although it will occur against the side of an AlGaAs mesa). The laser structure must end with the p-AlGaAs cladding layer instead of a p^+-GaAs contact layer, or regrowth will occur on top of the laser stripe. Since the active region is completely surrounded by AlGaAs, a BH has tight optical confinement. If the regrown layers are doped to produce a reverse biased junction (as illustrated in Figure 4.2) a BH laser can also provide good current confinement.

Narrow QW stripe lasers have been fabricated in all of the above structures. BHs are a well developed technology, while growth on patterned substrates (by MBE or MO-CVD) and stripe formation by impurity disordering are developing technologies for fabricating narrow stripes. At the time that the work reported on here was performed,* the lowest threshold current SQW stripe lasers which had been

---

* More recently SQW lasers with a threshold of 1.8 mA were fabricated by MBE growth on a patterned substrate.[9]

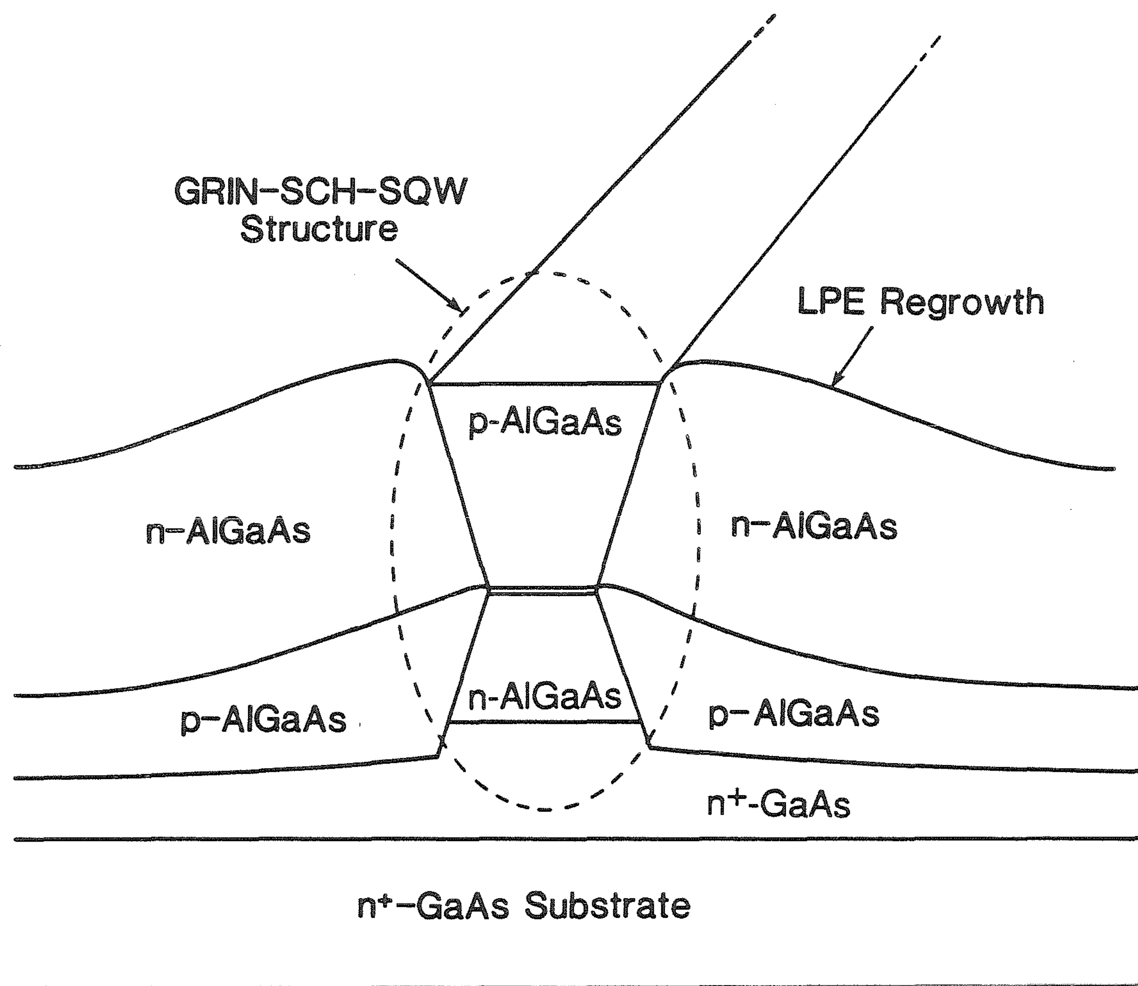

Figure 4.2: Schematic diagram of a buried heterostructure GRIN SCH SQW (Al,Ga)As stripe laser.

fabricated were BH lasers with a threshold current of 2.5 mA.[16] On the basis of the results already achieved with the BH, a BH stripe was chosen as a good structure for fabricating ultralow threshold SQW lasers by application of high reflectivity end facet coatings.

In this chapter the fabrication and threshold current properties of buried heterostructure GRIN SCH SQW lasers, with and without high reflectivity coatings, are described. The results are also explained on the basis of theory.

4.2 Planar GRIN SCH SQWs Grown by MBE

The first step in fabricating ultralow threshold buried heterostructure GRIN SCH SQW lasers is to grow high quality planar GRIN SCH SQW laser structures. LPE regrowth places some limitations on the structure. It cannot have a p^+-GaAs contact layer or regrowth will occur on top of the lasing structure. The best structure for low threshold current would have doping in the GRIN SCH structure for efficient carrier injection; however, when the p-side of the GRIN SCH was doped with Be, LPE regrowth destroyed the lasers. Be (discussed in Section 3.4) diffuses significantly at the temperature (~800°C) at which LPE growth is normally carried out. The problem was, therefore, attributed to Be diffusion past the SQW, which would move the active region to somewhere in the n-side of the GRIN SCH or the N-cladding layer, creating an inefficient laser structure. GRIN SCH SQW structures which were buried successfully had no Be doping in the GRIN SCH region. Since this should result in less efficient carrier injection in the planar material, wide contact stripe lasers fabricated from this material could not be expected to have as low a threshold current density as ones with better doping in the GRIN SCH.

All of the MBE material discussed here was grown in a Riber 2300 R & D MBE system. Substrate temperature during growth was measured with an optical

pyrometer. To achieve the best quality layers possible GaAs buffer layers were grown at ~600-620°C and the lasing structures were grown at ~720°C. The arsenic source was As_4.

BH lasers described here resulted from two different MBE growths. For MBE growth #1 the following layers (Figure 4.3) were grown on an n^+-GaAs (100) substrate: a 0.5 μm n^+-GaAs buffer layer, an n-doped 0.1 μm superlattice buffer layer (five periods of 100 Å GaAs and 100 Å $Al_{0.5}Ga_{0.5}As$), a 1.5 μm n-$Al_{0.5}Ga_{0.5}As$ cladding layer, a 0.2 μm parabolically graded n^--$Al_xGa_{1-x}As$ layer (x=0.5-0.2), a 100 Å undoped GaAs QW, a 0.2 μm parabolically graded undoped $Al_xGa_{1-x}As$ layer (x=0.2-0.5), and a 1.5 μm p-$Al_{0.5}Ga_{0.5}As$ cladding layer. The n-type dopant was Si, which does not diffuse as much as Be, so it could be included in the n-side of the GRIN SCH although its concentration was reduced gradually as the Al concentration decreased. As discussed in Section 3.6, the superlattice buffer layer is included to improve the quality of the "inverted" interface of the QW.[20] Contact stripe lasers 100 μm wide and 450 μm long fabricated from this material had threshold current densities of ~450 A/cm^2 with external differential quantum efficiencies of ~73%.

MBE Growth #2 was similar to growth #1, but the n^+-GaAs buffer layer was increased to a thickness of 1 μm, a graded 0.2 μm $Al_xGa_{1-x}As$ (x =0.2-0.5) buffer layer was introduced between the n^+-GaAs buffer layer and the superlattice buffer layer, and the QW was 70 Å thick. The thicker n^+-GaAs buffer layer and the graded buffer layer[21] were introduced to further improve the "inverted" interface of the QW. The difference in QW thickness is not expected to result in a change in threshold current[22] (see Section 2.5). Contact stripe lasers 100 μm wide and 500 μm long fabricated from growth #2 had threshold current densities of ~300 A/cm^2 with external differential quantum efficiencies of ~80%. It is not clear that the

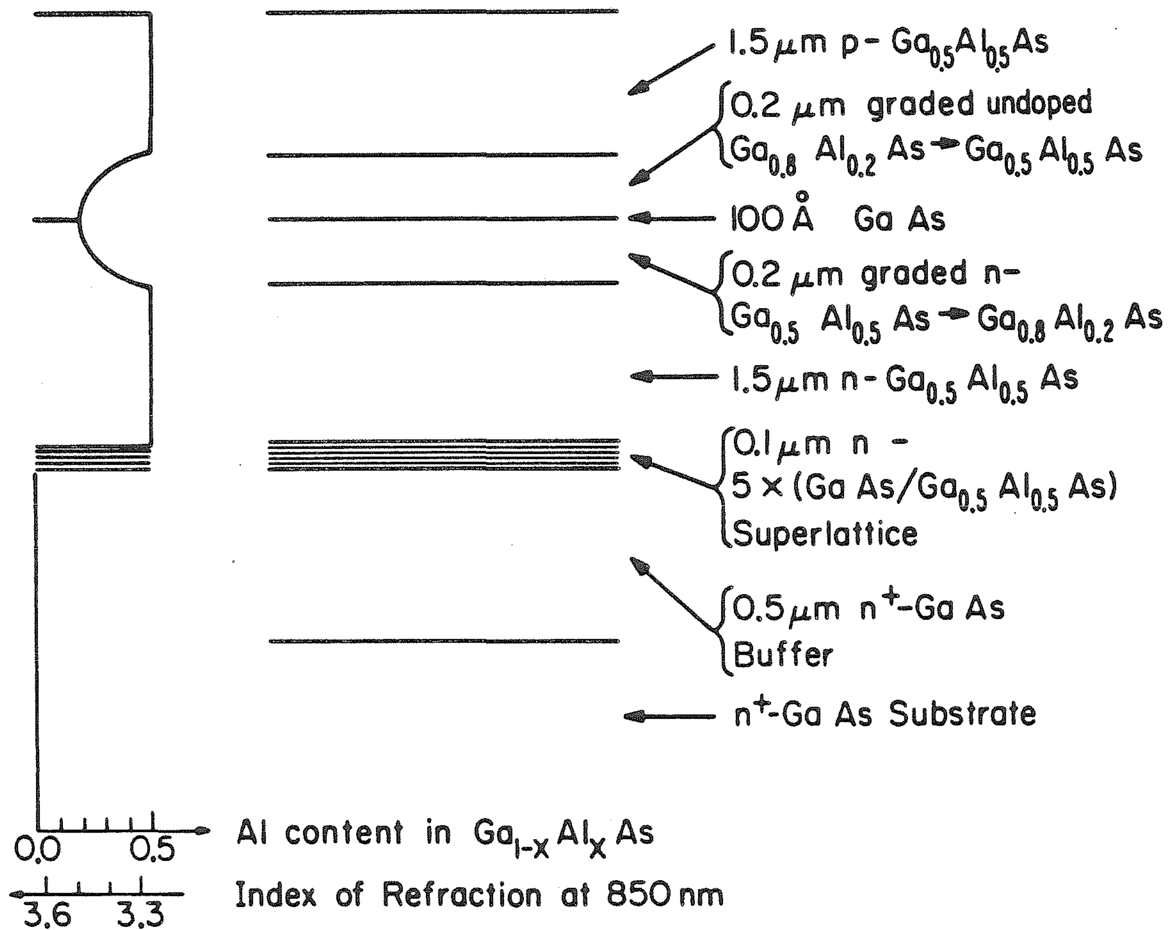

Figure 4.3: Schematic diagram of a GRIN SCH SQW AlGaAs laser showing layers and their indexes of refraction.

improvement in growth #2 as compared to growth #1 can be contributed to the added buffer layers, since the arsenic flux for growth #2 was more optimal (lower). As discussed in Section 3.3, too much As_4 flux can cause Ga vacancies, which would result in a higher threshold current. Also, the growths were made six months apart, which could introduce further unintentional variation in the growth conditions.

4.3 LPE Regrowth

To prepare for LPE regrowth, photoresist stripes oriented in the [011] direction were formed on the planar GRIN SCH SQW wafer. The material around the stripes was chemically etched in a solution of phosphoric acid, hydrogen peroxide, and water (1:2:3), deeply enough to reach n^+-GaAs. Wet chemical etching on stripes in the [011] direction typically produces a dovetail shape (as drawn in Figure 4.2); therefore the stripe width at the active region is less than that at the top of the mesa. For MBE growth #1 the etched mesa stripe width was ~2 μm at the top of the mesa and ~1 μm at the active region, while for MBE growth #2 the stripe width was ~5 μm at the top and ~4 μm at the active region. The photoresist was removed, leaving the mesa stripes of the GRIN SCH SQW material, where it had been. Just before LPE growth the wafer was cleaned, primarily by a dip etch in 3:1:1 (sulfuric acid, hydrogen peroxide, and water). This cleaning step is important for removing impurities on the surface of the wafer which could result in inferior growth. A ~1 μm p-$Al_{0.3}Ga_{0.7}As$ layer doped with Ge and a ~3 μm n-$Al_{0.3}Ga_{0.7}As$ layer doped with Sn were regrown by LPE (see Figure 4.2).

LPE is normally performed at ~800°C, but for a MBE growth #1 wafer, it was found that LPE regrowth at this temperature resulted in very poor lasers. When the LPE regrowth temperature was reduced to 710°C much better results were obtained for MBE growth #1. The poor results at 800°C are attributed to

Be diffusion from the MBE grown p-$Al_{0.5}Ga_{0.5}As$ cladding layer into or past the QW. For these regrowths, the wafer was held at the LPE growth temperature for an approximately two hour long bake plus the actual growth time (around 15-20 minutes at 800°C). For a MBE growth #2 wafer, however, the LPE regrowth was successfully performed at 800°C. For this regrowth the bake time was reduced to ~1.5 hours. The reduction in bake time could be the change which allowed growth at 800°C, since there was less time for Be diffusion. Another possibility is that a small unintentional downward variation in Be concentration occurred between MBE growth #1 and MBE growth #2, since they were grown six months apart. It is preferable to perform the LPE regrowth at the more optimal temperature of 800°C if possible. The optimal temperature for LPE growth of AlGaAs is that at which As is dissolved well in the Ga melt and defects are minimized.[23] It would be interesting to perform a detailed study on the optimal LPE regrowth conditions, i.e., bake time, and optimal Be concentration for the best buried heterostructure GRIN SCH SQWs. It is difficult to draw definite conclusions from the results presented here because too many variables are involved.

After regrowth, the regrown layers were masked with SiO_2, and Zn was diffused into the p-$Al_{0.5}Ga_{0.5}As$ cladding layer of the buried stripes to facilitate formation of an ohmic contact on the p-doped side of the devices. Ohmic contacts were applied to both the p- and n-sides of the devices. Electrical contact on the p-side of the devices was restricted to the opening in the SiO_2. Zn diffusion using as a mask the SiO_2, which will later act as an insulating barrier between the p-metallic contact and regions outside of the buried stripe, is an important step. It insures that the semiconductor material in electrical contact with the p-metallic contact is p-type even if the SiO_2 is slightly misaligned.

For cw operation single laser diodes (separated by cleaving) were indium sol-

dered p-side up to gold coated copper mounts which act as heat sinks. Electrical contact to the p-side of the devices was made with a probe or by ball bonding gold wire to the surface of the p-metallic contact.

4.4 Leakage Current

On the basis of Figure 4.2, in which the regrown reverse biased junction lines up perfectly with the QW, one might expect that the leakage current of BH SQWs would be insignificant. While the leakage current can be expected to be much smaller than that of many stripe structures, for a very narrow stripe ($\sim 1\ \mu$m) the leakage current of a BH laser is not insignificant. For a device like that in Figure 4.2 the only leakage current path is through the reverse biased junction. However LPE growth does not have the uniformity and control necessary to fabricate the ideal structure of Figure 4.2 reproducibly. In fact, across one regrown wafer one can expect variation substantial enough to produce both lasers like that diagrammed in Figure 4.4a and that in Figure 4.4b.

These variations in the regrowth create leakage current paths around the reverse biased junction. As diagrammed in Figure 4.4a, if the LPE regrown p-$Al_{0.3}Ga_{0.7}As$ is too thin, a current path results from the p-$Al_{0.5}Ga_{0.5}As$ cladding layer through the regrown n-$Al_{0.3}Ga_{0.7}As$ layer and the n-$Al_{0.5}Ga_{0.5}As$ cladding layer to n^{+}-GaAs, which avoids the QW (active region). Similarly, as diagrammed by Figure 4.4b, if the LPE regrown p-$Al_{0.3}Ga_{0.7}As$ is too thick a current path exists from the p-$Al_{0.5}Ga_{0.5}As$ cladding layer through the regrown p-$Al_{0.3}Ga_{0.7}As$ cladding layer directly to n^{+}-GaAs (or to n^{+}-GaAs via the n-$Al_{0.5}Ga_{0.5}As$ cladding layer).

Even the ideal structure of Figure 4.2 will have leakage current. Leakage current through reverse biased barriers of semiconductor layers has been considered by Namizaki et al.[24] and Dutta et al.[25] Assuming the p-type metallic contact only

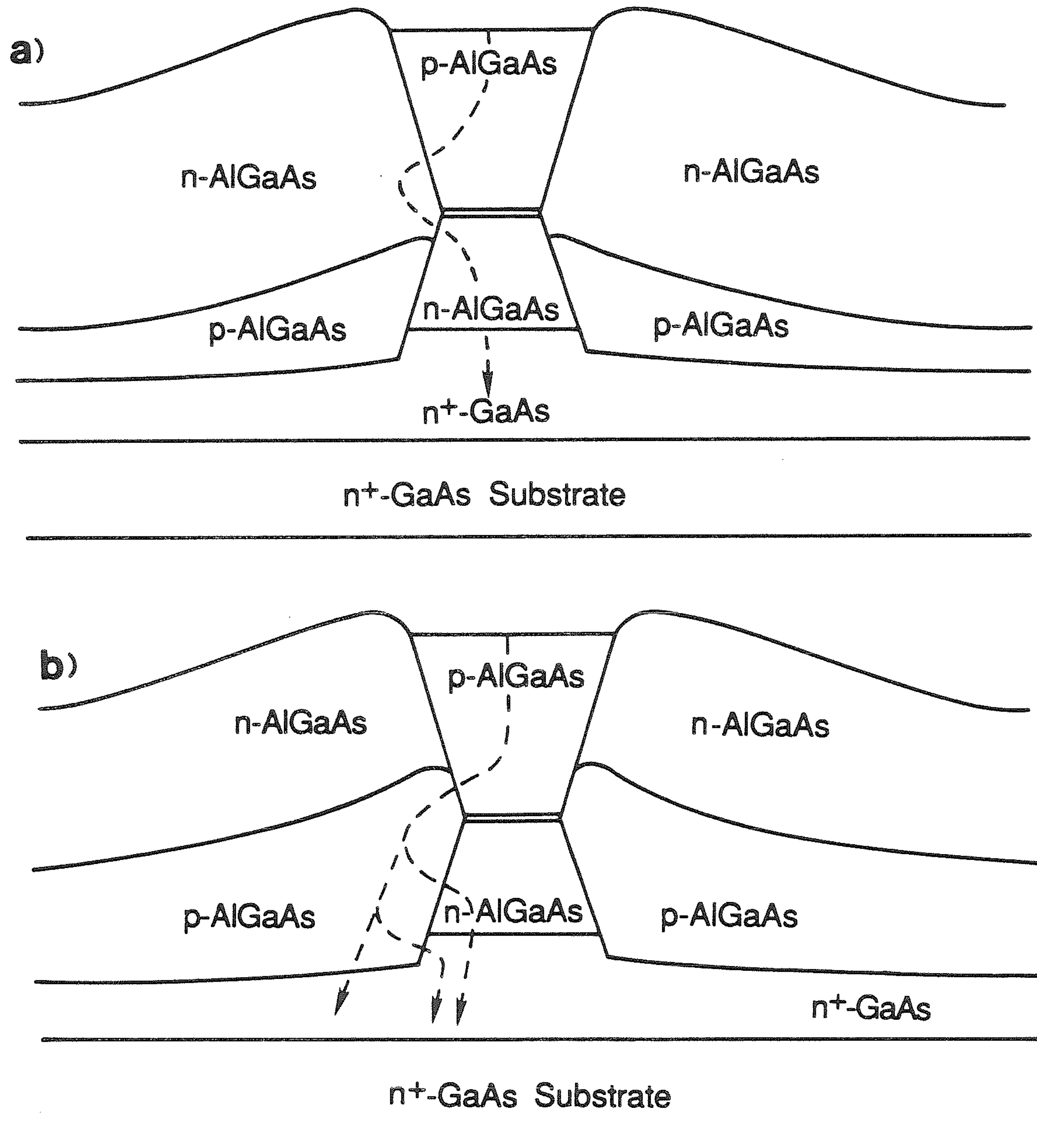

Figure 4.4: Schematic diagram of a buried heterostructure GRIN SCH SQW AlGaAs laser showing leakage current paths around the QW created by (a) a thin LPE regrown p-$Al_{0.3}Ga_{0.7}As$ layer and (b) a thick LPE regrown p-$Al_{0.3}Ga_{0.7}As$ layer.

contacts the p-$Al_{0.5}Ga_{0.5}As$ layer, the current path through the reverse biased junction is from the p-cladding layer through the n-regrown layer and the p-regrown layer to n^+-GaAs (or to n^+-GaAs through the n-cladding layer). This p-n-p-n path is a thyristor. (For a discussion of thyristors see Sze.[26]) As illustrated in Figure 4.5 a thyristor can be modeled as two connected transistors, a p-n-p transistor and a n-p-n transistor, which share the middle p and n layers.

As illustrated in Figure 4.6 at low voltages a thyristor has an OFF state with high impedance in which very little current flows; in this case the reverse biased junction works as intended. However when the forward breakover voltage V_{BF} (at which $dV/dI = 0$) is reached the thyristor goes through a negative resistance region after which it reaches an ON state with low impedance and high current flow. This is possible because a thyristor contains two forward biased junctions and only one reverse biased junction. At low voltages the reverse biased junction prevents current flow. In the ON state the middle n and p layers act like an insulating layer or in other words the n-p-n transistor of the two transistor model is saturated. In the ON state the whole thyristor therefore acts like a p^+-i-n^+ diode,[26] which allows current to flow.

If a semiconductor laser with an n-p-n-p blocking layer could be fabricated it would have much less leakage current, because that structure has two reverse biased junctions and only one forward biased junction. However, the laser diode must be forward biased, which means the first layer must be the p-cladding layer, so it is difficult to imagine a structure which could have an n-p-n-p blocking layer.

A thyristor can be turned on by an increase in voltage or an increase in temperature. The effect of temperature on a thyristor explains the poor temperature characteristics which have been observed for BH lasers.[24] If the intermediate p-layer or n-layer has an external electrical connection, an increase in current through this

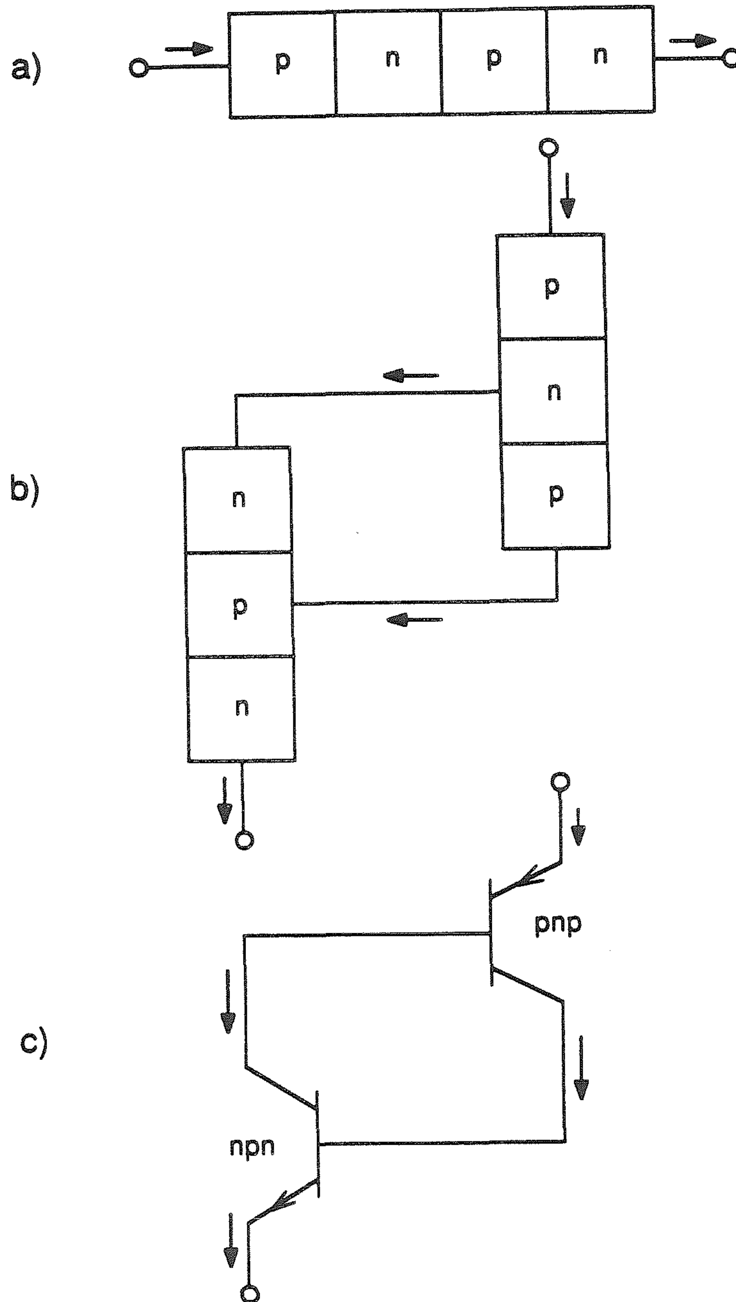

Figure 4.5: Schematic diagram of (a) a thyristor (b) the two transistor model of a thyristor (c) the two transistor model using transistor notation. The arrows indicate the direction of current flow.

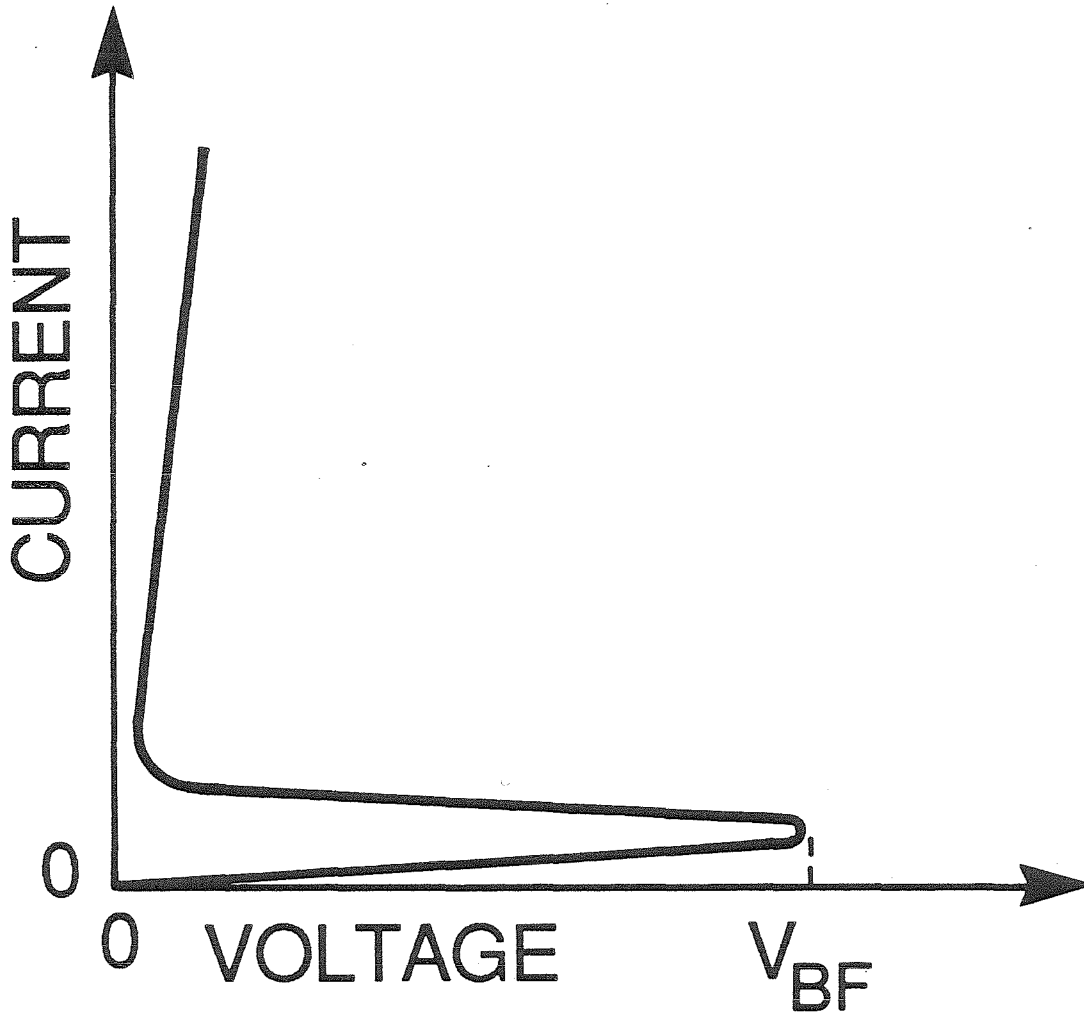

Figure 4.6: Sketch of the forward biased current-voltage characteristics of a thyristor.

connection can also turn on the thyristor.

By realizing that the blocking layers form a thyristor, we can produce equivalent electrical circuit models for the BH lasers diagrammed in Figure 4.2 and Figure 4.4. For the ideal SQW BH of Figure 4.2 the circuit model is that of Figure 4.7a. The thyristor is represented by the two transistors. There are two possible current paths: through the laser diode or through the thyristor. For a thin p-$Al_{0.3}Ga_{0.7}As$ blocking layer (Figure 4.4a), the additional path through the n-$Al_{0.3}Ga_{0.7}As$ around the active region creates a connection to the middle n-layer of the thyristor (Figure 4.7b). For a thick p-$Al_{0.3}Ga_{0.7}As$ blocking layer, the additional path through it around the active region produces a connection to the middle p-layer of the thyristor (Figure 4.7c). It is also possible to have a laser for which the p-$Al_{0.3}Ga_{0.7}As$ layer is too thin on one side of the buried stripe, but too thick on the other side. In that case, both the leakage path modeled by Figure 4.7b and that modeled by Figure 4.7c will exist.

4.5 High Reflectivity End Facet Coatings

There are many materials which could be used as high reflectivity end facet coatings for (Al,Ga)As lasers. Generally the coating is simply evaporated onto the entire cleaved facet by orienting the laser diode so that the facet is perpendicular to the flux of the evaporating material. One might think that the best high reflectivity coating is simply a reflecting metal such as aluminum or silver, but this is not the case. Coatings are generally the last processing step so they are applied after metallic contacts. A conductive coating will make the laser inoperable by shorting the contacts. It is possible to evaporate a dielectric such as Al_2O_3 before the metal to prevent shorting, however, shorting due to pinholes in the dielectric can still occur.[27] In addition, if the laser is soldered to a mount after application of this

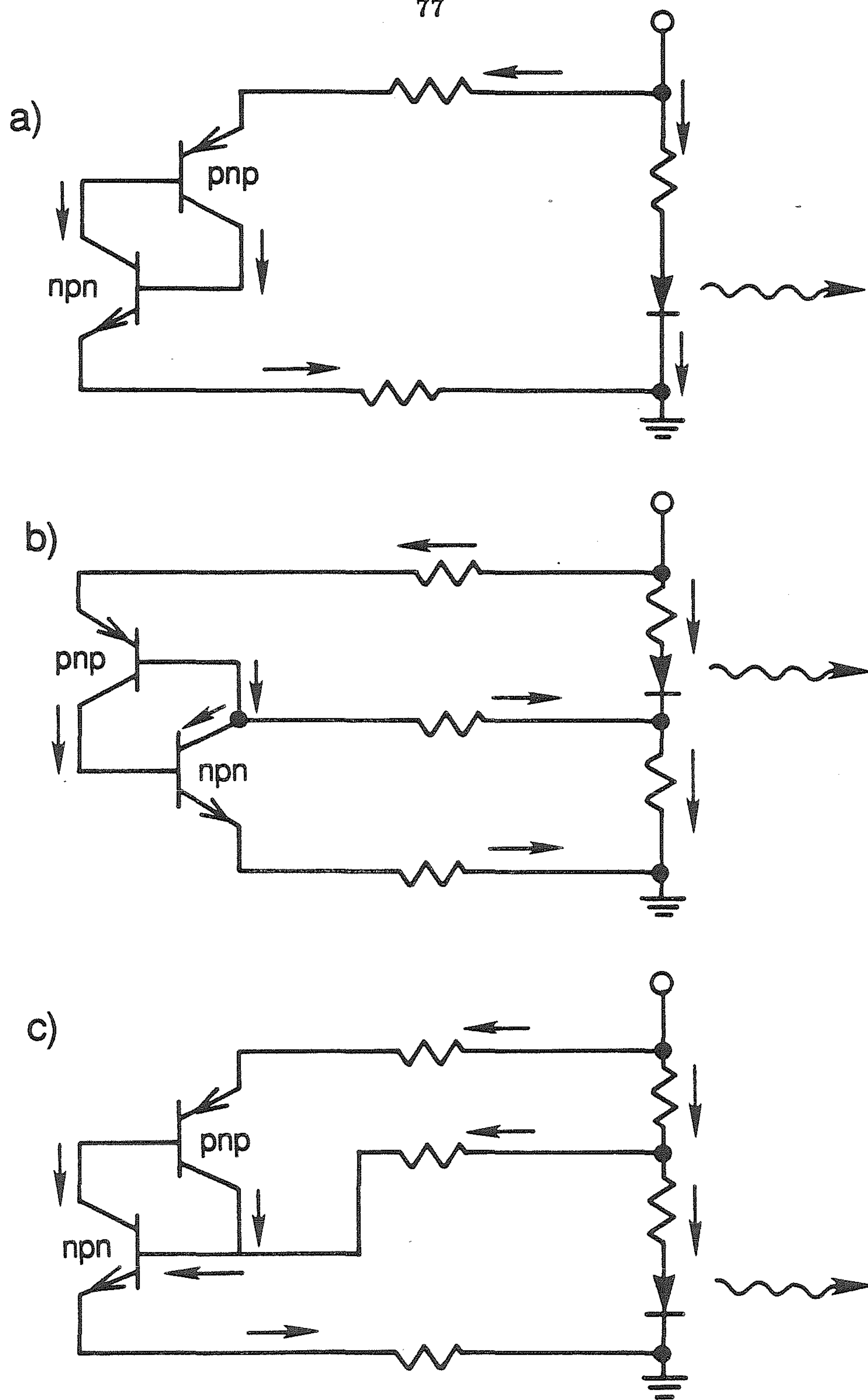

Figure 4.7: Equivalent electrical circuit model for (a) an ideal buried heterostructure GRIN SCH SQW, (b) one with a thin p-$Al_{0.3}Ga_{0.7}As$ blocking layer , and (c) one with a thick p-$Al_{0.3}Ga_{0.7}As$ blocking layer. The arrows indicate the direction of current flow.

coating it is possible to dissolve the metal.

A dielectric quarter-wavelength stack of Al_2O_3 and Si avoids these problems, since it withstands soldering and is insulating since the evaporated Si is amorphous and not intentionally doped. The reflectivity at normal incidence of a dielectric stack of N periods (each period is a $\frac{\lambda}{4n_2}$ layer of Al_2O_3 and a $\frac{\lambda}{4n_3}$ layer of Si, where λ is the wavelength of the lasing mode) from GaAs to air is:[28]

$$R = \left(\frac{1 - (n_4/n_1)(n_2/n_3)^{2N}}{1 + (n_4/n_1)(n_2/n_3)^{2N}} \right)^2 \tag{4.1}$$

where n_1 is the refractive index of GaAs, n_2 is the refractive index of Al_2O_3, n_3 is the refractive index of Si, and n_4 is the refractive index of air. The refractive indices of Al_2O_3 and Si will depend on the evaporation and on the wavelength of the lasing mode. Using values of $n_1 = 3.6$, $n_2 = 1.75$, $n_3 = 3.6$, and $n_4 = 1$, the reflectivity of a one period coating is 77%, with two periods it increases to 94%, and with three periods to 99%.

It is clear that reflectivities as high as those possible with a metallic coating can be achieved with Al_2O_3/Si coatings, although experimental reflectivities are usually less than the calculated values. It is desirable to limit the number of periods in a stack since Si is absorptive in the wavelength range of (Al,Ga)As semiconductor lasers. Significant absorption could cause localized facet heating.[29] A buried heterostructure GRIN SCH SQW typically has a lasing wavelength of ~8400-8500 Å so a $\frac{\lambda}{4n_2}$ layer of Al_2O_3 is ~1200 Å thick and a $\frac{\lambda}{4n_3}$ layer of Si is ~590 Å thick. Since the Si layer is thin, with a two or three period coating the absorption in Si is not significant.[27]

An Al_2O_3/Si coating must be evaporated in an electron beam evaporator instead of a resistance evaporator, because of the high temperature necessary to evaporate Si. Since the refractive indices of Al_2O_3 and Si depend on the evaporation, and the thickness monitor of an evaporator cannot be expected to be extremely

accurate, the proper amount of deposition for high reflectivity must be carefully calibrated for a particular evaporator. When the calibration is good, the coating will look pinkish since the reflectivity peak will be in the infrared, which is invisible to the naked eye. To reach this point the Al_2O_3 and Si must first be calibrated individually. From air a single $\frac{\lambda}{4n}$ coating on a substrate with a higher index of refraction (than the layer) will have a reflectivity minimum for light of wavelength λ at normal incidence. If the reflectivity of the substrate is smaller than that of the coating, light of wavelength λ at normal incidence will have a reflectivity maximum.[28]

Calibration of the proper evaporator setting for the Al_2O_3 layer can be accomplished by evaporating ~1200 Å of Al_2O_3 on a GaAs wafer. The reflectivity spectrum at normal incidence of the coating can then be examined with the setup diagramed in Figure 4.8. To compensate for a nonuniform white light source a mirror with a known reflectivity spectrum should be placed in the same position as the sample; the reflectivity spectrum of the sample can then be corrected. The reflectivity minimum (since $n_2 < n_1$) of the Al_2O_3 coated GaAs sample can then be found and the amount of Al_2O_3 evaporated can be adjusted to produce a minimum at the appropriate wavelength.

Calibration of a Si coating on a GaAs wafer is more complicated because the refractive indices of Si and GaAs are so close. It is not clear whether to look for a reflectivity minimum or a maximum, since the refractive index of Si could be either less or more than that of GaAs. It is preferable to calibrate Si coatings on substrates of other materials, which have a more dissimilar refractive index.

After the individual layer thicknesses of Al_2O_3 and Si are calibrated, multilayer coatings can be fabricated. If a multilayer coating evaporated on an end facet of a laser is also evaporated on a piece of GaAs wafer, the reflectivity can be checked

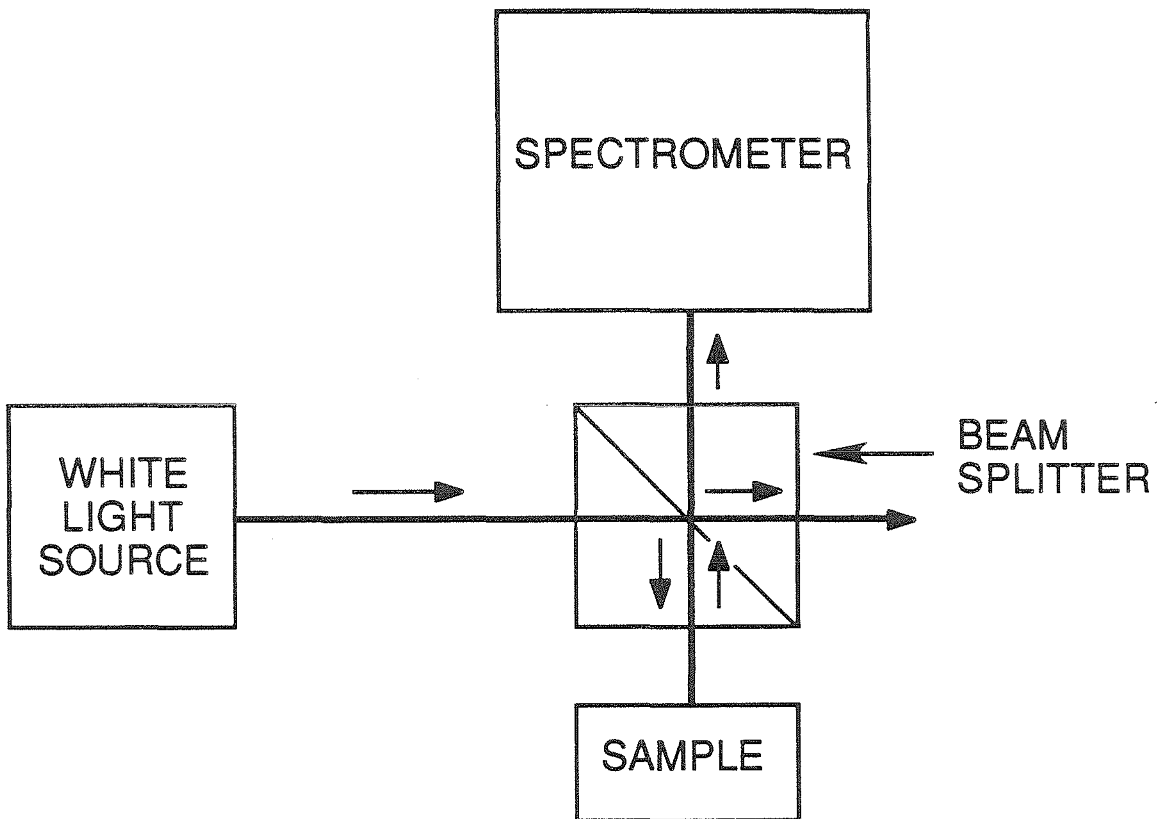

Figure 4.8: Schematic diagram of optical setup for calibration of high reflectivity coatings.

using the setup illustrated in Figure 4.8. For absolute reflectivity measurement, the reflectivity spectrum of the coating can be compared with that of a mirror of known reflectivity. It is better, however, to test the coating which was actually evaporated on the laser since: (1) changes may be introduced in the alignment of the optical setup when the samples are switched; (2) the coating on the laser may be slightly different from that on the the GaAs wafer, since they cannot be placed at exactly the same spot in the evaporator; and (3) the lasing wavelength will vary slightly for different lasers.

The reflectivity of a coating on the end facet of a laser can be determined by examining the ratio of the power output (P_1 and P_2) from the two ends of the laser. When the reflectivities R_1 and R_2 have different values, P_1 and P_2 will of course have different values. When the stimulated emission power is much greater than the spontaneous emission power the ratio of P_1/P_2 is:[30]

$$\frac{P_1}{P_2} = \frac{(1 - R_1)\sqrt{R_2}}{(1 - R_2)\sqrt{R_1}} \tag{4.2}$$

In another form Equation (4.2) becomes

$$R_2^2 - R_2\left(2 + \frac{(1 - R_1)^2}{R_1}\frac{P_2^2}{P_1^2}\right) + 1 = 0 \tag{4.3}$$

If the ratio of P_1/P_2 is measured and R_1 is known, R_2 can be solved for. Setting

$$F = \frac{(1 - R_1)}{\sqrt{R_1}}\frac{P_2}{P_1} \tag{4.4}$$

$$R_2 = 1 + \frac{F^2}{2} - F\sqrt{1 + \frac{F^2}{4}} \tag{4.5}$$

If R_1 is the reflectivity of an uncoated facet, it is ~31%. If both end facets are to be coated, the reflectivity of the first coating must be measured before the second coating is applied, if the reflectivity is to be measured in this manner.

The total η_{ext} is the sum of η_{ext}^1 and η_{ext}^2, which are the external differential quantum efficiencies from each facet. Note that the ratio of η_{ext}^1 to η_{ext}^2 is equal to P_1/P_2, which is given by the right hand side of Equation (4.2). When the facet reflectivity is increased, the external differential quantum efficiency at that facet will decrease. With high reflectivity coatings on both facets, η_{ext} can be expected to decrease significantly. This is an important point, since the amount of power required for a particular application could limit the facet reflectivity that could be used. The optimal reflectivity coating will, therefore, depend on the requirements of a particular application. In general, there will be a trade off between low threshold and high power. For the application of optical interconnects over short distances in an optical supercomputer, high power is not required, so this is not a significant limitation for that application.

4.6 Threshold Current Results

Cw threshold currents for 1 μm wide stripe lasers from MBE growth #1 (100 Å SQWs) were measured at room temperature for a variety of laser cavity lengths and facet reflectivities. Table 4.1 summarizes data for two 250 μm long lasers. Figure 4.9 shows the light output versus current curves for laser A of Table 4.1 before and after application of high reflectivity coatings. The results show that the predictions of a dramatic reduction in threshold current I_{th} with application of high reflectivity coatings are borne out by experimental results. For these 250 μm long lasers, application of ~70% reflectivity coatings on both facets reduces threshold current by a factor of more than three. Surprisingly, however, this result was achieved with very little reduction in η_{ext}.

It is of interest to try to interpret these results and predict what results can be expected for other cavity lengths and facet reflectivities. The threshold current

Laser A

R_1	R_2	$\frac{1}{2L}\ln\frac{1}{R_1R_2}$	I_{th}	η_{ext}	α_i	η_i
31%	31%	46.8 cm^{-1}	3.3 mA	0.62	2.3 cm^{-1}	0.65
31%	67%	31.4 cm^{-1}	1.6 mA	0.62	4.8 cm^{-1}	0.71
71%	67%	14.9 cm^{-1}	0.95 mA	0.56	12.3 cm^{-1}	1.0

Laser B

R_1	R_2	$\frac{1}{2L}\ln\frac{1}{R_1R_2}$	I_{th}	η_{ext}	α_i	η_i
31%	31%	46.8 cm^{-1}	4.3 mA	0.55	6.9 cm^{-1}	0.63
31%	67%	31.4 cm^{-1}	1.95 mA	0.58	8.3 cm^{-1}	0.73
71%	67%	14.9 cm^{-1}	1.15 mA	0.52	15.5 cm^{-1}	1.0

Table 4.1: Threshold characteristics for 250 μm long 1 μm wide buried GRIN SCH 100 Å SQW (Al,Ga)As lasers at room temperature.

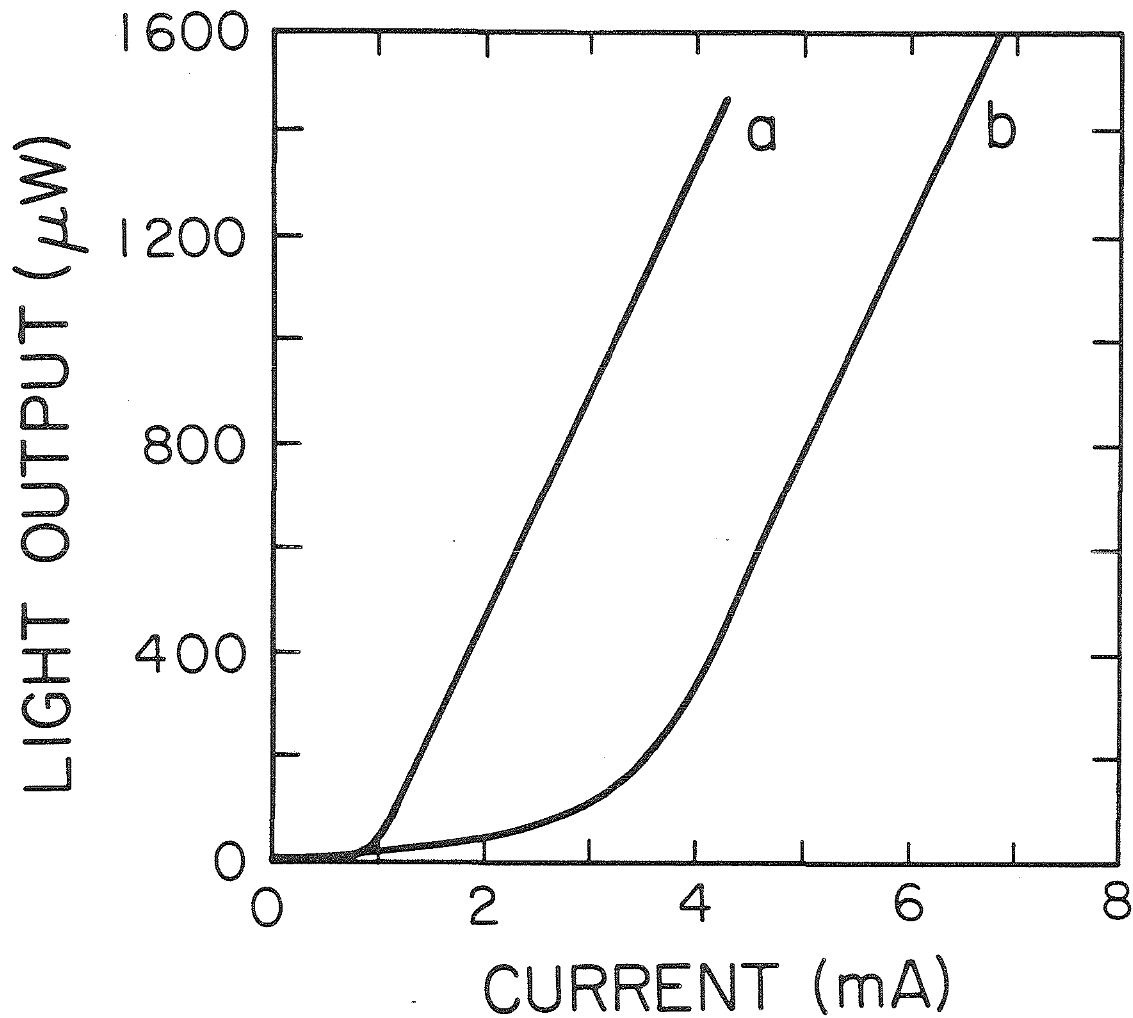

Figure 4.9: Light output vs. current for a 250 μm long 1 μm wide buried GRIN SCH 100 Å SQW (Al,Ga)As laser with (a) ~70% high reflectivity coated end facets and (b) uncoated end facets. Both curves are for the *same* laser.

is determined by the modal threshold gain:

$$g_{th} = \alpha_i + \frac{1}{2L}\ln\frac{1}{R_1 R_2} \tag{4.6}$$

The length and facet reflectivities are known, but the internal loss α_i must be calculated. If the threshold current is converted into threshold current density J_{th}, the threshold gain can be estimated from the calculations of Chapter 2 (see Figure 2.3). An estimate of α_i can then be reached by subtracting the end loss from g_{th}. $J_{th} = I_{th}/(LW)$ where W is the stripe width through which the current flows. W depends on how much leakage current is present. For simplicity in the calculations W is taken as 2 μm. In doing so it is assumed that the leakage current is always half of the total current. Note that this assumption is a reasonable approximation only if the thyristor leakage path is either always ON, always OFF, or an insignificant fraction of the leakage current because a large leakage current, through one of the paths diagrammed in Figure 4.4, dominates. With this assumption, the calculated value of α_i (see Table 4.1) appears to increase when the laser facets are coated.

Since α_i is small for wide QW stripe lasers[1], a large portion of α_i in the narrow buried lasers is expected to be waveguide loss at the buried interface. One would normally expect α_i to be approximately constant for a particular laser. It is, however, possible that the change in α_i is real and is due to gradual degradation in the lasers over time. This possibility is supported by the experimental results for MBE growth #1 since both the uncoated and coated BH lasers from growth #1 showed threshold current increases within a few hours of operation and generally had short lifetimes. This type of degradation can be attributed to darkline defects,[31] which are believed to grow from defects in the laser structure. Defects due to aluminum oxide[32] at the interface of the regrown LPE material with the AlGaAs layers of the lasing stripe can be expected. BH stripe lasers generally have lower yields and poorer reliability than some other stripe laser structures because of this

problem.[33] This problem could be expected to be especially bad in the regrown MBE growth #1 lasers, because the regrowth was performed at the nonoptimal temperature of 710°C and the lasing stripe is very narrow, which would lead to greater domination of waveguide defects than would occur in a wider stripe. In fact the wider (~4 μm) stripe lasers regrown at 800°C from MBE growth #2 had much improved degradation characteristics.

Another possibility is that the change in α_i is not real and is due to inaccuracy in the calculations. Error in the calculated gain curve (Figure 2.3) is quite possible, since the quantized energy levels of the QW were approximated with those of an infinitely deep well, rigorous k-selection was assumed, and a Lorentzian lineshape function was used to account for intraband relaxations. In a real laser one might actually expect partial k-selection, since a finite relaxation time allows a range of wavevectors to be involved in a transition.[34] Partial k-selection is difficult to model accurately in calculations; most gain calculations have assumed rigorous k-selection. A few authors[34,35] have made calculations with no k-selection. These calculations were, however, simplistic in that they did not include a lineshape function to model intraband relaxations. It is therefore difficult to compare the results with other calculations, which do account for intraband relaxations. They do not, however, suggest that with no k-selection, the calculated maximum value of the gain would be significantly changed; they do show a change in the shape of the gain profile.

Some lineshape broadening function is required to account for intraband relaxations. Recent theorectical work[36] has suggested that the Lorentzian lineshape function is inaccurate and causes the gain to be underestimated. This sort of error in the calculations could cause the calculated gain to saturate at too low a value. In that case the gain in the uncoated devices could be larger than that calculated. This would make α_i larger for the uncoated lasers, which could result in more constant

values of α_i.

Another possibility is that the leakage current assumptions made are in error; however, that would not cause change in α_i in the observed direction. If the thyristor leakage path were ON in the uncoated devices and OFF in the coated devices, a constant leakage current assumption would cause an apparent *decrease* in α_i instead of an *increase* for the coated devices. Note, however, that if the thyristor leakage current went from ON to OFF, it would cause an increase in η_i, since η_i is a measure of how many of the injected carriers are converted to photons. Using the calculated values of α_i η_i (from Equation (4.2)) in the coated devices appears to be larger than that in the uncoated devices, which suggests that this is the case. These points will be considered further after discussion of more experimental results.

Using the average value of α_i (8.4 cm^{-1}) from the results in Table 4.1, threshold current estimates for various laser cavity lengths and facet reflectivities can be made. This is the opposite calculation from that to find α_i. g_{th} is calculated, J_{th} is predicted from the calculations graphed in Figure 2.3, and I_{th} is estimated to be LWJ_{th}. The results of these calculations are graphed in Figures 4.10 and 4.11 along with experimental data points. In spite of the potential sources of inaccuracy the calculations explain threshold current trends.

Figure 4.10 shows that the threshold current increases dramatically for lasers with large end losses, i.e., short uncoated lasers, because they operate in the region in which the gain versus current curve (Figure 2.3) flattens out due to saturation of the first quantized energy level. The most dramatic reduction in threshold current and lowest absolute threshold currents can be achieved when high reflectivity coatings are applied to these short lasers (see Figure 4.11). Experimentally, a 120 μm long laser had a 5.5 mA threshold current, which was reduced to 0.55 mA when $\sim$80% reflectivity coatings were applied to both facets (see Figure 4.12). This is

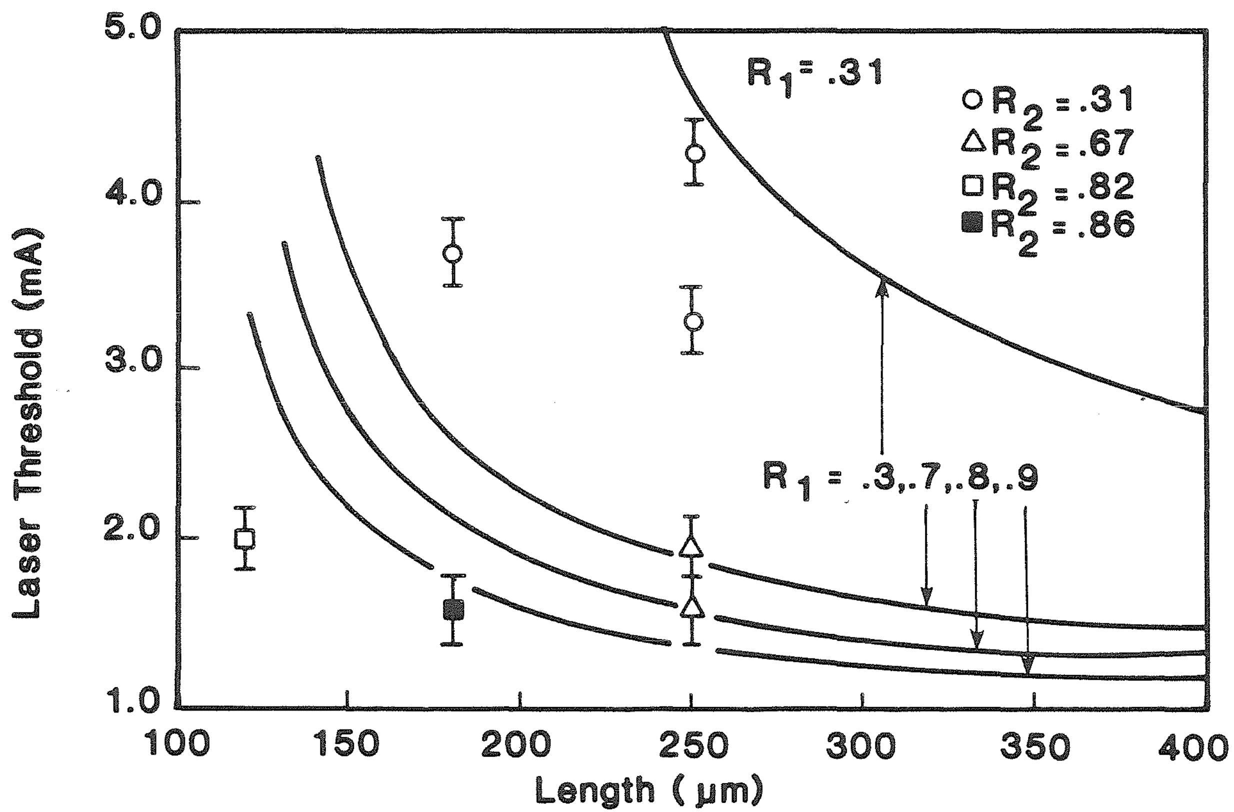

Figure 4.10: Calculated threshold current for ~1 μm stripe buried GRIN SCH 100 Å SQW (Al,Ga)As lasers with R_1= 31%, various cavity lengths, and various values of R_2.

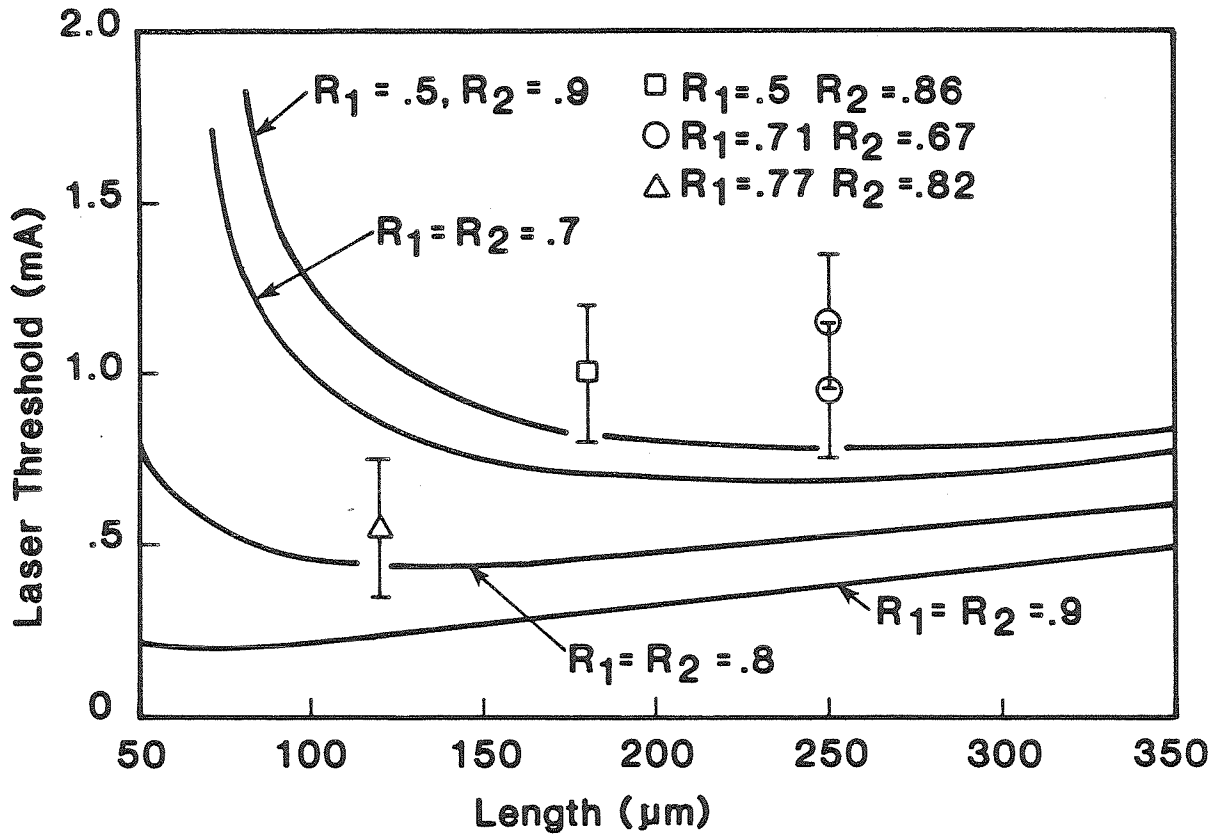

Figure 4.11: Calculated threshold current for ~1 μm stripe buried GRIN SCH 100 Å SQW (Al,Ga)As lasers with various cavity lengths and high reflectivity coatings on both facets.

believed to be the lowest threshold current so far reported for any semiconductor laser at room temperature. Still lower threshold currents should be achieved for slightly shorter lasers with 90% reflectivity coatings. The calculations suggest that the lowest threshold current that could be achieved in this manner would be ~0.2-0.3 mA.

Threshold currents for 250 μm long, 4 μm wide buried lasers from MBE growth #2 were also examined. Results for two lasers with and without high reflectivity coatings are given in Table 4.2. Note that with ~90% reflectivity coatings on both end facets the threshold was reduced by only a factor of approximately two, while η_{ext} is reduced significantly, as is expected theoretically. Compare these results with those of the 250 μm long 1 μm wide lasers (Table 4.1). The narrow stripe lasers had a more substantial threshold reduction with only ~70% reflectivity coatings. For the wider stripe lasers, leakage current is expected to be a much less significant factor; the difference can, therefore, be attributed to leakage current in the narrower lasers. If the thyristor leakage path is ON in the uncoated narrow devices and OFF in the coated narrow devices, it could contribute significantly to the observed reduction in threshold current and reduce the effect of high reflectivity coatings on the external quantum efficiency. In the wider stripe lasers, however, the leakage current is relatively small, so any nonlinear change in leakage current would not have as significant an effect on the properties of the lasers. As discussed earlier, this change in leakage current for the narrower stripe lasers would tend to cause an apparent *decrease* in α_i for the coated lasers when a constant leakage current was assumed. Since the opposite was observed, the results suggest either error in the calculation of the gain curve or a real significant increase in α_i.

A real increase in α_i for the narrow lasers is possible, because of their poor lifetime characteristics, but it is unlikely in the wider stripe lasers since they had

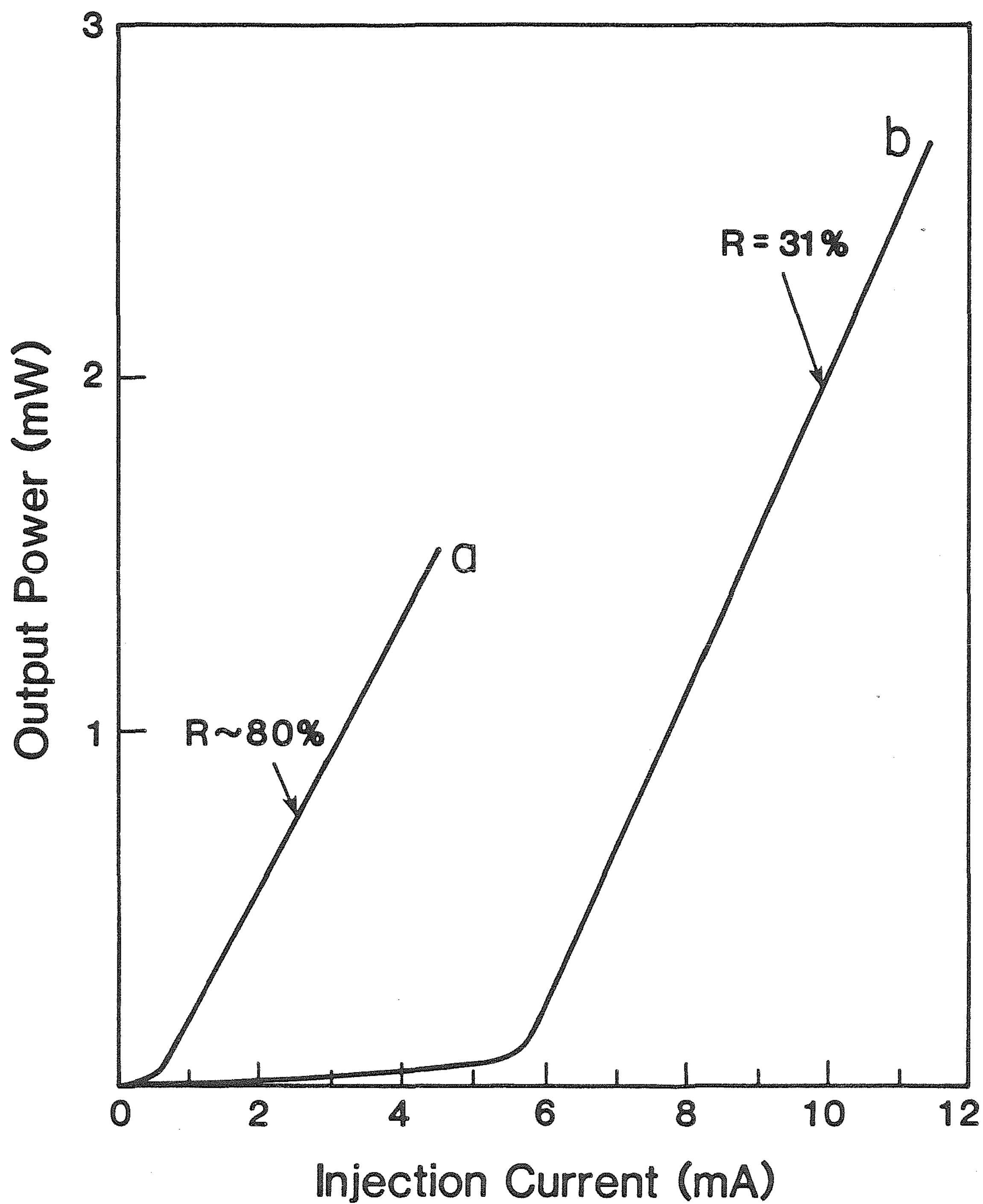

Figure 4.12: Light output vs. current for a 120 μm long 1 μm wide buried GRIN SCH 100 Å SQW (Al,Ga)As laser with (a) ~80% high reflectivity coated end facets and (b) uncoated end facets. Both curves are for the *same* laser.

Laser A

R_1	R_2	$\frac{1}{2L}\ln\frac{1}{R_1R_2}$	I_{th}	η_{ext}
31%	31%	46.8 cm^{-1}	7.3 mA	0.75
31%	93%	24.9 cm^{-1}	5.1 mA	0.50
85%	93%	4.7 cm^{-1}	3.8 mA	0.32

Laser B

R_1	R_2	$\frac{1}{2L}\ln\frac{1}{R_1R_2}$	I_{th}	η_{ext}
31%	31%	46.8 cm^{-1}	6.6 mA	0.80
31%	92%	25.1 cm^{-1}	4.6 mA	0.55
92%	92%	3.3 cm^{-1}	2.9 mA	0.41

Table 4.2: Threshold characteristics for 250 μm long 4 μm wide buried GRIN SCH 70 Å SQW (Al,Ga)As lasers at room temperature.

much more stable operation over time. It is, however, impossible to fit the numerical results for the wider stripe lasers to the calculations unless a very large increase in α_i is assumed when the facets are coated. This suggests that the gain calculations are too inaccurate for a numerical fit. If the gain versus current density curve (Figure 2.3) had a steeper slope and saturated at a higher value of gain, it should be possible to fit the numerical results to it. Measurements of gain by K. Y. Lau[37] indicate that the real gain curve for the narrow stripe lasers does have these characteristics.

A parameter in the gain calculations which could be adjusted is the intraband relaxation time τ_{in}. It is found, however, that varying it produces little change in the gain curve. For the calculations described in Chapter 2 τ_{in} is taken as 0.2 psec, which is the maximum value at which it has been measured.[38,39,40] Using a lower value of τ_{in} reduces the calculated gain (see Figure 4.13). Using a value of τ_{in} slightly larger than the measured values does not increase the gain enough to fit the measured results. Unless τ_{in} is huge compared to its measured values, changing it cannot remove this discrepancy.

Recent theoretical work by Yamanishi and Lee[36] suggests that using a Lorentzian lineshape function to account for intraband relaxations is inaccurate because the Lorentzian lineshape is too broad. Using it causes transitions far away from the lasing transition to contribute to the calculated gain. Yamanishi and Lee show that using a narrower lineshape function results in larger calculated gains. The experimental results reported here appear to support this theoretical conclusion. (The results reported in Chapter 6 also support it.) The Lorentzian lineshape function has become the established method for accounting for intraband relaxations in QW lasers[41,42,43,44,45] so possible inaccuracy inherent in this method and possible alternative lineshape functions certainly deserve further investigation. As mentioned earlier, there are other possible sources of inaccuracy in the calculations

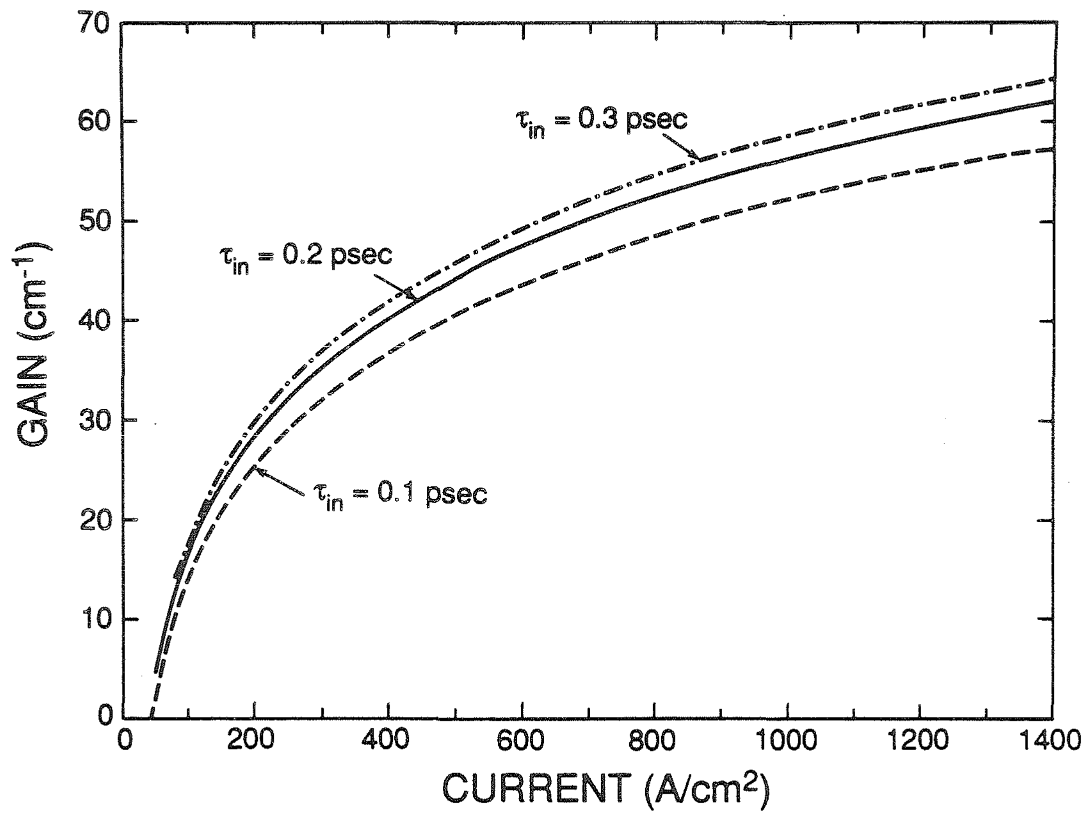

Figure 4.13: Calculated modal gain as a function of current density for a 100 Å SQW with intraband relaxation times of 0.1, 0.2, and 0.3 psec.

that could also contribute to the observed error.

The discussion here should not be taken as refuting the basic shape of the calculated gain curve or the basic premise that high reflectivity coatings have a large effect on the threshold current of a QW laser. It appears, however, that the effect on narrow BH lasers is enhanced because of the nonlinear leakage current characteristics of the thyristor leakage path through the burying layers of the lasers. It is, therefore, possible that less dramatic threshold reduction would be obtained if a different narrow stripe structure were employed.

4.7 Steps for Improvement

Although very low threshold currents were achieved for the 1 μm wide stripe buried heterostructure GRIN SCH 100 Å SQW (Al,Ga)As lasers with high reflectivity coatings, it should be possible to reach even lower threshold currents. It is likely that a substantial portion of the current, even in the coated lasers, is leakage current. If this leakage current could be reduced lower threshold currents should result. With LPE regrowth, the lack of uniformity and control makes it virtually impossible to avoid the leakage paths illustrated in Figure 4.4. With more uniform and controlled growths, the probability of reducing the leakage through these paths would be increased. Since current through one of these paths could turn on the thyristor leakage path, this would have the added advantage of making it easier to reach the OFF state of the thyristor.

One way to achieve this would be an MBE regrowth instead of an LPE regrowth. This MBE regrowth, however, would not be easy to accomplish. The normal MBE cleaning process would etch away the mesa to be buried. Reducing the cleaning would increase the probability of impurities and defects which would result in inferior growth. Another potential problem would be achieving quality

growth against the sides of the mesa. The overhang on a dovetail-shaped mesa could shadow the walls of the mesa from the evaporation material fluxes. This would result in inferior growth or an actual space next to the mesa. These problems with MBE growth against a mesa have been observed experimentally.[46,47] As already discussed, defects at the interface will tend to cause unreliable lasers. This problem could possibly be solved by a bromine/methanol polish, which would remove some of the overhang.[7] Another solution would be to orient the lasers in the $[0\bar{1}1]$ direction instead of the [011] direction. Mesa stripes oriented along the $[0\bar{1}1]$ direction have a triangular shape, which is oriented with the base of the triangle towards the substrate with no overhang. It might be more difficult to contact an narrow stripe oriented in this direction, since more of the P-cladding layer would be etched away.

Once these problems were solved, the processing of the buried lasers would be more complicated than that of those formed with LPE regrowth, because regrowth would occur on top of the buried mesa. This material would have to be etched away carefully. One way to simplify this step would be to mask the top of the mesa with a layer of SiO_2. MBE growth over SiO_2 is polycrystalline.[48] The MBE growth rate of GaAs on SiO_2 is reduced, especially at high substrate temperatures.[49] After growth, it is easily lifted off when the SiO_2 is etched away with buffered hydrofluoric acid. Since buffered hydrofluoric acid does not attack (Al,Ga)As and the layer to be lifted off should be relatively thin, this is a simple processing step. With MBE regrowth a p^+-GaAs contact layer could be included in the laser structure, since not including it will not prevent MBE regrowth from occuring on the mesa.

In spite of the difficulty of fabricating buried heterostructure lasers with MBE regrowth the potential reduction in threshold current makes it worthwhile to develop the technique. Other possibilities for achieving lower threshold current would

be to make the active region stripe width narrower and/or use one of the other stripe structures discussed in Section 4.1. MBE growth on patterned substrates is especially promising, since this structure has recently resulted in threshold currents as low as 1.8 mA for QW lasers without high reflectivity coatings.[8]

4.8 Conclusion

Buried heterostructure GRIN SCH SQW (Al,Ga)As lasers with threshold currents as low as 0.55 mA have been fabricated. This is the lowest threshold current reported so far for any semiconductor laser at room temperature. This result was achieved through the use of high reflectivity coatings. As predicted, high reflectivity coatings have a dramatic effect on the threshold current of SQW lasers because of the low transparency current of QW lasers. The effect is, however, enhanced for narrow buried heterostructure SQW lasers. The enhancement is attributed to turn off of the thyristor leakage current paths through the burying layers when the current is reduced.

While gain calculations correctly predict the trends observed, the numerical results obtained exhibit significant error when compared to the experimental results. It is possible that some of the error is caused by the use of a Lorentzian lineshape function to account for intraband relaxations. Since this is the established method of accounting for intraband relaxations, the results suggest that its theoretical basis for semiconductor lasers may be in need of further examination; a narrower lineshape function might be more accurate.

4.9 References

[1] M. Mittelstein, Y. Arakawa, A. Larsson, and A. Yariv, *Appl. Phys. Lett.* **49**(25), pp. 1689-1691 (1986).

[2] A. Sugimura, *IEEE J. Quantum Electron.* **QE-20**(4), pp. 336-343 (1984).

[3] A. Kurobe, H. Furuyama, S. Naritsuka, Y. Kokubun, and M. Nakamura, *Electron. Lett.* **22**(21), pp. 1117-1118 (1986).

[4] H. Nobuhara, T. Fujii, and O. Wada, *Electron. Lett.* **23**(12), pp. 645-647 (1987).

[5] H. Furuyama, A. Kurobe, S. Naritsuka, N. Sugiyama, Y. Kokubun, M. Nakamura, and Y. Uematsu, *Conference on Lasers and Electro-Optics*, Baltimore (1987).

[6] Y.-H. Wu, M. Werner, K.-L. Chen, and S. Wang, *Appl. Phys. Lett.* **44**(9), pp. 834-846 (1984).

[7] J. S. Smith, P. L. Derry, S. Margalit, and A. Yariv, *Appl. Phys. Lett.* **47**(7), pp. 712-714 (1985).

[8] E. Kapon, J. P. Harbison, C. P. Yun, and N. G. Stoffel, *Appl. Phys. Lett.* **52**(8), pp. 607-609 (1988).

[9] E. Kapon, J. P. Harbison, C. P. Yun, and N. G. Stoffel, *Conference on Lasers and Electro-Optics*, Anaheim (1988).

[10] D. Fekete, D. Bour, J. M. Ballantyne, and L. F. Eastman, *Appl. Phys. Lett.* **50**(11), pp. 635-637 (1987).

[11] K. Meehan, P. Gavrilović, N. Holonyak, Jr., R. D. Burnham, and R. L. Thornton, *Appl. Phys. Lett.* **46**(1), pp. 75-77 (1985).

[12] R. L. Thornton, R. D. Burnham, T. L. Paoli, N. Holonyak, Jr., and D. G. Deppe, *IEEE Trans. Electron. Dev.* **ED-32**(11), pp. 2541-2542 (1985).

[13] J. E. Epler, R. D. Burnham, R. L. Thornton, and T. L. Paoli, *Appl. Phys. Lett.* **50**(23), pp. 1637-1639 (1987).

[14] D. G. Deppe, W. E. Plano, J. M. Dallesasse, D. C. Hall, L. J. Guido, and N. Holonyak, Jr., *Appl. Phys. Lett.* **52**(10), pp. 825-827 (1988).

[15] T. Tsukada, *J. Appl. Phys.* **45**(11), pp. 4899-4906 (1974).

[16] W. T. Tsang, R. A. Logan, and J. A. Ditzenberger, *Electron. Lett.* **18**(19), pp. 845-847 (1982).

[17] K. Wohlleben and W. Beck, *Z. Naturforsch.* **A21**, pp. 1057-1071 (1966).

[18] J. C. Dyment, J. C. North, and L. A. D'Asaro, *J. Appl. Phys.* **44**(1), pp. 207-213 (1973).

[19] K. Ishida, K. Matsui, T. Fukunaga, T. Takamori, and H. Nakashima, *Jpn. J. Appl. Phys.* **25**(8), pp. L690-L692 (1986).

[20] T. Fujii, S. Hiyamizu, S. Yamakoshi, and T. Ishikawa, *J. Vac. Sci. Technol.* **B3**(2), pp. 776-778 (1985).

[21] T. Hayakawa, T. Suyama, M. Kondo, K. Takahashi, S. Yamamoto, and T. Hijikata, *Appl. Phys. Lett.* **49**(4), pp. 191-193 (1986).

[22] H. Chen, A. Ghaffari, H. Morkoç, and A. Yariv, *Electron. Lett.* **23**(25), pp. 1334-1335 (1987).

[23] G. H. B. Thompson, *Physics of Semiconductor Laser Devices,* pp. 16-20, John Wiley & Sons, New York (1980).

[24] H. Namizaki, R. Hirano, H. Higuchi, E. Oomura, Y. Sakakibara, and W. Susaki, *Electron. Lett.* **18**(16), pp. 703-705 (1982).

[25] N. K. Dutta, D. P. Wilt, and R. J. Nelson, *J. Lightwave Tech.* **LT-2**(3), pp. 201-208 (1984).

[26] S. M. Sze, *Physics of Semiconductor Devices,* 2nd Edition, pp. 190-242, John Wiley & Sons, New York (1981).

[27] M. Ettenberg, *Appl. Phys. Lett.* **32**(11), pp. 724-725 (1978).

[28] M. Born and E. Wolf, *Principles of Optics,* 4nd Edition, pp. 61-70, Pergamon, New York (1970).

[29] D. M. Fye, *IEEE J. Quantum Electron.* **QE-17**(9), pp. 1950-1954 (1981).

[30] G. H. B. Thompson, Ibid, p. 106.

[31] H. C. Casey, Jr. and M. B. Panish, *Heterostructure Lasers Part B: Materials and Operating Characteristics,* pp. 287-300, Academic Press, Orlando (1978).

[32] T. Tsukada, *Appl. Phys. Lett.* **28**(12), pp. 697-699 (1976).

[33] D. Botez, private communication.

[34] P. T. Landsberg, M. S. Abrahams, and M. Osiński, *IEEE J. Quantum Electron.* **QE-21**(1), pp. 24-28 (1985).

[35] B. Saint-Cricq, F. Lozes-Dupuy, and G. Vassilieff, *IEEE J. Quantum Electron.* **QE-22**(5), pp. 625-630 (1986).

[36] M. Yamanishi and Y. Lee, *IEEE J. Quantum Electron.* **QE-23**(4), pp. 367-370 (1987).

[37] K. Y. Lau, P. L. Derry, and A. Yariv, *Appl. Phys. Lett.* **52**(2), pp. 88-90 (1988).

[38] M. Yamada and Y. Suematsu, *J. Appl. Phys.* **52**(4), pp. 2653-2664 (1981).

[39] M. Yamada, H. Ishiguro, and H. Nagato, *Jpn. J. Appl. Phys.* **19**(1), pp. 135-142 (1980).

[40] E. H. Stevens and S. S. Yee, *J. Appl. Phys.* **44**(2), pp. 715-722 (1973).

[41] A. Arakawa and A. Yariv, *IEEE J. Quantum Electron.* **QE-21**(10), pp. 1666-1674 (1985).

[42] M. Asada, A. Kameyama, and Y. Suematsu, *IEEE J. Quantum Electron.* **QE-20**(7), pp. 745-753 (1984).

[43] P. T. Landsberg, M. S. Abrahams, and M. Osiński, *IEEE J. Quantum Electron.* **QE-21**(1), pp. 24-27 (1985).

[44] P. W. A. McIlroy, A. Kurobe, and Y. Uematsu, *IEEE J. Quantum Electron.* **QE-21**(12), pp. 1958-1963 (1985).

[45] A. Arakawa and A. Yariv, *IEEE J. Quantum Electron.* **QE-22**(9), pp. 1887-1899 (1987).

[46] W. T. Tsang and A. Y. Cho, *Appl. Phys. Lett.* **30**(6), pp. 293-296 (1977).

[47] S. Nagata and T. Tanaka, *J. Appl. Phys.* **48**(3), pp. 940-942 (1977).

[48] A. Y. Cho, J. V. Dilorenzo, and G. E. Mahoney, *IEEE Trans. Electron Dev.* **ED-24**(9), pp. 1186-1187 (1977).

[49] A. Okamoto and K. Ohata, *Appl. Phys. Lett.* **51**(19), pp. 1512-1514 (1987).

Chapter 5

Spectral Characteristics of Buried Heterostructure Single Quantum Well (Al,Ga)As Lasers

5.1 Introduction

The spectral linewidth of a semiconductor laser is of interest since it is a measure of the phase coherence of the lasing mode. Highly coherent lasers are needed for applications such as phase modulation. The linewidths of quantum well lasers have been predicted to be significantly narrower than those of conventional double heterostructures,[1] and the reduction in linewidth caused by use of a multiquantum well active region has been measured for the distributed feedback structure.[2] The measurements of linewidth described in this chapter are, however, believed to be the first reported for SQW lasers. The further dramatic linewidth reduction caused by application of high reflectivity coatings is also described. The theoretical reasons behind these results are explained and theoretical predictions are compared to the measured values for the linewidth and the linewidth enhancement factor. The theory assumes that the laser is lasing in a single mode, so the spectra of the SQW lasers were measured. Single mode operation is also important since linewidth is measured as a function of output power in the mode. If multiple lasing modes exist, it is difficult to determine accurately what fraction of the power is in a particular mode.

5.2 Spectrum

The possible spectrum of a semiconductor laser includes lateral modes, which are perpendicular to the plane of the active region and the direction of light propagation, transverse modes, which are in the plane of the active region and perpendicular

to the direction of light propagation, and longitudinal modes, which are in the direction of light propagation. The GRIN SCH SQW lasers described here support only the fundamental lateral mode.[3]

Multiple longitudinal modes are supported by the optical resonator structure of a semiconductor laser since its cavity length is much longer than the lasing wavelength. Guided longitudinal modes have an integral number of half wavelengths in the cavity length. $\lambda/n_r = 2L/m$, where λ is the mode wavelength in free space, n_r is the index of refraction of GaAs, and m is the longitudinal mode number. For normal cavity lengths, the mode number of longitudinal modes of the proper wavelength is on the order of 2000. The wavelength separation between adjacent longitudinal modes (with the same transverse mode number) is given by:[4]

$$\Delta\lambda = \frac{\lambda^2}{(n_{eff} - \lambda(dn_{eff}/d\lambda))2L} \tag{5.1}$$

where $\Delta\lambda$ is the wavelength separation, L is the cavity length, n_{eff} is the effective refractive index of the active region, and $n_{eff} - \lambda(dn_{eff}/d\lambda)$ has a value of $\sim$4.5. The buried GRIN SCH SQW stripe lasers of interest here lase at a wavelength of $\sim$8400 Å and were cleaved to a length of 250 μm, which results in a calculated longitudinal mode spacing of $\sim$3.2 Å.

If the stripe waveguide structure of a semiconductor laser supports multiple transverse modes, they can all be excited since each transverse mode can have a different longitudinal mode number, which allows a range of possible lasing wavelengths. Which of the possible modes is excited will depend on which has the most gain. To insure single transverse mode operation, the stripe structure should be designed to support only the fundamental transverse mode. To determine accurately how many transverse modes are supported and what their spacing will be, the guiding in the plane of the active region and that perpendicular to the plane must be taken into account.

The waveguide of a buried GRIN SCH SQW stripe laser may be visualized schematically by Figure 5.1a. Here a is the width of the GRIN SCH (~4000 Å) and W is the stripe width. The z-axis is along the direction of light propagation, the x-axis is along the width of the GRIN SCH, and the y-axis is along the stripe width. Since a is smaller than W, the stronger confinement is along the x-axis. The confinement in the x-direction is illustrated by Figure 5.1b where n_2 is the refractive index of the $Al_{0.5}Ga_{0.5}As$ cladding layers and n_1 is the refractive index at the center of the GRIN SCH. This waveguide is the one referred to in describing whether the modes are TE or TM. The end facet reflectivity of a DH is greater for TE modes[5] (which have the electric field vector polarized in the y-direction). The lasing modes of a DH semiconductor laser are therefore TE polarized since these modes have lower losses.

Finding the modes of the three dimensional dielectric waveguide of Figure 5.1a is not trivial; however, approximate methods such as the effective index method have been developed to solve it. (See for example Reference 6.) The effective index approximation involves finding the longitudinal propagation constant β of the lateral TE mode supported by the waveguide of Figure 5.1b (only one exists for this case). The effective index of this guide is defined as

$$n_{eff} = \frac{\beta}{k} \tag{5.2}$$

where $k = 2\pi/\lambda$. The waveguide in the other direction (illustrated in Figure 5.1c) is then considered to have an index of refraction n_{eff} in its confining region. The outer regions of this waveguide still have their original refractive index n_3 which is the refractive index of the $Al_{0.3}Ga_{0.7}As$ burying layers. The TM modes of this waveguide can then be solved for. Their spacing is the transverse mode spacing.

For a GRIN SCH SQW even solving for the propagation constant of the first waveguide (Figure 5.1b) is not trivial. Neglecting the SQW, which is very small

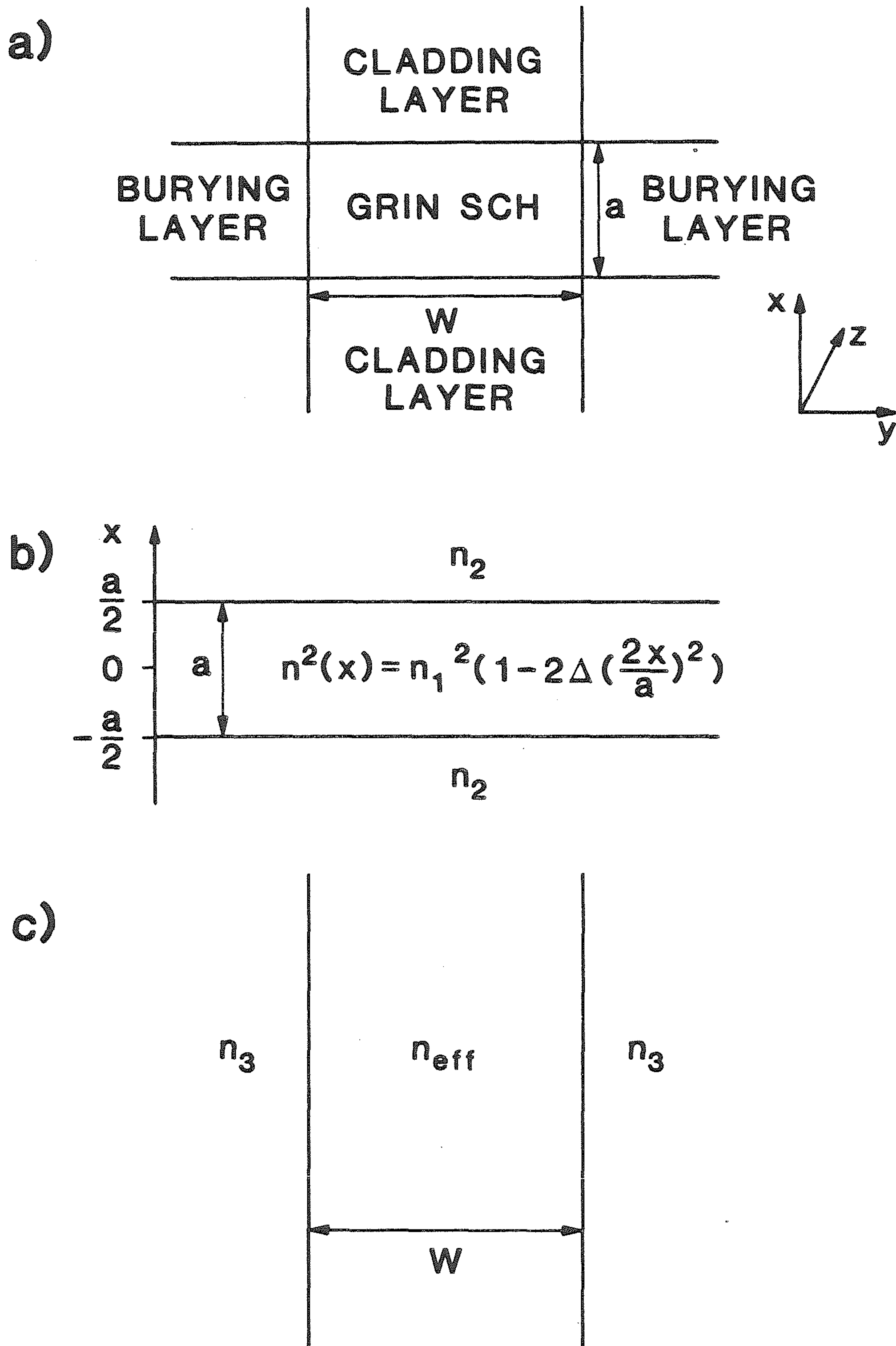

Figure 5.1: Schematic diagrams of (a) the waveguide formed by a buried GRIN SCH SQW, (b) waveguide in the lateral direction, and (c) effective waveguide in the transverse direction.

compared to the total waveguide structure, the refractive index profile of a parabolic GRIN SCH is

$$n^2(x) = n_1^2\left(1 - 2\Delta\left(\frac{2x}{a}\right)^2\right) \tag{5.3}$$

where $x = 0$ is at the center of the GRIN SCH and $2\Delta = (n_1^2 - n_2^2)/n_1^2$. The modes of a cladded parabolic index waveguide near cutoff can be found by finding the modes for $n(x) = n_1$ and then considering the parabolic change as a perturbation.[6] For the GRIN SCH SQWs discussed here $n_1 = 3.452$ and $n_2 = 3.258$. For a lasing wavelength of ~8400 Å the resulting n_{eff} is 3.4. The number of transverse modes supported by the waveguide is[6]

$$M = \left[\frac{ak}{\pi}\sqrt{n_{eff}^2 - n_3^2}\right]_{int} \tag{5.4}$$

where "*int*" means take the next largest integer. For a 1 μm wide buried GRIN SCH only one transverse mode will be supported, but for a 4 μm buried stripe approximately four modes will be supported.

The transverse spacing of these modes can be determined by considering the value of q for two adjacent modes. q is defined by

$$q^2 = n_{eff}^2 k^2 - \beta^2 \tag{5.5}$$

where β is the longitudinal propagation constant of these modes, i.e., the z dependence is of the form $e^{i\beta z}$. $\beta = m\pi/L$, where m is the longitudinal mode number, which will not change for adjacent transverse modes with the same longitudinal mode number. By realizing that $d\beta/d\lambda = 0$, Equation (5.5) can be used to solve for the transverse mode spacing. The result is [7]

$$\frac{\Delta\lambda}{\lambda} = \frac{q_l^2 - q_{l-1}^2}{2n_{eff}(n_{eff} - \lambda(dn_{eff}/d\lambda)k^2} \tag{5.6}$$

where l is the transverse mode number. For a 4 μm wide buried stripe GRIN SCH SQW the transverse mode spacing is ~7 Å.

A buried heterostructure is relatively tightly confining because of the abrupt refractive index change between the burying layers and the active region; a more weakly confining structure is one with a gradual refractive index change. Such a structure supports fewer transverse modes than the same width buried stripe.[8] A good example of a more weakly confining structure is the channeled-substrate laser[9] illustrated in Figure 5.2. A channeled-substrate laser is formed by LPE growth over a channel of a patterned substrate. Optical confinement is caused by the wider active region and wider lower cladding layer formed over the channel. The active region over the channel has a larger effective index of refraction than the GaAs layer grown over the flat portion of the substrate.

A waveguide structure which supports only a single transverse mode has a great advantage for achieving single mode operation since stable single transverse mode operation is required for single longitudinal operation.[10,11] The width of the gain spectrum of a semiconductor laser is wider than the separation between longitudinal modes; however, if the gain spectrum is homogeneously broadened, single longitudinal operation is possible.[12] Homogeneously broadened means the gain spectrum shape is not changed as the stimulated emission power increases. The main factors which determine if the gain spectrum is homogeneously broadened are spontaneous emission, carrier distribution, carrier diffusion, and photon distribution.

A large fraction of spontaneous emission at the lasing energy increases the probability of multilongitudinal mode operation.[13,14,15] A tightly confining waveguide structure like a buried heterostucture will have a relatively large proportion of spontaneous emission at the lasing energy[16] and is therefore less ideal for single mode operation than a structure like a channeled substrate laser.

Nonuniform carrier distribution could also cause an inhomogeneously broadened gain spectrum.[8] This could be caused by poor fabrication, for example a

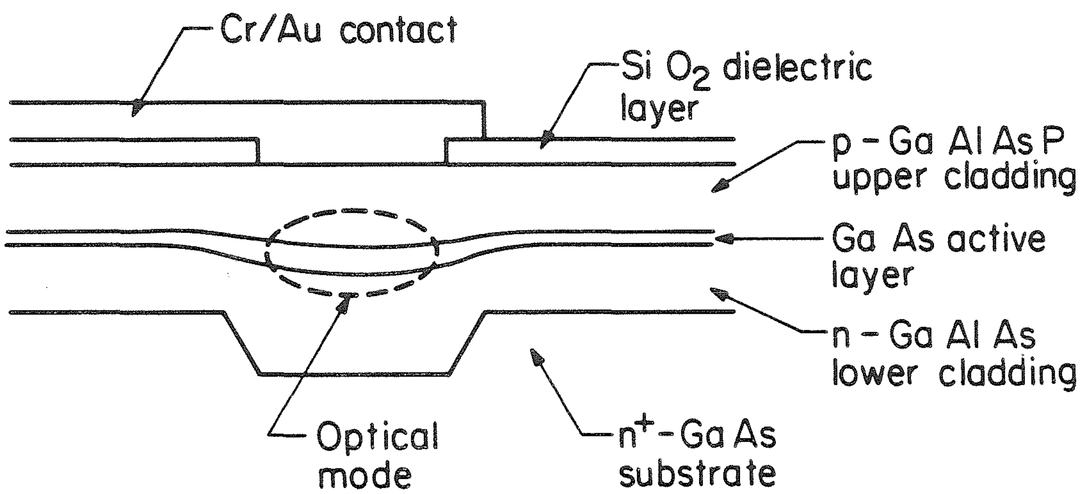

Figure 5.2: Schematic diagram of a channeled-substrate stripe laser formed by LPE growth on a patterned substrate.

contact not centered over a narrow stripe laser. A nonuniform carrier distribution could also be caused by spectral hole burning.[11,17] If carrier relaxation times are long, the gain at a lasing mode can be reduced by intense lasing. As the gain for this mode is reduced other modes may be excited. This phenomenon is caused by depletion of carriers at peaks in the standing wave pattern of the lasing mode.

The spectra of 250 μm long buried GRIN SCH SQW (Al,Ga)As lasers, whose fabrication is described in Chapter 4, were resolved with a spectrometer. An optical isolator was placed between the lasers and the spectrometer to prevent optical feedback into the lasers, which could influence the results. Lasers with a 1 μm stripe width were expected to be more likely to have single mode operation than those with a 4 μm stripe width since a 1 μm stripe is narrow enough to support only the fundamental transverse modes while a 4 μm stripe will support several transverse modes. Single mode operation, however, was not observed for the 1 μm stripe lasers. Lasing typically occurred in two or three longitudinal modes. This result can be attributed to either a large degree of spontaneous emission or nonuniform carrier distribution due to spectral hole burning or problems with fabrication. Application of high reflectivity coatings did not switch these lasers to single mode operation. High reflectivity coatings are theoretically expected to increase the probability of single mode operation, since the internal stimulated emission power is increased by their application.[15]

Surprisingly, the 4 μm stripe lasers had superior spectra. Typical spectra of an uncoated 250 μm long laser at various current levels are shown in Figure 5.3. The cw threshold current I_{th} for this laser was 6.9 mA. As is typical for a single mode semiconductor laser near threshold, multiple longitudinal modes were observed because of low internal stimulated emission power,[15] but at higher currents single mode operation took over. The mode spacing is 3.4 Å which suggests that

the modes are multiple longitudinal modes (calculated spacing ~3.2 Å). Transverse modes would have a wider spacing (~7 Å), but since adjacent transverse modes tend to operate in different longitudinal modes, some irregular spacing would probably be observed. No spectra which showed this were observed although there was some sporadic mode hopping which could be caused by multiple transverse modes, but could also be caused by changes in temperature.[18] Since the transverse mode spacing is approximately twice the longitudinal spacing, it might be difficult to recognize transverse modes with the same longitudinal mode number as such; it is therefore not clear whether multiple transverse modes were excited. Single mode operation was achieved over a wide range of currents, but at very high currents (5-6I_{th}) multiple modes began to appear. This was probably caused by spectral hole burning unless multiple transverse modes were present.

As the current was raised, the lasing mode tended to shift to longer wavelengths. This is a typical result and is caused by resistive heating.[18] An increase in temperature reduces the band gap energy of the active region. The energy gap is inversely proportional to the lasing wavelength, so the lasing wavelength is increased by the shift.

The spectra of the 4 μm stripe lasers with high reflectivity coatings were very similar to those without coatings. Figure 5.4 shows the spectra of a 4 μm wide 250 μm long laser with one 57% reflectivity coating, one 89% reflectivity coating, and a cw threshold current of 3.25 mA. The only significant difference is that with coatings the lasing wavelength is longer. With coatings the threshold gain is low, which means that most of the transitions contributing to the gain are from the first quantized state of the quantum well. A laser with higher loss, i.e., no coatings, will have higher threshold gain. At higher gains, transitions from the second quantized state contribute more. This means that the gain peak shifts toward the second

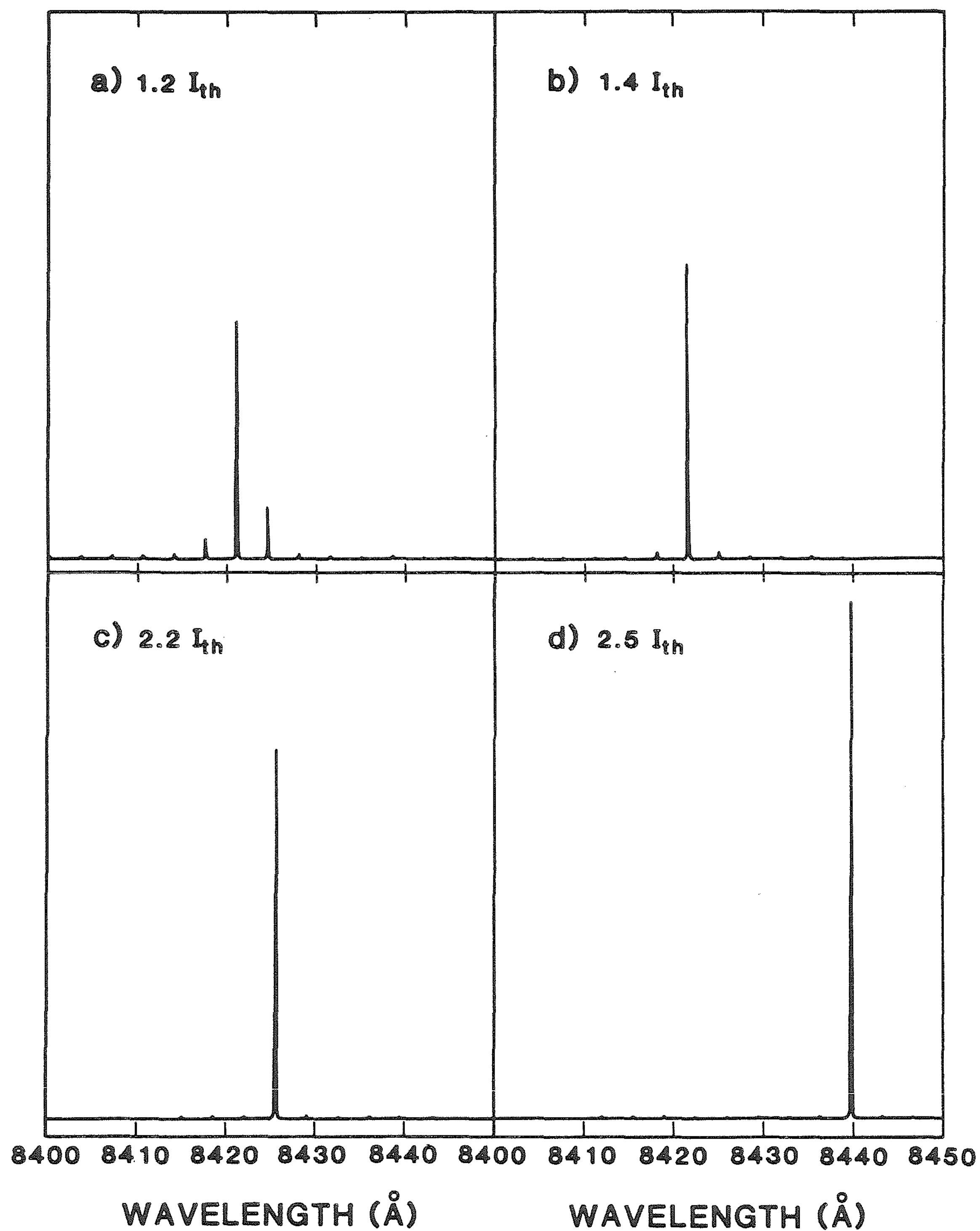

Figure 5.3: Spectra of an uncoated 250 μm long 4 μm wide buried GRIN SCH 70 Å SQW (Al,Ga)As laser at currents of (a) $1.2I_{th}$, (b) $1.4I_{th}$, (c) $2.2I_{th}$, and (d) $2.5I_{th}$. Intensity scales are arbitrary and are not the same for all the spectra.

quantized state transition energy,[19] which is larger than that of the first quantized state. The uncoated lasers, therefore, have a larger lasing energy (smaller lasing wavelength) than the coated lasers.

There are several mechanisms which could explain the superiority of the spectra of the 4 μm lasers compared to those of the 1 μm lasers. The fraction of spontaneous emission at the lasing energy should be larger for the narrower stripe lasers[20] just as the spontaneous emission factor n_{sp}, which is discussed later in this chapter, is. This is also an explanation of why high reflectivity coatings did not improve the spectra.

It may be that the carrier distribution in the narrower lasers is more sensitive to nonuniformity in the LPE regrowth and contact formation. For instance, different regrown thicknesses on either side of the buried stripe or a misaligned contact stripe could cause a nonuniform carrier distribution, which could cause multilongitudinal mode operation. It is also possible that the poor lifetime characteristics of these lasers (see Chapter 4) caused instabilities, which resulted in multiple modes. It is not clear whether this is a problem inherent in the narrower buried stripe structure. It is true that buried heterostructure lasers are not usually used for applications which require single mode operation, since other structures such as the channeled-substrate laser have more reliable single mode operation, because of less spontaneous emission into the lasing mode.

Since single mode operation is required for the measurement of spectral linewidth, all the spectral linewidth measurements reported in Section 5.4 are for the 4 μm stripe lasers.

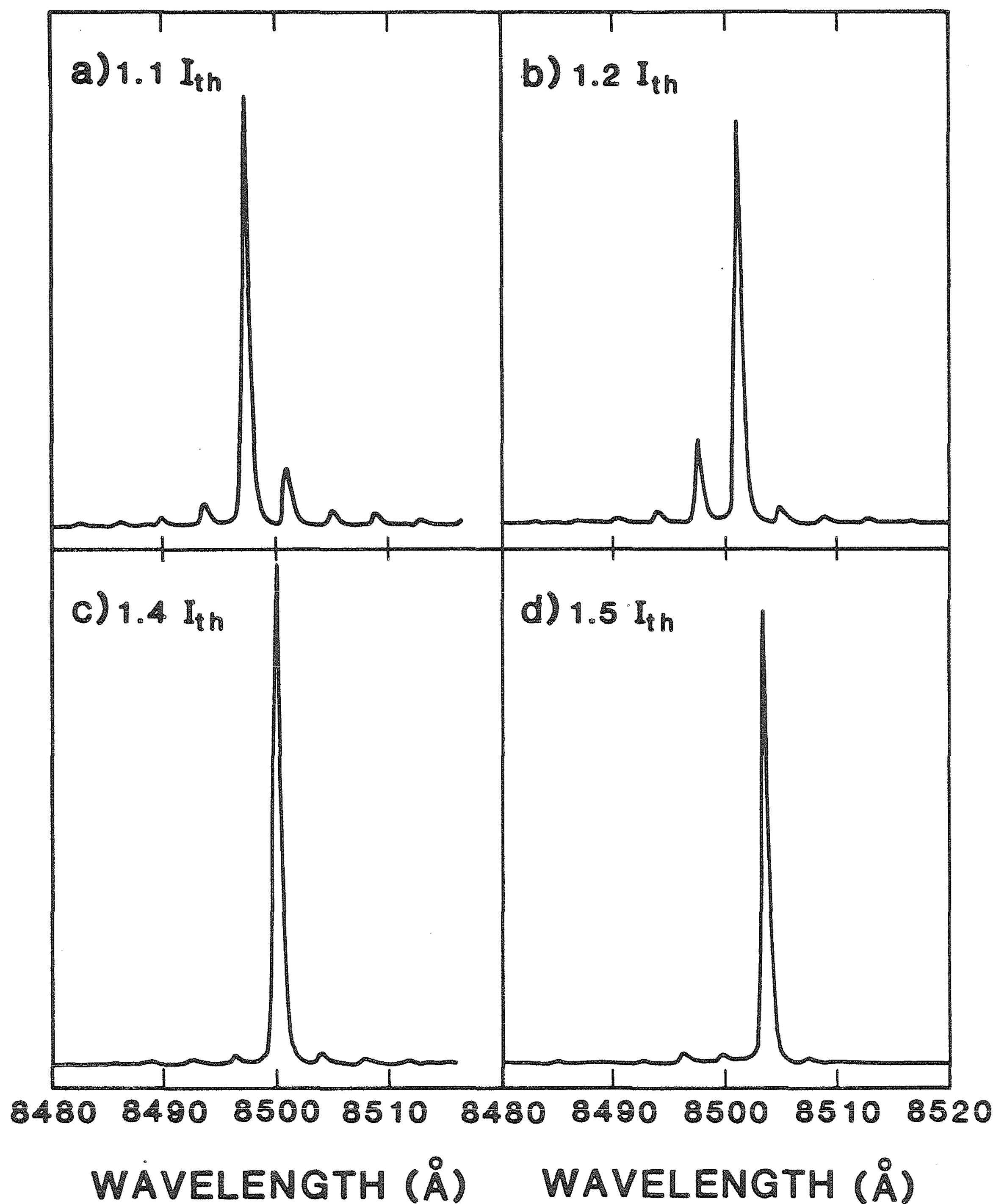

Figure 5.4: Spectra of an 250 μm long 4 μm wide buried GRIN SCH 70 Å SQW (Al,Ga)As laser with one 57% reflectivity coating and one 89% reflectivity coating at currents of (a) $1.1 I_{th}$, (b) $1.2 I_{th}$, (c) $1.4 I_{th}$, and (d) $1.5 I_{th}$. Intensity scales are arbitrary and are not the same for all the spectra.

5.3 Spectral Linewidth: Theory

The spectral linewidth of a semiconductor laser is:[21,22]

$$2\Gamma = \frac{v_g^2 E_L\big(\alpha_i + (1/2L)\ln(1/R_1R_2)\big)^2 n_{sp}(1+\alpha^2)}{4\pi P_{stim}} \tag{5.7}$$

where 2Γ is the full width at half-maximum of the lasing mode at photon energy E_L, v_g is the group velocity, α_i is the internal loss, L is the laser cavity length, R_1 and R_2 are the end facet reflectivities, P_{stim} is the total stimulated power inside the laser, n_{sp} is the spontaneous emission factor, and α is the linewidth enhancement factor.

n_{sp} is the ratio of spontaneous emission power into the lasing mode to stimulated emission power of the mode.[23] Assuming rigorous k-selection and accounting for intraband relaxations with a Lorentzian broadening function:

$$n_{sp} = \frac{\int \frac{|M(E_L)|^2 \mathcal{D}(E) f_c(E,N)\big(1-f_v(E,N)\big)\hbar\gamma}{(E-E_L)^2+(\hbar\gamma)^2}\,dE}{\int \frac{|M(E_L)|^2 \mathcal{D}(E)\big(f_c(E,N)-f_v(E,N)\big)\hbar\gamma}{(E-E_L)^2+(\hbar\gamma)^2}\,dE} \tag{5.8}$$

where the notation is that of Chapter 2. Some factors common to both the spontaneous and stimulated emission rates, which can be moved outside of the integral, are omitted since they cancel out. In the case of a SQW, $\mathcal{D}(E)$ is given by Equation (2.9). Substituting (2.9) into Equation (5.8) and neglecting the light hole contribution, which is insignificant compared to the heavy hole contribution, n_{sp} for a SQW is

$$n_{sp} = \frac{\int \sum_{n=1}^{\infty} \frac{m_r^h H(E-E_g-E_n^c-E_{n,h}^v)|M(E_L)_{QW}|^2 f_c(E,N)\big(1-f_v(E,N)\big)}{(E-E_L)^2+(\hbar\gamma)^2}\,dE}{\int \sum_{n=1}^{\infty} \frac{m_r^h H(E-E_g-E_n^c-E_{n,h}^v)|M(E_L)_{QW}|^2\big(f_c(E,N)-f_v(E,N)\big)}{(E-E_L)^2+(\hbar\gamma)^2}\,dE} \tag{5.9}$$

Putting in the limits of integration

$$n_{sp} = \frac{\sum_{n=1}^{\infty} m_r^h |M(E_L)_{QW}|^2 \int_{E_g+E_{n,h}}^{\infty} \frac{f_c(E,N)\big(1-f_v(E,N)\big)}{(E-E_L)^2+(\hbar\gamma)^2}\,dE}{\sum_{n=1}^{\infty} m_r^h |M(E_L)_{QW}|^2 \int_{E_g+E_{n,h}}^{\infty} \frac{\big(f_c(E,N)-f_v(E,N)\big)}{(E-E_L)^2+(\hbar\gamma)^2}\,dE} \tag{5.10}$$

where $E_{n,h} = E_n^c + E_{n,h}^v$. If only the first quantized state contributes significantly, then Equation (5.10) reduces to

$$n_{sp} \approx \int_{E_g+E_{n,h}}^{\infty} \frac{f_c(E,N)\big(1-f_v(E,N)\big)}{(E-E_L)^2+(\hbar\gamma)^2}\,dE \Bigg/ \int_{E_g+E_{n,h}}^{\infty} \frac{\big(f_c(E,N)-f_v(E,N)\big)}{(E-E_L)^2+(\hbar\gamma)^2}\,dE \tag{5.11}$$

If the energy broadening due to intraband relaxations is not large, the Lorentzian broadening function can be neglected, in which case the integrals become delta functions at $E = E_L$. Equation (5.11) then simplifies to

$$n_{sp} \approx \frac{f_c(E_L,N)\big(1-f_v(E_L,N)\big)}{f_c(E_L,N)-f_v(E_L,N)} \tag{5.12}$$

Note that the same approximation would be reached for a conventional DH laser. $f_c(E_L,N)$ and $f_v(E_L,N)$ are defined by Equations (2.11) and (2.12). Substituting in their values:

$$n_{sp} \approx \frac{exp\big(-(E_v+F_v)/kT\big)}{exp\big(-(E_v+F_v)/kT\big) - exp\big((E_g+E_c-F_c)/kT\big)} \tag{5.13}$$

which reduces to

$$n_{sp} \approx \frac{1}{1-exp\big((E_g+E_c-F_c+E_v+F_v)/kT\big)} \tag{5.14}$$

$E_L = E_g + E_c + E_v$ so Equation (5.14) simplifies to

$$n_{sp} \approx \frac{1}{1-exp\big((E_L+F_v-F_c)/kT\big)} \tag{5.15}$$

n_{sp} depends strongly on the carrier density and the quantized energy levels since those are the factors which determine E_L, F_c, and F_v. Approximating the energy levels of the SQW with those of an infinitely deep well was found to cause significant error in n_{sp}; consequently, the actual energy levels, which M. Mittelstein computed by numerically solving the Schrödinger equation for a QW of finite depth,[19] were

used in calculating n_{sp}. Figure 5.5 is a plot of the calculated value of n_{sp} as a function of carrier density for a GRIN SCH 70 Å SQW. At very low carrier densities (near transparency) n_{sp} is large, but it approaches 1 as the carrier density increases. In SQW lasers n_{sp} is calculated to approach 1 more quickly than in bulk double heterostructure lasers.[1] The carrier density in the active region and the gain of a semiconductor laser are clamped at their threshold values when lasing begins. If the carrier density is clamped and the temperature is constant, E_L, F_c, and F_v are clamped, which means that n_{sp} is clamped at its threshold value.

The linewidth enhancement factor α exists because of coupling between amplitude and phase fluctuations. This coupling occurs because changes in carrier density cause changes in the refractive index of the active region and vice versa. α is defined as[21,22]

$$\alpha = \frac{\partial \chi_R(E_L, N)/\partial N}{\partial \chi_I(E_L, N)/\partial N} \tag{5.16}$$

where $\chi_R(E_L, N)$ and $\chi_I(E_L, N)$ are the real and imaginary parts of the electronic susceptibility. $\chi_I(E_L, N)$ is proportional to the gain, which is given by Equation (2.10). $\chi_R(E_L, N)$ is the Kramers-Kronig inverse[24] of $\chi_I(E_L, N)$. Neglecting common terms, which cancel out in the ratio, assuming rigorous k-selection, and accounting for intraband relaxations with a Lorentzian lineshape function

$$\frac{\partial \chi_R(E_L, N)}{\partial N} \propto \int \frac{|M(E_L)|^2 \mathcal{D}(E)\big(\partial f_c(E,N)/\partial N - \partial f_v(E,N)/\partial N\big)(E - E_L)}{(E - E_L)^2 + (\hbar\gamma)^2} \, dE \tag{5.17}$$

$$\frac{\partial \chi_I(E_L, N)}{\partial N} \propto \int \frac{|M(E_L)|^2 \mathcal{D}(E)\big(\partial f_c(E,N)/\partial N - \partial f_v(E,N)/\partial N\big)\hbar\gamma}{(E - E_L)^2 + (\hbar\gamma)^2} \, dE \tag{5.18}$$

Equation (5.17) neglects the free carrier contribution to $\chi_R(E_L, N)$; however, the intraband component is normally dominant.[25] Figure 5.6 shows the calulated values of $|\alpha|$ for a bulk DH and for 70 Å and 100 Å SQWs as a function of carrier density.

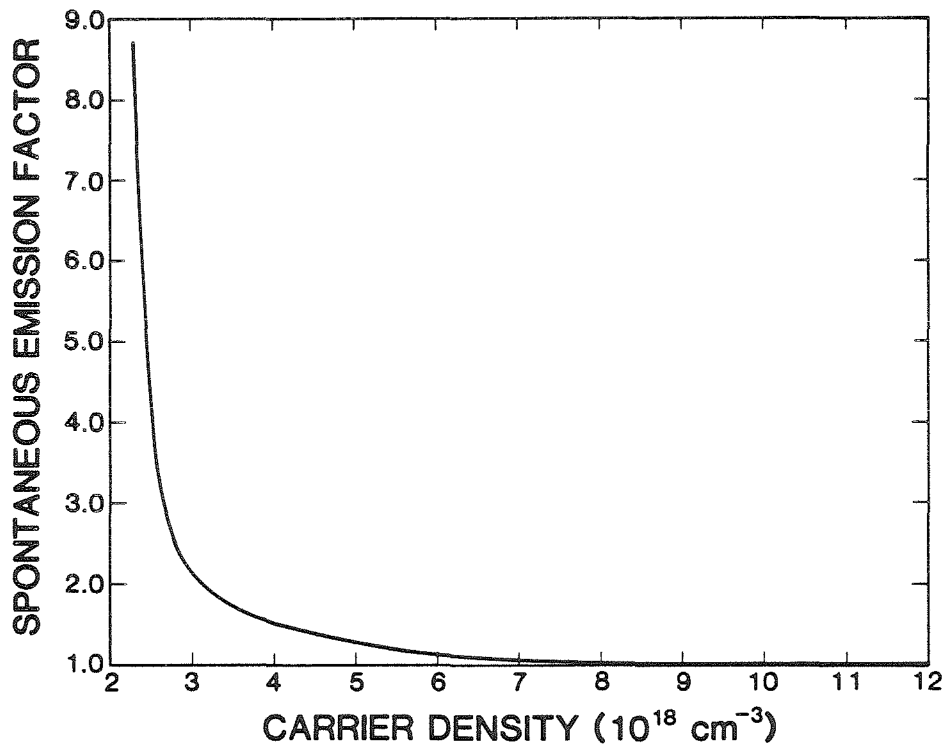

Figure 5.5: Calculated spontaneous emission factor for an (Al,Ga)As GRIN SCH 70 Å SQW as a function of carrier density.

Since the carrier density is clamped at its threshold value, $|\alpha|$ is clamped at its threshold value, too. The calculations show that $|\alpha|$ is expected to be much smaller for a SQW than for a conventional DH. Since α is squared in Equation (5.7), this should result in a very significant reduction in linewidth for a SQW laser. The much smaller internal loss[19] (< 2 cm^{-1} in the best SQWs) and the smaller values of n_{sp} should also contribute to the linewidth reduction.

Equation (5.7) is in terms of P_{stim}; however, linewidth is measured as a function of the output power at one facet. The relationship between the total output power $P_1 + P_2$ and P_{stim} is given by Equation (2.22), and the ratio of P_1/P_2 is given by Equation (4.2). Combining Equations (2.22) and (4.2) the relationship between P_{stim} and output power P_1 at the facet with reflectivity R_1 is

$$P_{stim} = \frac{P_1\big(\alpha_i + (1/2L)\ln(1/R_1R_2)\big)\left(1 + \sqrt{\frac{R_1}{R_2}}\frac{(1-R_2)}{(1-R_1)}\right)}{(1/2L)\ln(1/R_1R_2)} \tag{5.19}$$

Substituting Equation (5.19) into Equation (5.7):

$$2\Gamma = \frac{v_g^2 E_L\big(\alpha_i + (1/2L)\ln(1/R_1R_2)\big)(1/2L)\ln(1/R_1R_2)n_{sp}(1+\alpha^2)}{4\pi P_1\left(1 + \sqrt{\frac{R_1}{R_2}}\frac{(1-R_2)}{(1-R_1)}\right)} \tag{5.20}$$

The comparisons between the linewidth of a QW and of a conventional DH still hold when 2Γ is expressed as a function of P_1.

To understand the dramatic effect of facet reflectivity on the linewidth in a QW laser, consider Equation (5.20) when $R_1 = R_2 = R$:

$$2\Gamma = \frac{v_g^2 E_L\big(\alpha_i + (1/L)\ln(1/R)\big)(1/L)\ln(1/R)n_{sp}(1+\alpha^2)}{8\pi P_1} \tag{5.21}$$

Examining Equation (5.21), it is clear that as $R \to 1$, 2Γ is reduced; this effect has already been appreciated for conventional double heterostructure lasers.[26] The much smaller internal loss in a QW laser will make the reduction significantly greater

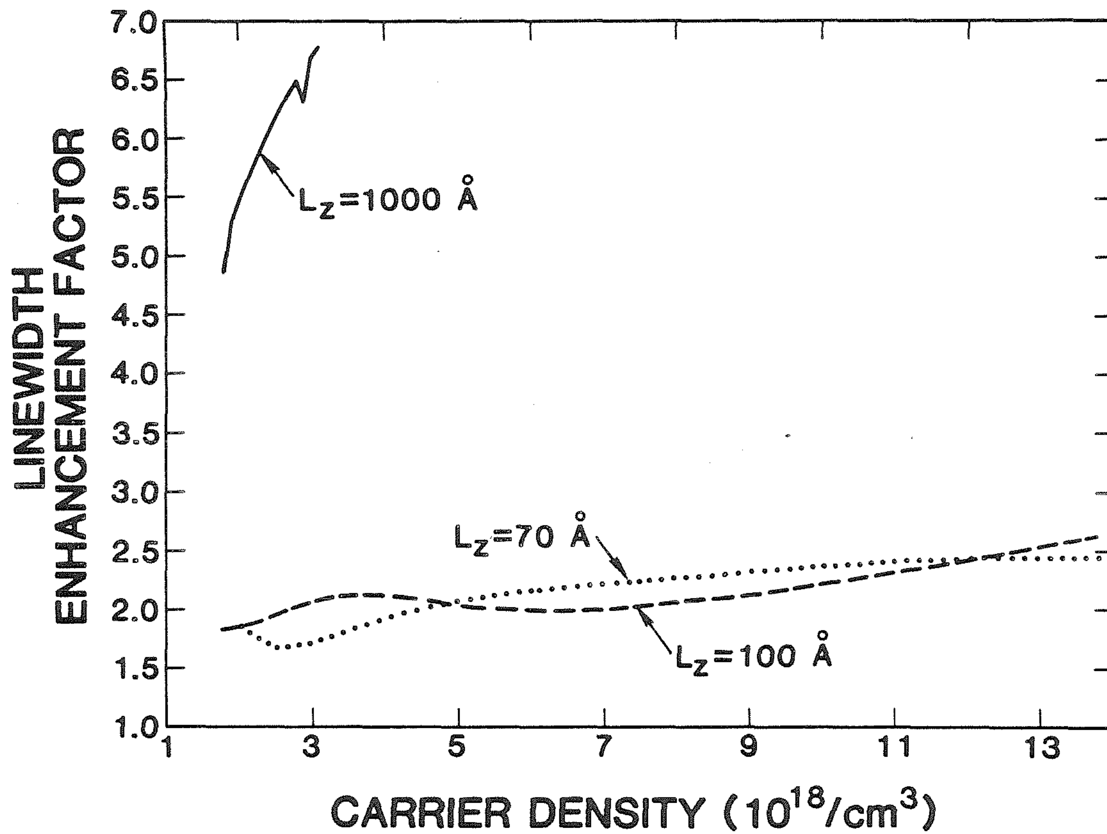

Figure 5.6: Calculated linewidth enhancement factor as a function of carrier density for a conventional DH with an active region thickness of 1000 Å and for 70 Å and 100 Å SQWs.

for a QW. In the limit of $\alpha_i \ll \frac{1}{L}\ln(1/R)$

$$2\Gamma \approx \frac{v_g^2 E_L (1/L)^2 \left(\ln(1/R)\right)^2 n_{sp}(1+\alpha^2)}{8\pi P_1} \tag{5.22}$$

For small x, $\ln(1+x) \to x$. $(1/L)\ln(1/R) = (-1/L)\ln R$ so as $R \to 1$ $(1/L)\ln(1/R) \to (1/L)(1-R)$. In this limit Equation (5.22) becomes

$$2\Gamma \approx \frac{v_g^2 E_L (1/L)^2 (1-R)^2 n_{sp}(1+\alpha^2)}{8\pi P_1} \tag{5.23}$$

One would therefore expect the linewidth to approach zero in the limit of $R \to 1$ and very low α_i, however, n_{sp} limits the reduction since it increases exponentially as the threshold current density decreases (see Figure 5.5). Therefore, in a SQW with enhanced facet reflectivities and low loss, the linewidth will be dramatically reduced, but for very high facet reflectivities, the increase in n_{sp} will become a significant limiting factor in the reduction. While $|\alpha|$ is expected to decrease slightly at lower threshold current densities,[27] calculations (see Figure 5.6) indicate that this will not be a significant factor for a QW compared to the end loss $(1/2L)\ln(1/R_1R_2)$ and n_{sp}.

5.4 Spectral Linewidth: Experiment

The spectral linewidths of 250 μm long 4 μm wide uncoated and coated buried GRIN SCH 70 Å SQW (Al,Ga)As lasers at room temperature were measured with a confocal scanning Fabry-Perot interferometer with a free spectral range of 1500 MHz. The Fabry-Perot response was measured with a photomultiplier. The optical setup is schematically illustrated in Figure 5.7. Great care was taken to prevent optical feedback into the lasers by isolating them from the Fabry-Perot interferometer with an optical isolator and neutral density filters with at least 10^4 attenuation for all measurements. The neutral density filters were oriented at an

angle other than 90° from the beam to insure that reflections from them did not produce feedback into the laser. In addition the spherical lens used to focus the laser beam had an antireflection coating. Wires in the circuit powering the lasers were shielded. It was found that unshielded wires sometimes picked up noise at ~90 MHz, which was attributed to FM radio signals. If the wires were not shielded, this noise affected the measured linewidth since it modulated the lasers.

Linewidths were measured at output powers at which single mode laser operation had been observed. Figures 5.8, 5.9, and 5.10 show typical mode profiles obtained for the buried GRIN SCH SQW lasers. The spectral linewidth is defined as the full width at half maximum of the mode. Figures 5.8 and 5.9 show linewidths of an uncoated laser. Figure 5.10 shows how narrow the linewidth becomes when high reflectivity coatings are applied. It is likely that even narrower linewidths could be achieved since the lasers could be operated at higher powers, however, the limited resolution of the Fabry-Perot interferometer prevented examination of narrower linewidths.

Figure 5.11 shows the linewidth of a typical GRIN SCH SQW with and without coatings as a function of $1/P_1$. Results for this device and others are tabulated in Table 5.1. The measured slope, 28.3 MHz mW, as a function of $1/P_1$ for uncoated lasers is significantly smaller than that of bulk double heterostructure stripe lasers. For instance Welford and Mooradian[28] measured 74.7 MHz mW at 273 K for Mitsubishi TJS lasers.

Figure 5.11 shows that when the end facet reflectivities were increased to 85% and 93%, the slope was reduced from 28.3 to 5.9 MHz mW, but the intercept increased to 2.2 MHz. The narrowest linewidth measured for this device was 6.0 MHz at 1.27 mW (see Figure 5.10). For other coated lasers, slightly narrower linewidths were measured at higher powers (4.9 MHz at 2.45 mW). All the coated

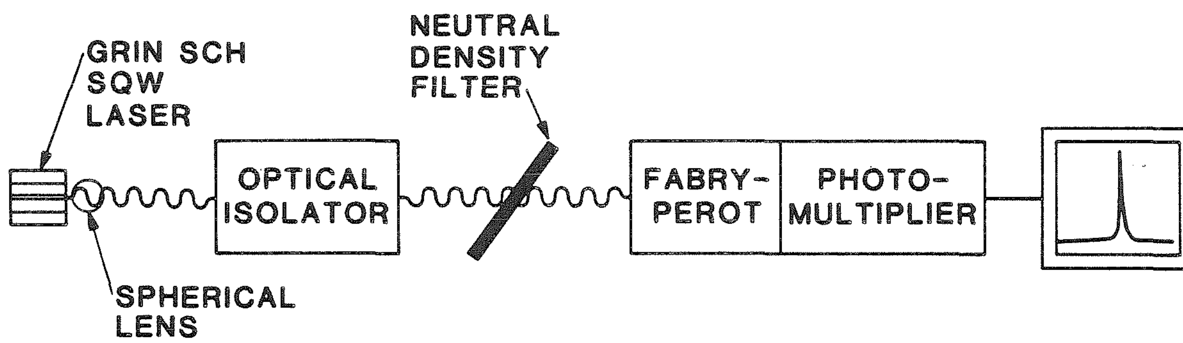

Figure 5.7: Optical setup for measuring the spectral linewidth of buried GRIN SCH SQW lasers.

a)

$P_1 = 1.34$ mW
$1/P_1 = 0.75$ mW^{-1}
$2\Gamma = 27.7 \pm 1.9$ MHz

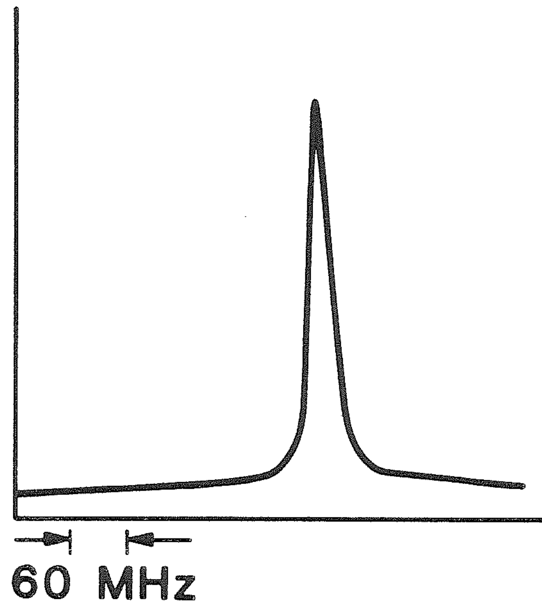

b)

$P_1 = 2.66$ mW
$1/P_1 = 0.38$ mW^{-1}
$2\Gamma = 13.2 \pm 1.9$ MHz

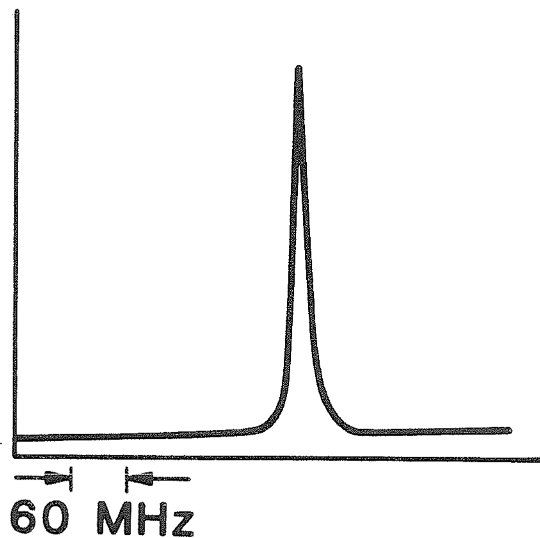

Figure 5.8: Spectra of an uncoated 250 μm long 4 μm wide buried GRIN SCH 70 Å SQW (Al,Ga)As laser at (a) P_1 = 1.34 mW and (b) P_1 = 2.66 mW. The horizontal scale is 60 MHz per division. The intensity scales are arbitrary.

a)

$P_1 = 2.66$ mW

$1/P_1 = 0.38$ mW^{-1}

$2\Gamma = 13.2 \pm 1.9$ MHz

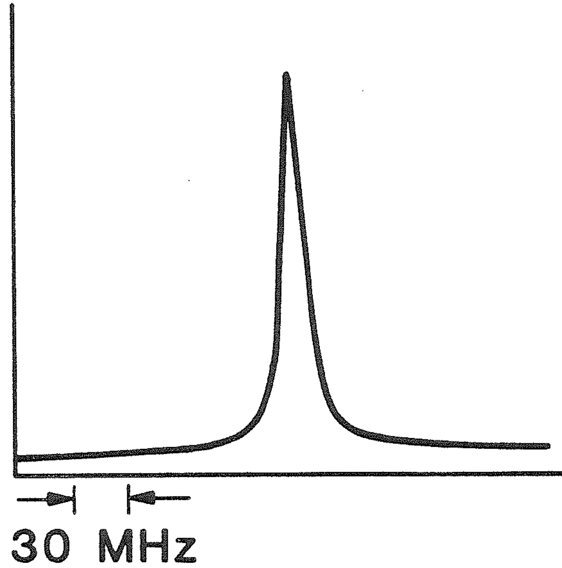

b)

$P_1 = 4.76$ mW

$1/P_1 = 0.21$ mW^{-1}

$2\Gamma = 7.9 \pm 1.0$ MHz

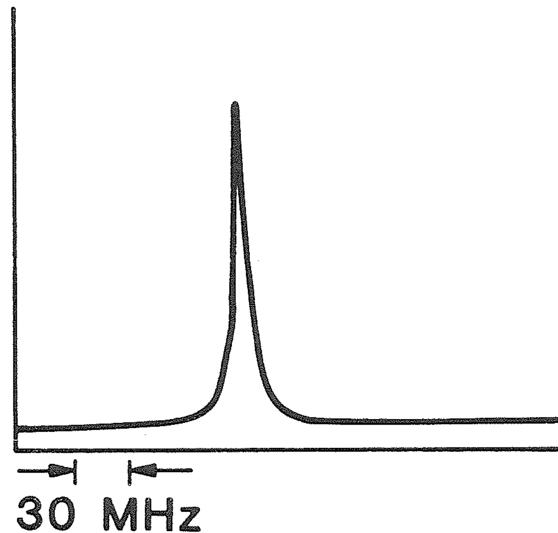

Figure 5.9: Spectra of an uncoated 250 μm long 4 μm wide buried GRIN SCH 70 Å SQW (Al,Ga)As laser at (a) P_1 = 2.66 mW and (b) P_1 = 4.76 mW. The horizontal scale is 30 MHz per division. The intensity scales are arbitrary.

a)

$P_1 = 1.27$ mW

$1/P_1 = 0.79$ mW^{-1}

$2\Gamma = 6.0 \pm 1.2$ MHz

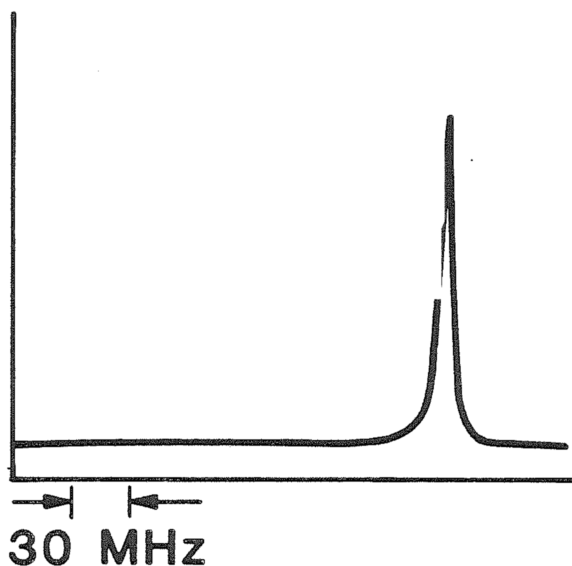

b)

$P_1 = 2.45$ mW

$1/P_1 = 0.41$ mW^{-1}

$2\Gamma = 4.9 \pm 0.8$ MHz

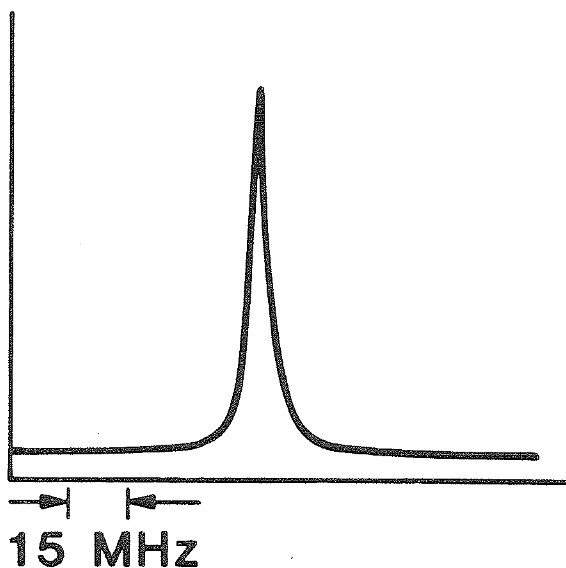

Figure 5.10: Spectra of coated 250 μm long 4 μm wide buried GRIN SCH 70 Å SQW (Al,Ga)As lasers. The intensity scales are arbitrary. (a) $R_1 = 85\%$, $R_2 = 93\%$, and $P_1 = 1.27$ mW. The horizontal scale is 30 MHz per division. (b) $R_1 = 57\%$, $R_2 = 89\%$, and $P_1 = 2.45$ mW. The horizontal scale is 15 MHz per division.

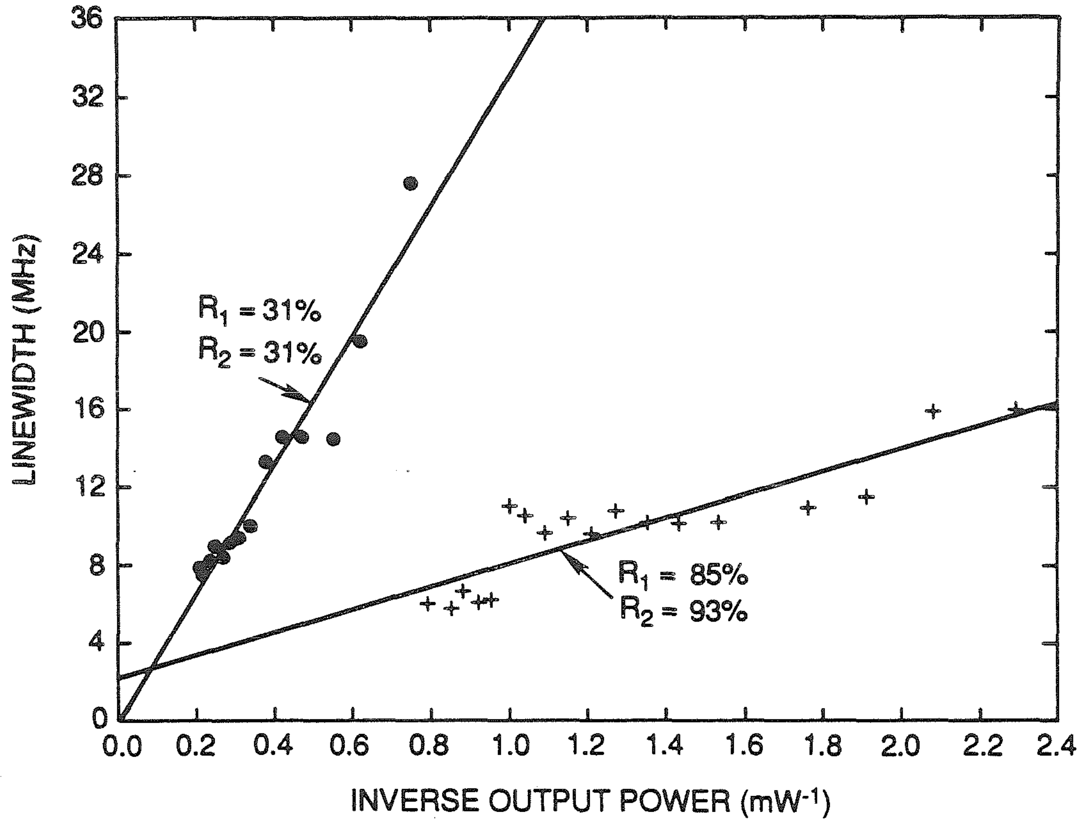

Figure 5.11: Spectral linewidth as a function of the reciprocal of the output power at facet with reflectivity R_1 for an uncoated 250 μm long 4 μm wide buried GRIN SCH 70 Å SQW (Al,Ga)As laser and for the *same* laser with coated facets reflectivities R_1=85% and R_2=93%.

SQW lasers (Table 5.1) examined had significant nonzero intercepts. A nonzero intercept is not predicted by Equation (5.20), but has been observed experimentally for other semiconductor lasers[26,29] and has been attributed to several possible mechanisms.[30,31] Although very narrow linewidths have been measured for lasers with coupled cavities,[32] the present linewidth slopes, $2\Gamma P_1$, are believed to be the smallest so far reported for a solitary semiconductor laser at room temperature. Examination of Table 5.1 reveals that for the most highly coated devices, the increase in n_{sp} becomes a significant factor, as predicted theoretically.

For the theoretical estimates of linewidth given in Table 5.1 a value of 7 cm^{-1} was used for α_i; this average value was determined from experimental SQW gain curves.[33] The theoretical value of $|\alpha|$ used is 2.3. This is an average value from the calculations discussed in the previous section (see Figure 5.6). While SQWs have significantly narrower linewidths than bulk double heterostructures, the linewidths are not as narrow as predicted theoretically. If the calculated value for n_{sp} is accurate, $|\alpha|$ for uncoated devices is 3.9. It is reasonable that $|\alpha|$ is somewhat larger than predicted, since the calculations neglect the free-carrier absorption contribution to $\chi_R(E_L, N)$. The interband component is normally dominant;[25] however, the free-carrier contribution is expected to be dependent on the device structure.[34] In bulk BH (Al,Ga)As lasers $|\alpha|$ has been measured to be 6.2,[25] which is significantly larger than what is measured for other stripe bulk (Al,Ga)As heterostructure lasers such as channeled-substrate lasers. Therefore this discrepancy may be due to the relatively large free-carrier contribution in a buried stripe. The present results for uncoated devices confirm that $|\alpha|$ is reduced in SQW lasers. It is likely that other SQW stripe laser structures might have even narrower linewidths because of smaller free carrier contributions to $|\alpha|$. In the most highly coated devices the value of $|\alpha|$ depends strongly on how much n_{sp} is increased; however, the results suggest that

R_1	31%	31%	57%	85%	92%
R_2	31%	92%	89%	93%	92%
End Loss (cm^{-1})	46.8	25.1	13.6	4.7	3.3
n_{sp} Theory	1.0	1.4	1.9	7.3	8.2
$n_{sp}(1+\alpha^2)$ Theory	6.3	8.8	12.0	45.9	51.6
$2\Gamma P_1$ (MHz mW) Theory	10.7	8.1	2.9	0.79	0.34
$2\Gamma P_1$ (MHz mW) Experiment	28.3	17.5	5.3	5.9	2.1
Intercept (MHz) Experiment	0.9	5.9	2.7	2.2	6.8
$n_{sp}(1+\alpha^2)$ Experiment	17.1	17.9	17.9	120.7	95.4
$\|\alpha\|$ Experiment	3.9	3.4	2.9	3.9	3.3

Table 5.1: A summary of measured data and theoretical estimates for the spectral linewidth of 250 μm long 4 μm stripe buried GRIN SCH 70 Å SQW (Al,Ga)As SQW lasers with and without high reflectivity facet coatings. The theoretical estimates used for $|\alpha|$ and α_i are 2.3 and 7 cm^{-1}.

as expected, $|\alpha|$ is decreased slightly from its value in uncoated lasers.

Although the calculations explain the experimental results well when allowance is made for the free carrier contribution to $|\alpha|$, it should be remembered that they can only be considered to be estimates, since they depend on gain calculations which show inaccuracy compared to threshold current measurements (see Chapter 4) and differential gain values inferred from measurements of relaxation oscillation frequencies (see Chapter 6). α is directly proportional to the differential gain, so this inaccuracy could directly effect its calculated value.

5.5 Steps for Improvement

Although very narrow spectral linewidths were achieved for buried GRIN SCH SQWs with high reflectivity coatings, it is likely that the linewidth measurements reported can be improved upon. A buried heterostructure stripe laser is not the best structure for single mode operation[15] or for small linewidth enhancement factor;[34] for bulk DH active regions channeled-substrate lasers give better results than BH lasers. The channeled-substrate laser structure, however, requires LPE growth of the active region, which is not desirable for a QW. QW structures with similar waveguide properties, which should result in similar spectral properties, can be grown with MBE or MO-CVD growth over patterned substrates (see Figure 4.1). While narrow QW stripe structures like this have been fabricated[35,36,37,38] and single mode operation has been observed[35] their spectral linewidths have not been reported. It would be worthwhile to develop further the technology of fabricating these structures (in as narrow a stripe as possible for low threshold current) for applications which require a coherent laser source. The linewidth of QW stripe lasers formed by impurity induced disordering would also be interesting to investigate, since this structure has also shown single mode operation.[39] These other SQW

stripe structures are described in more detail in Chapter 4.

5.6 Conclusion

As predicted,[1] SQW lasers have much narrower spectral linewidths than bulk double heterostructure lasers. SQW lasers with high reflectivity coatings have dramatically narrower linewidths due to their low losses. Linewidths as narrow as 6.0 MHz at 1.27 mW output power were measured. If allowance is made for the free carrier contribution to the linewidth enhancement factor, the experimental results appear to fit theoretical predictions well.

While high reflectivity coatings result in a dramatic reduction in spectral linewidth for a SQW laser, for coherent applications it is not desirable to increase the reflectivity of the front facet as much as is possible. Increasing it beyond a certain point does not result in further significant linewidth reduction because the spontaneous emission factor increases, but does result in lower output power.

5.8 References

[1] A. Arakawa and A. Yariv, *IEEE J. Quantum Electron.* **QE-21**(10), pp. 1666-1674 (1985).

[2] S. Noda, K. Kojima, K. Kyuma, K. Hamanaka, and T. Nakayama, *Appl. Phys. Lett.* **50**(14), pp. 863-865 (1987).

[3] W. T. Tsang, *Electron. Lett.* **16**(25), pp. 939-941 (1980).

[4] G. H. B. Thompson, *Physics of Semiconductor Laser Devices,* p. 118, John Wiley & Sons, New York (1980).

[5] H. C. Casey and M. B. Panish, *Heterostructure Lasers, Part A: Fundamental Principles,* pp. 79-82, Academic Press, Orlando (1978).

[6] M. J. Adams, *An Introduction to Optical Waveguides,* John Wiley & Sons, New York (1981).

[7] G. H. B. Thompson, Ibid., p. 227.

[8] S. Wang, C.-Y. Chen, A. S.-H. Liao, and L. Figueroa, *IEEE J. Quantum Electron.* **QE-17**(4), pp. 453-468 (1981).

[9] P. A. Kirkby and G. H. B. Thompson, *J. Appl. Phys.* **47**(10), pp. 4578-4589 (1976).

[10] M. Yamada, *IEEE J. Quantum Electron.* **QE-19**(9), pp. 1365-1380 (1983).

[11] M. Nakamura, K. Aiki, N. Chinone, R. Ito, and J. Umeda, *J. Appl. Phys.* **49**(9), pp. 4644-4648 (1978).

[12] R. F. Kazarinov, C. H. Henry, and R. A. Logan, *J. Appl. Phys.* **53**(7), pp. 4631-4644 (1982).

[13] M. Nakamura and S. Tsuji, *IEEE J. Quantum Electron.* **QE-17**(6), pp. 994-1005 (1981).

[14] W. Streifer, D. R. Scifres, and R. D. Burnham, *Appl. Phys. Lett.* **40**(4), pp. 305-307 (1982).

[15] K. Y. Lau and A. Yariv, *Appl. Phys. Lett.* **40**(9), pp. 763-765 (1982).

[16] K. Y. Lau and A. Yariv, in *Semiconductors and Semimetals Volume 22: Lightwave Communications Technology* edited by W. T. Tsang, p. 86, Academic Press, New York (1985).

[17] T.-P. Lee, C. A. Burrus, J. A. Copeland, A. G. Dentai, and D. Marcuse, *IEEE J. Quantum Electron.* **QE-18**(7), pp. 1101-1113 (1982).

[18] D. Botez, *J. Opt. Commun.* **1**(2), pp. 42-50 (1980).

[19] M. Mittelstein, Y. Arakawa, A. Larsson, and A. Yariv, *Appl. Phys. Lett.* **49**(25), pp. 1689-1691 (1986).

[20] C. S. Harder, thesis, *Bistability, High Speed Modulation, Noise, and Pulsations in GaAlAs Semiconductor Lasers*, p. 15, California Institute of Technology, Pasadena (1983).

[21] K. Vahala and A. Yariv, *IEEE J. Quantum Electron.* **QE-19**(6),pp. 1096-1101 (1983).

[22] C. H. Henry, *IEEE J. Quantum Electron.* **QE-18**(2), pp. 259-264 (1982).

[23] H. Haug and H. Haken, *Z. Physik* **204**, pp. 262-275 (1967).

[24] J. I. Pankove, *Optical Processes in Semiconductors,* pp. 89-90, Dover Pub. Inc., New York (1971).

[25] C. H. Henry, R. A. Logan, and K. A. Bertness, *J. Appl. Phys.* **52**(7), pp. 4457-4461 (1981).

[26] W. Lenth, *Appl. Phys. Lett.* **44**(3), pp. 283-285 (1984).

[27] K. Vahala, L. C. Chiu, S. Margalit, and A. Yariv, *Appl. Phys. Lett.* **42**(8), pp. 631-633 (1983).

[28] D. Welford and A. Mooradian, *Appl. Phys. Lett.* **40**(10), pp. 865-867 (1982).

[29] D. Welford and A. Mooradian, *Appl. Phys. Lett.* **40**(7), pp. 560-562 (1982).

[30] K. Vahala and A. Yariv, *Appl. Phys. Lett.* **43**(2), pp. 140-142 (1983).

[31] R. J. Lang, K. J. Vahala, and A. Yariv, *IEEE J. Quantum Electron.* **QE-21**(5), pp. 443-451 (1985).

[32] T. P. Lee, C. A. Burrus, K. Y. Liou, N. A. Olsson, R. A. Logan, and D. P. Wilt, *Electron. Lett.* **20**(24), pp. 1011-1012 (1984).

[33] K. Y. Lau, P. L. Derry, and A. Yariv, *Appl. Phys. Lett.* **52**(2), pp. 88-90 (1988).

[34] M. Osiński, and J. Buus, *IEEE J. Quantum Electron.* **QE-23**(1), pp. 9-29 (1987).

[35] Y.-H. Wu, M. Werner, K.-L. Chen, and S. Wang, *Appl. Phys. Lett.* **44**(9), pp. 834-846 (1984).

[36] D. Fekete, D. Bour, J. M. Ballantyne, and L. F. Eastman, *Appl. Phys. Lett.* **50**(11), pp. 635-637 (1987).

[37] E. Kapon, J. P. Harbison, C. P. Yun, and N. G. Stoffel, *Appl. Phys. Lett.* **52**(8), pp. 607-609 (1988).

[38] E. Kapon, J. P. Harbison, C. P. Yun, and N. G. Stoffel, *Conference on Lasers and Electro-Optics*, Anaheim (1988).

[39] R. L. Thornton, R. D. Burnham, T. L. Paoli, N. Holonyak, Jr., and D. G. Deppe, *Appl. Phys. Lett.* **49**(3), pp. 133-134 (1986).

Chapter 6

Dynamic Characteristics of Buried Heterostructure Single Quantum Well (Al,Ga)As Lasers

6.1 Introduction

Buried heterostructure GRIN SCH SQW lasers with high reflectivity coatings are of great interest for applications such as optical interconnects in optical supercomputers. The dynamic characterstics of these lasers are clearly of interest, since these applications require high frequency modulation.

Semiconductor laser dynamics are commonly described by the rate equations for the photon and carrier densities:[1,2]

$$\frac{dN}{dt} = \frac{J}{eL_z} - \frac{c}{n_r}\frac{g(E_L,N)}{\Gamma}P - \frac{N}{\tau_s} \tag{6.1}$$

$$\frac{dP}{dt} = \frac{c}{n_r}g(E_L,N)P - \frac{P}{\tau_p} + \Gamma\beta\frac{N}{\tau_s} \tag{6.2}$$

where N is the carrier density, P is the photon density, J is the current density, L_z is the active region thickness, e is the absolute value of the electron charge, c is the speed of light, n_r is the refractive index of the active region, $g(E_L,N)$ is the modal gain at photon energy E_L, Γ is the optical confinement factor, τ_s is the carrier lifetime, and τ_p is the photon lifetime of the cavity.

$$\tau_p = \frac{n_r}{c\big(\alpha_i + (1/2L)\ln(1/R_1R_2)\big)} \tag{6.3}$$

where α_i is the internal loss, L is the cavity length, and R_1 and R_2 are the end facet reflectivities.

β is called the spontaneous emission factor, but is not equal to the spontaneous emission factor n_{sp}, which was defined in Chapter 5. β is the ratio of the spontaneous emission power into the lasing mode to the total spontaneous emission rate,[3]

while n_{sp} is the ratio of the spontaneous emission power into the lasing mode to the stimulated emission power of the mode.

In this chapter, some of the modulation properties of buried GRIN SCH SQW (Al,Ga)As lasers with and without high reflectivity coatings are examined. The time delay for switching the lasers on with no prebias is discussed. Measurement of the relaxation oscillation frequency, which is commonly considered to be the limit of the useful bandwidth of a semiconductor laser[2] is described and values of differential gain are derived from the measured relaxation oscillation frequencies. The results are compared with theoretical predictions made on the basis of Equations (6.1) and (6.2) and the gain calculations of Chapter 2.

6.2 Modulation Without Prebias

It is desirable to amplitude modulate semiconductor lasers without current prebias or a feedback circuit. When a current pulse of amplitude I is applied to an unbiased semiconductor laser, there is a time delay before lasing begins, because it takes time for a carrier population to build up. When the current pulse ends, it takes time for the carrier population to decay. If another identical pulse is applied before the carrier population decays fully, it will produce a larger light pulse than the first current pulse did. This phenomenon, which is illustrated in Figure 6.1, is called the pattern effect.[4] The pattern effect is clearly undesirable as it will distort information carried by the laser modulation. The pattern effect can be eliminated by prebiasing the laser at a current below threshold sufficient to maintain a carrier population. If the laser is prebiased, the prebias current must be monitored by a feedback circuit. This is undesirable since power and space are wasted.

Once a semiconductor laser reaches its threshold carrier density, the carrier density in the active region is clamped at approximately that value since additional

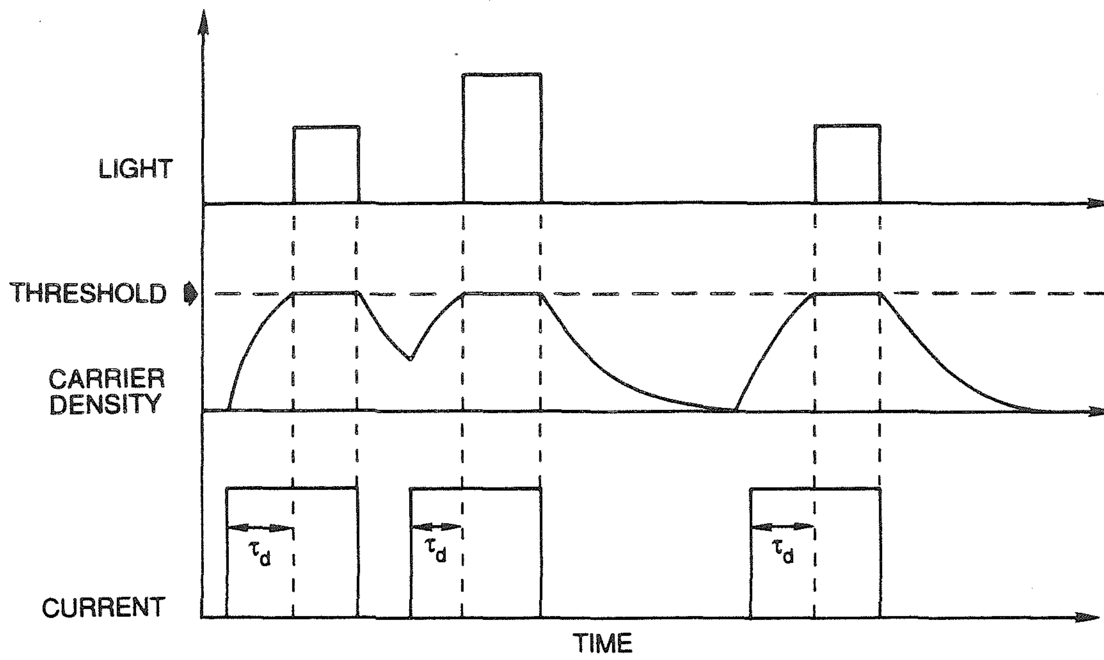

Figure 6.1: Schematic illustration of the pattern effect.

injected carriers will recombine by induced transitions. The turn-on time τ_d is therefore longer than the turn-off time, which is just the time for the carrier density to drop below its threshold value. τ_d can be determined from Equation (6.1). Before lasing begins $P = 0$. Substituting in $J = I/LW$, where I is the amplitude of the current pulse and W is the stripe width, below threshold Equation (6.1) simplifies to

$$\frac{dN}{dt} = \frac{I}{eL_zLW} - \frac{N}{\tau_s} \tag{6.4}$$

A solution of the form

$$N(t) = A + Be^{-Ct} \tag{6.5}$$

can be tried. At $t = 0$, $N(0) = 0$, so $B = -A$. Equation (6.4) becomes

$$\frac{I}{eL_zLW} - \frac{A}{\tau_s} + Ae^{-Ct}\left(\frac{1}{\tau_s} - C\right) = 0 \tag{6.6}$$

The coefficents of e^{-Ct} must equal zero so, $C = 1/\tau_s$. Similarly $A = I\tau_s/eL_zLW$. Substituting in the values of A and C Equation (6.5) becomes

$$N(t) = \frac{I\tau_s}{eL_zLW}(1 - e^{-t/\tau_s}) \tag{6.7}$$

When $t = \tau_d$, $N(\tau_d)$ equals the threshold carrier density N_{th}. N_{th} is the steady state solution of Equation (6.4) so

$$N_{th} = \frac{I_{th}\tau_s}{eL_zLW} \tag{6.8}$$

where I_{th} is the cw threshold current. Equating Equation (6.7) at $t = \tau_d$ and Equation (6.8) gives

$$\frac{I_{th}}{I} = 1 - e^{-\tau_d/\tau_s} \tag{6.9}$$

Equation (6.9) can be solved for τ_d

$$\tau_d = -\tau_s \ln\left(1 - \frac{I_{th}}{I}\right) \tag{6.10}$$

In the limit of I much larger than I_{th} Equation (6.10) becomes

$$\tau_d \approx \tau_s \frac{I_{th}}{I} \tag{6.11}$$

Therefore if I_{th} is very small compared to I, τ_d should be short. If τ_d is small enough the pattern effect will be eliminated without any prebias. Unfortunately the current pulse required for a conventional DH stripe laser with a normal I_{th} is too large to be practical. Taking $\tau_s \sim 2$ ns with $I_{th} = 10$ mA a current pulse of ~400 mA would be required to reduce τ_d to 50 ps. If I_{th} is very low (submilliampere) it should be possible to solve this problem. If $I_{th} = 0.9$ mA a current pulse of only ~36 mA would be sufficient to reduce τ_d to 50 ps. As described in Chapter 4 narrow (1 μm wide) buried GRIN SCH SQW (Al,Ga)As lasers with high reflectivity coatings have submilliampere threshold currents.

The turn-on time delay without prebias has been measured for these lasers by K. Y. Lau.[5,6] The drive pulse amplitude was controlled by a broadband continuously variable rf attenuator. The pulse shape was maintained in all measurements. To accurately measure the switch-on delay down to <50 ps time scale it was assumed that the laser turns off without delay at the termination of the current pulse; this assumption was well supported by the observed data. Figure 6.2 shows the measured τ_d as a function of I for a buried GRIN SCH 100 Å SQW laser with a cavity length of 250 μm, ~70% reflectivity coatings on both end facets and a cw threshold current of 0.9 mA. The results demonstrate that the laser had a τ_d of only 20 to 50 ps with a modest 30 mA pulse drive.

Relaxation oscillations are small amplitude oscillations about the steady state values of the carrier and photon densities. These oscillations occur when a semiconductor laser first reaches threshold, because of the time required for the carrier and photon populations to come into equilibrium.[1] Figure 6.3 is a schematic illustration of relaxation oscillations of the photon density. The pulse responses of

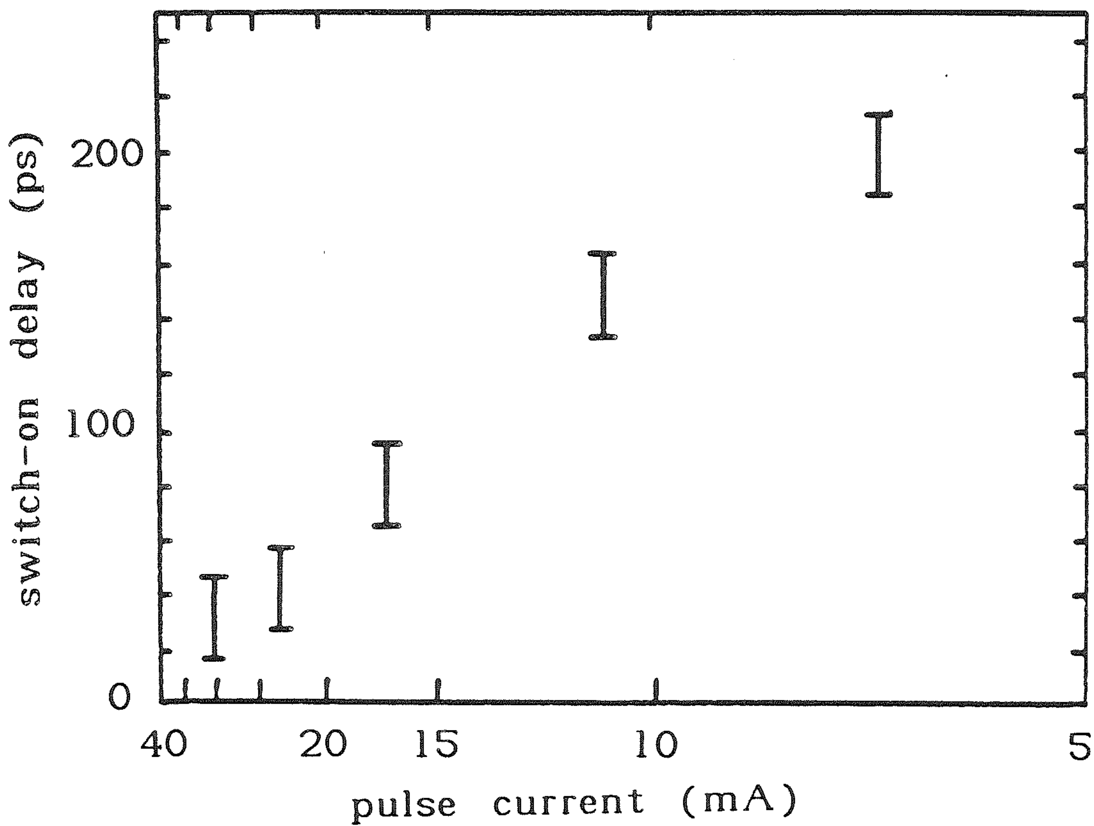

Figure 6.2: Measured switch-on delay vs pulse current amplitude for a 250 μm long 1 μm wide buried GRIN SCH 70 Å SQW (Al,Ga)As laser with ~70% reflectivity end facet facet coatings and a CW threshold current of 0.9 mA.

narrow buried GRIN SCH SQW lasers showed no relaxation oscillations; this is not believed to be related to the QW since it is also observed for conventional BH lasers. It may be caused by critical damping due to the relatively large β of the BH laser structure.[2,7]

When driven by two consecutive current pulses separated by as little as 200 ps (limited by the risetime of the pulser) the narrow buried GRIN-SCH SQW lasers with high reflectivity coated facets showed no pattern effect.

The modulation characteristics of narrow buried GRIN SCH SQW (Al,Ga)As lasers, with high reflectivity coatings and without prebias, are discussed further in References 5 and 6. The experimental results show significant improvement over what would be achieved with conventional DH stripe lasers. The improvement is due to the submilliampere threshold currents of these lasers. This is an important result, since a short τ_d is needed for successful implementation of optical interconnects in optical supercomputers.

6.3 Relaxation Oscillation Frequency: Theory

Although relaxation oscillations were not observed in the pulse response of narrow buried GRIN SCH SQW lasers, the relaxation oscillation frequency is still an important parameter. For many communication applications, semiconductor lasers which are modulated to carry information are prebiased at a current greater than the threshold current. They are then modulated at high frequencies through small amplitudes about the continous current prebias. The frequency response of a semiconductor laser has the typical shape expected from a second order system. (For a discussion of the frequency response of a second order system see Reference 8.) The laser amplitude response is fairly uniform at frequencies less than the relaxation oscillation frequency f_r. At f_r the response goes through a resonance

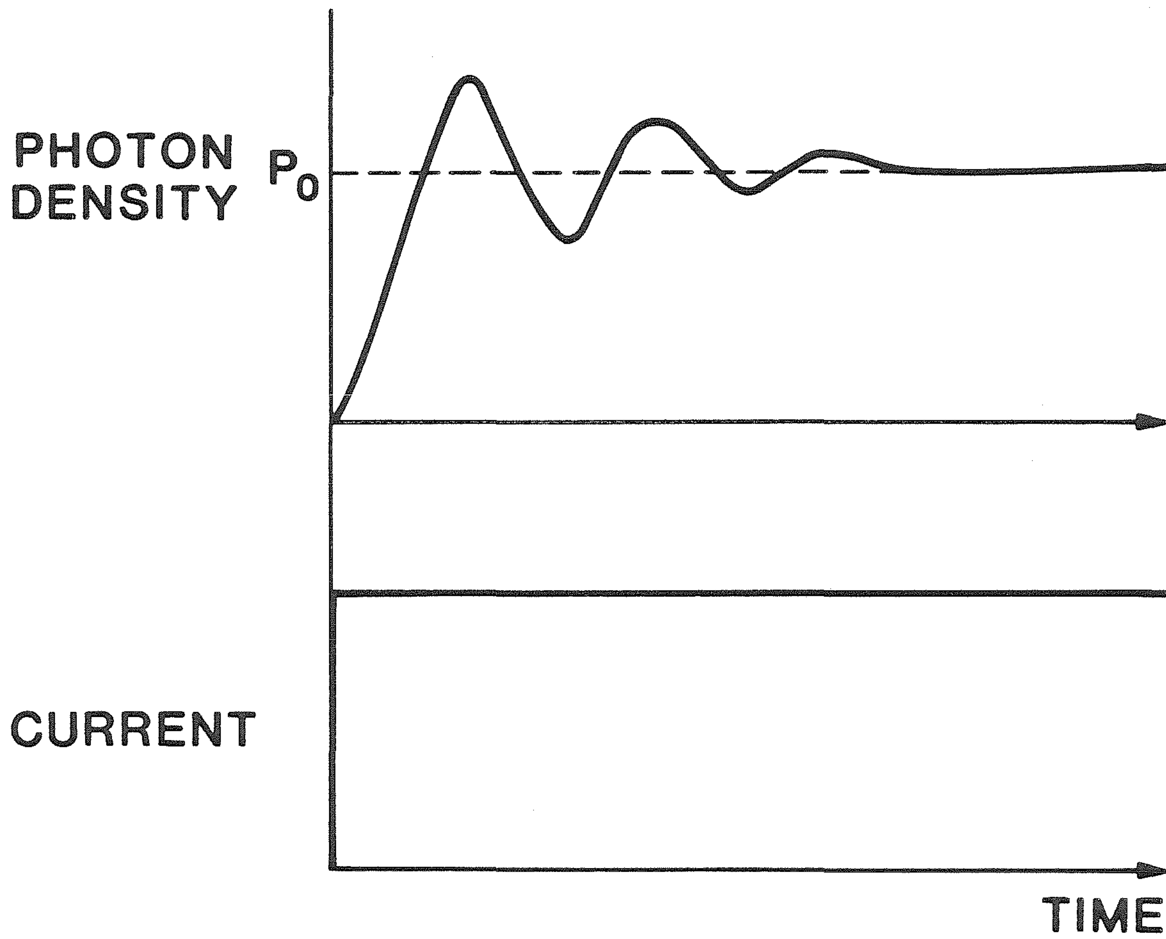

Figure 6.3: Schematic illustration of relaxation oscillations of the photon density of a semiconductor laser when current is first applied.

and then drops off sharply. The relaxation oscillation frequency, which is also called the corner frequency, is therefore commonly considered to be the limit of the useful modulation bandwidth of a semiconductor laser.[2]

The value of f_r can be derived from Equations (6.1) and (6.2).[1] First consider the steady state values of N and P above threshold. The steady state value of N is the threshold value N_{th} since the carrier density in the active region is clamped above threshold. Above threshold the spontaneous emission term in Equation (6.2) is small compared to the other terms and can be neglected. For the steady state photon density P_o for a particular current above threshold Equation (6.2) becomes

$$P_o\left(\frac{c}{n_r}g(E_L,N_{th})-\frac{1}{\tau_p}\right)\approx 0 \tag{6.12}$$

therefore

$$\frac{c}{n_r}g(E_L,N_{th})=\frac{1}{\tau_p} \tag{6.13}$$

Using Equations (6.13) (in terms of I) and (6.8) for the steady state above threshold Equation (6.1) is

$$\frac{I}{eL_zLW}-\frac{P_o}{\Gamma\tau_p}-\frac{I_{th}}{eL_zLW}=0 \tag{6.14}$$

Solving for P_o

$$P_o=\Gamma\tau_p\frac{(I-I_{th})}{eL_zLW} \tag{6.15}$$

Now consider small deviations from the steady state where $N=N_{th}+\Delta N$ and $P=P_o+\Delta P$. Using the first two terms of a Taylor expansion around N_{th}

$$g(E_L,N)\approx g(E_L,N_{th})+\Delta N\frac{dg(E_L,N_{th})}{dN} \tag{6.16}$$

Equations (6.1) and (6.2) become

$$\frac{d\Delta N}{dt}=-\frac{c}{n_r\Gamma}\frac{dg(E_L,N_{th})}{dN}P_o\Delta N-\frac{\Delta P}{\Gamma\tau_p}-\frac{\Delta N}{\tau_s} \tag{6.17}$$

$$\frac{d\Delta P}{dt} = \frac{c}{n_r}\frac{dg(E_L, N_{th})}{dN} P_o \Delta N \tag{6.18}$$

where Equation (6.13) has been used, the terms equal to dN_{th}/dt and dP_o/dt are omitted since their sums are zero, and terms containing $\Delta N \Delta P$ are neglected since they are small compared to the others. Consider solutions of the form

$$\Delta N = Be^{-(\xi - i)\omega t}, \ \Delta P = Ce^{-(\xi - i)\omega t} \tag{6.19}$$

Equations (6.17) and (6.18) become

$$-(\xi - i)\omega B = -\frac{c}{n_r \Gamma}\frac{dg(E_L, N_{th})}{dN} P_o B - \frac{C}{\Gamma \tau_p} - \frac{B}{\tau_s} \tag{6.20}$$

$$-(\xi - i)\omega C = -\frac{c}{n_r}\frac{dg(E_L, N_{th})}{dN} P_o B \tag{6.21}$$

Solving Equation (6.21) for C, substituting this value for C into Equation (6.20) and separating the resulting equation into real and imaginary parts results in

$$\xi\omega - \frac{c}{n_r \Gamma}\frac{dg(E_L, N_{th})}{dN} P_o + \frac{\xi}{\omega(\xi^2 + 1)}\frac{c}{n_r \Gamma}\frac{dg(E_L, N_{th})}{dN}\frac{P_o}{\tau_p} - \frac{1}{\tau_s} = 0 \tag{6.22}$$

$$1 - \frac{1}{\omega^2(\xi^2 + 1)}\frac{c}{n_r \Gamma}\frac{dg(E_L, N_{th})}{dN}\frac{P_o}{\tau_p} = 0 \tag{6.23}$$

Equation (6.23) simplifies to

$$\omega^2 = \frac{1}{(\xi^2 + 1)}\frac{c}{n_r \Gamma}\frac{dg(E_L, N_{th})}{dN}\frac{P_o}{\tau_p} \tag{6.24}$$

Substituting $\xi^2 + 1$ from Equation (6.24) into Equation (6.22) and solving for ξ results in

$$\xi = \frac{1}{2\omega}\left(\frac{c}{n_r \Gamma}\frac{dg(E_L, N_{th})}{dN} P_o + \frac{1}{\tau_s}\right) \tag{6.25}$$

It turns out that ξ^2 is normally small compared to 1 so

$$\omega \approx \sqrt{\frac{c}{n_r \Gamma}\frac{dg(E_L, N_{th})}{dN}\frac{P_o}{\tau_p}} \tag{6.26}$$

$f_r = \omega/2\pi$ therefore

$$f_r = \frac{1}{2\pi}\sqrt{\frac{c}{n_r\Gamma}\frac{dg(E_L, N_{th})}{dN}\frac{P_o}{\tau_p}} \tag{6.27}$$

This is the same equation as is normally obtained with a simple linear gain dependence on carrier density although it is usually written as[2]

$$f_r = \frac{1}{2\pi}\sqrt{A\frac{P_o}{\tau_p}} \tag{6.28}$$

where A is the optical gain parameter, which is defined as

$$A = \frac{c}{n_r\Gamma}\frac{dg(E_L, N_{th})}{dN} \tag{6.29}$$

Normally for a conventional DH $dg(E_L, N_{th})/N$ and A are approximated as being independent of N_{th}; however, this is not a good approximation for a QW since the gain is not a linear function of carrier density (see Figure 2.2), because of gain saturation as the first quantized level is filled.

For an uncoated SQW and a conventional DH laser of the same dimensions, values of P_o should be in the same range although P_o is of course a function of I. (Since P_o increases as I increases, higher values of f_r can be expected for large values of I.) τ_p (see Equation (6.3)) will be sightly larger for the SQW because of the lower internal loss, but since the end loss is much larger for an uncoated device of normal length the difference in τ_p should not be large. Therefore any large change in f_r for a QW compared to that of a bulk DH laser will be due to the value of A. A typical value of A for a conventional (Al,Ga)As DH laser at room temperature is 2.8×10^{-6} cm^3 sec^{-1}.[9] For the SQW the predicted value of A can be determined from the derivative of Equation (2.10) with respect to N.

$$A(E_L, N_{th}) = \frac{c}{n_r}\int \frac{C_{QW}(E_L)\mathcal{D}_{QW}(E)\big(df_c(E, N_{th})/dN - df_v(E, N_{th})/dN\big)\hbar\gamma}{(E - E_L)^2 + (\hbar\gamma)^2}\, dE \tag{6.30}$$

where rigorous k-selection is assumed and intraband relaxations are accounted for with a Lorentzian broadening function. For an uncoated 4 μm wide 250 μm long buried GRIN SCH 70 Å SQW with a cw threshold current of ~7 mA the predicted value of A is 1.1×10^{-6} cm^3 sec^{-1}. The calculations therefore predict that f_r for a SQW will be smaller than that of a bulk DH laser.

Now consider f_r for a SQW laser with high reflectivity end facet coatings, which will have a lower N_{th} than an uncoated SQW. A should be larger, since the slope of the gain curve versus carrier density is larger for low carrier densities (see Figure 2.2). Since less of the stimulated power leaves the lasing cavity, larger P_o's will be possible than without coatings. The increase in A and P_o will increase f_r; however, τ_p will also increase, which will decrease f_r. It is not immediately clear which factors will dominate, since P_o cannot be measured directly. Equation (6.15) relates P_o to measurable quantities. Substituting it into Equation (6.27) results in

$$f_r = \frac{1}{2\pi}\sqrt{\frac{\Gamma ALWI_{th}}{eL_z}\left(\frac{I}{I_{th}} - 1\right)} \tag{6.31}$$

Here everything except A is a known or measurable quantity, which makes numerical comparison between uncoated and coated SQW lasers easier. The calculated value of f_r is plotted in Figure 6.4 as a function of $\sqrt{I/I_{th} - 1}$ for a 4 μm wide 250 μm long GRIN SCH 70 Å SQW without coatings and one with R_1=60% and R_2=90%. The calculated value of A for the coated laser is 3.2×10^{-6} cm^3 sec^{-1}.

As a function of $\sqrt{I/I_{th} - 1}$ the calculated f_r is very similar for coated and uncoated lasers. The calculations therefore suggest that A is not increased sufficiently to increase f_r (as a function of $\sqrt{I/I_{th} - 1}$) when high reflectivity coatings are applied. However, since I_{th} is decreased significantly by high reflectivity coatings, as a function of I f_r is improved. In addition it might be possible to operate a coated laser at higher values of $\sqrt{I/I_{th} - 1}$ resulting in higher values of f_r than could be reached without coatings.

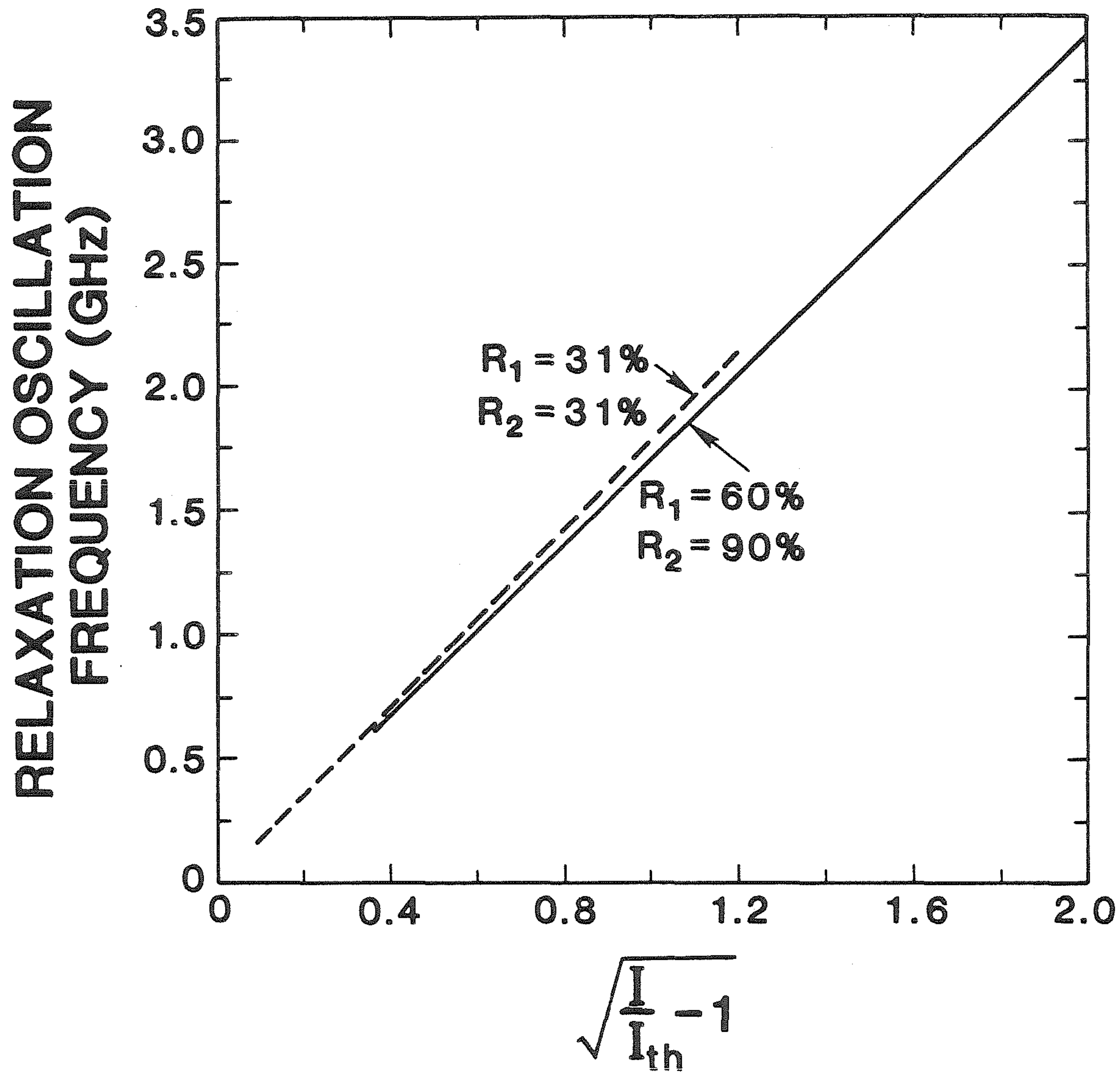

Figure 6.4: Calculated relaxation oscillation frequency as a function of $\sqrt{I/I_{th} - 1}$ for an uncoated 250 μm long 4 μm wide buried GRIN SCH 70 Å SQW (Al,Ga)As laser and one with R_1 = 60% and R_2 =90%.

6.4 Parasitics

The derivation of the relaxation oscillation frequency given in the previous section is rather simplistic since it is based on the rate equations, which consider only one type of carrier, neglect the spatial dependences of the carrier and photon distributions, and neglect carrier diffusion. In addition the spontaneous emission term of Equation (6.2) was neglected in the derivation. Generally the neglected effects are important when considering damping of the relaxation oscillations.[2,10,11] The formula derived for f_r is accurate for most semiconductor lasers for values of f_r up to several GHz. To understand the typical behavior when f_r is expected to be higher, it is necessary to consider the laser parasitics.

Figure 6.5 is a simple equivalent circuit, which describes the parasitic elements influencing a semiconductor laser under modulation when it is driven by a 50 Ω voltage source,[2] which is a typical experimental condition. Here L is inductance from the bond wire to the p-type contact, R_c is contact resistance, and C is parasitic capacitance between the laser contacts through layers surrounding the laser. For the case of a buried stripe laser, C is capacitance through the burying layers. Contributions through the laser diode itself are neglected since they are small compared to the external elements. The resonant frequency of this circuit is

$$f_o = \frac{1}{2\pi}\sqrt{\frac{50 + R_c}{LR_cC}} \tag{6.32}$$

The circuit is strongly damped so no resonance peak occurs; instead, the response simply drops off.[2,12] Depending on the values of L, R_c, and C, the damping can be large enough to cause appreciable drop off at frequencies below f_o. The amplitude response of a modulated semiconductor laser will begin to drop off at frequencies at which the response of the parasitics drops off even if f_r (as calculated by Equation (6.28)) is higher. Therefore the maximum measured value of f_r will be in the

vicinity of f_o. When laser modulation response is strongly affected by parasitics, the resonance peak at f_r will be reduced because of the damping in the circuit.

The amount of inductance depends on the length of the bond wire; typical values are from 0.2 nH to 1.0 nH. R_c and C depend on the laser structure. For a buried heterostructure on a conducting substrate typical values[2,13] are $R_c \approx 10\ \Omega$ and $C \approx 10$ pF. Taking L as 0.5 nH the resulting f_o for a BH laser is ~5.5 GHz. Thus for this laser structure the measured f_r cannot be expected to be greater than approximately 5 GHz even if the laser parameters (A, τ_p, etc.) suggest higher values.

6.5 Relaxation Oscillation Frequency: Experiment

For frequency response measurements a standard measurement system[2] was utilized. 250 μm long 4 μm wide buried GRIN SCH 70 Å SQW (Al,Ga)As lasers with and without high reflectivity end facet coatings were mounted in a microwave package, and DC bias currents I and microwave signals were applied through a bias-T. The frequency responses were measured with a high speed p-i-n photodiode. The modulation was generated by a sweep oscillator (Hp8350A) used in conjunction with a network analyser (Hp8410B) and a microwave s-parameter test set (Hp8746B). The actual measured response expressed in dB is $20\log(I_{pd}(f)/I_{mod}(f))$ plus a frequency independent offset, where $I_{pd}(f)$ is the current response of the photodiode to the modulated laser at frequency f, and $I_{mod}(f)$ is the amplitude of the current modulation applied to the laser at freqency f. The quantity of interest, the modulation response of the laser expressed in dB, is $20\log(P(f)/I_{mod}(f))$, where $P(f)$ is the output power from the laser when it is modulated at frequency f. $P(f) = KI_{pd}(f)T(f)$, where K is a constant, and $T(f)$ is a factor which accounts for nonuniform frequency response of the photodiode detector. The amplitude re-

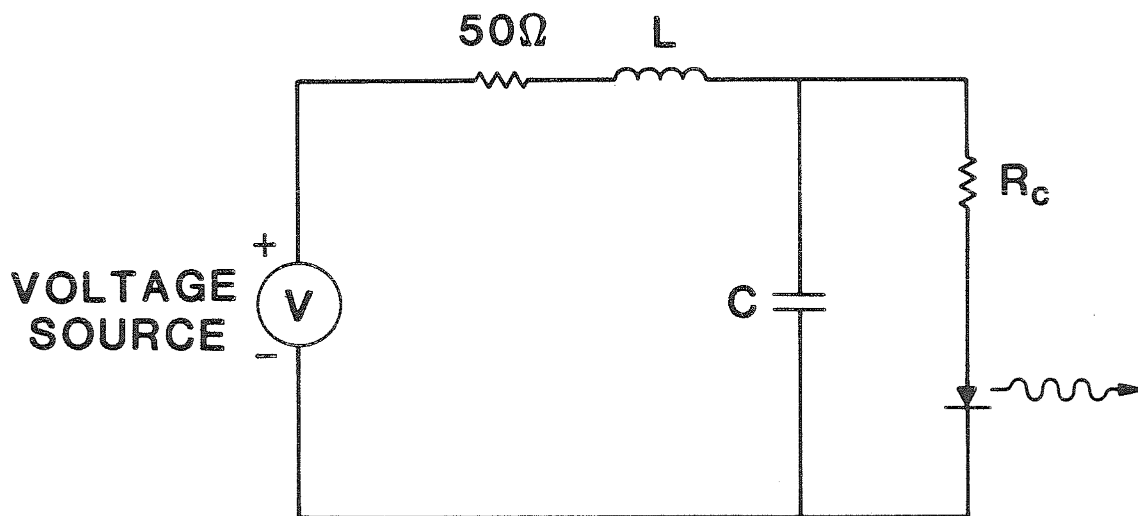

Figure 6.5: Equivalent circuit of the parastic elements affecting the modulation of a semiconductor laser driven by a 50 Ω voltage source.

sponse of the laser in dB is related to the measured value as follows:

$$20\log\frac{P(f)}{I_{mod}(f)} = 20\log\frac{I_{pd}(f)}{I_{mod}(f)} - 20\log T(f) + f \text{ independent offset} \quad (6.33)$$

The frequency dependence of the response of the photodiode $20\log T(f)$ was determined by examining the photodiode's response to a mode-locked dye laser. The dye laser produced pulses of 3-4 ps so the pulses have a flat spectrum in the frequency range of interest (0.6-8 GHz). The frequency of the pulse repetition was 100 MHz so the points at which the frequency response could be measured were separated by this amount. Under these conditions the response of the photodiode was measured with a microwave spectrum analyzer. Figure 6.6 is a plot of the frequency response of the photodiode after smoothing. The response is clearly nonuniform, which is why it was necessary to calibrate the photodiode.

It was necessary to smooth all of the measured data to lessen the effects of noise. Figure 6.7 is a plot of the amplitude response of an uncoated buried GRIN SCH SQW at several DC bias levels after smoothing and correcting for the photodiode response. This laser had a cw threshold current of 7.4 mA. Figure 6.8 is a similar plot for a laser with coated facet reflectivities of 57% and 89% and a cw threshold current of 3.7 mA.

For each bias level f_r is the frequency at which the resonance peak occurs. The measured f_r's determined from the amplitude responses at various bias levels are plotted as a function of $\sqrt{I/I_{th} - 1}$ in Figure 6.9. The measured values of f_r reached 5 GHz for both devices. f_r for the coated laser was similar to that of the uncoated laser as predicted theoretically. For both the coated and uncoated lasers, however, f_r was higher than predicted (compare Figure 6.9 with Figure 6.4). The calculations therefore explain the results qualitatively but not quantitatively. On the basis of the measured values of f_r, A in the uncoated laser was 3.3×10^{-6} cm^3 sec^{-1}, which is very similar to A (2.8×10^{-6} cm^3 sec^{-1}) in conventional DH

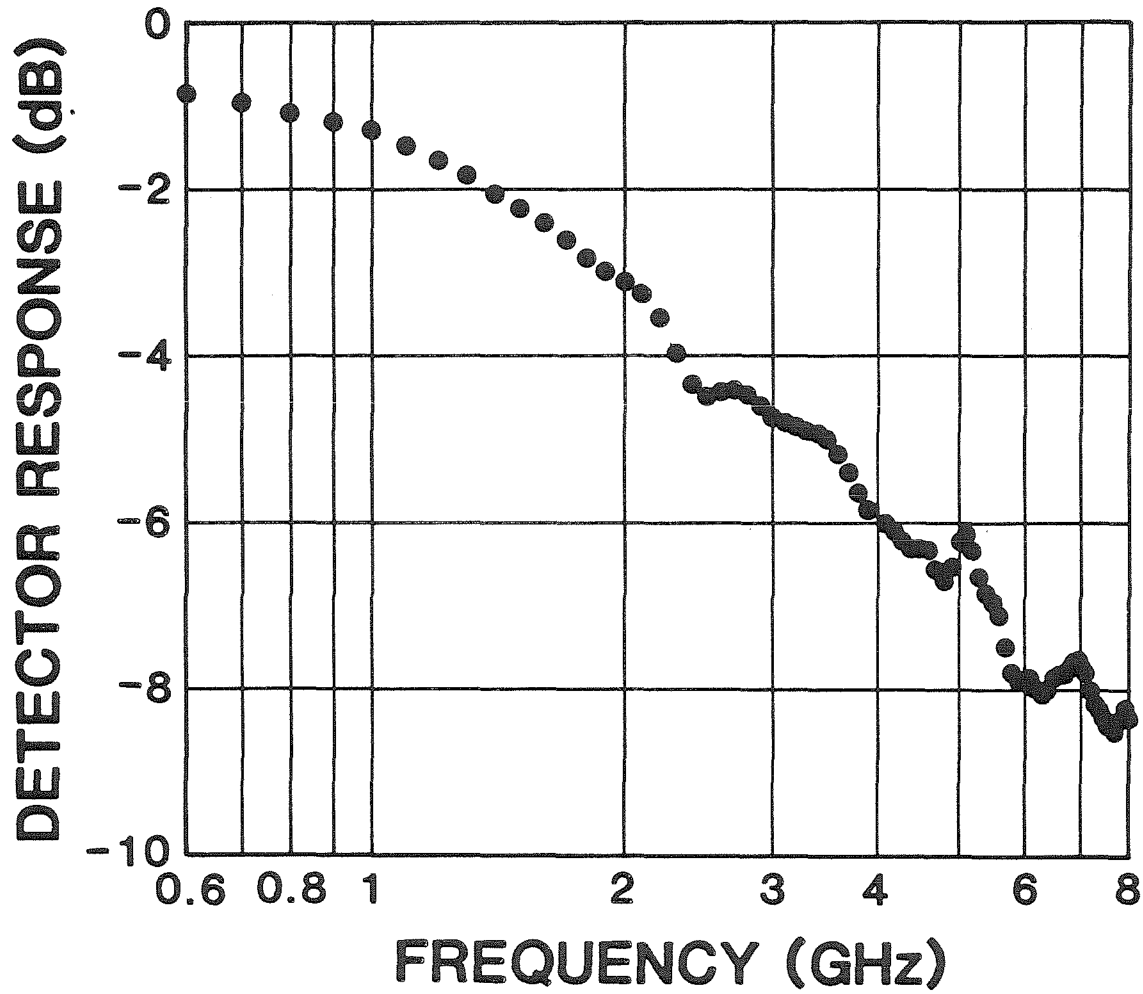

Figure 6.6: Smoothed frequency response of the p-i-n photodiode detector.

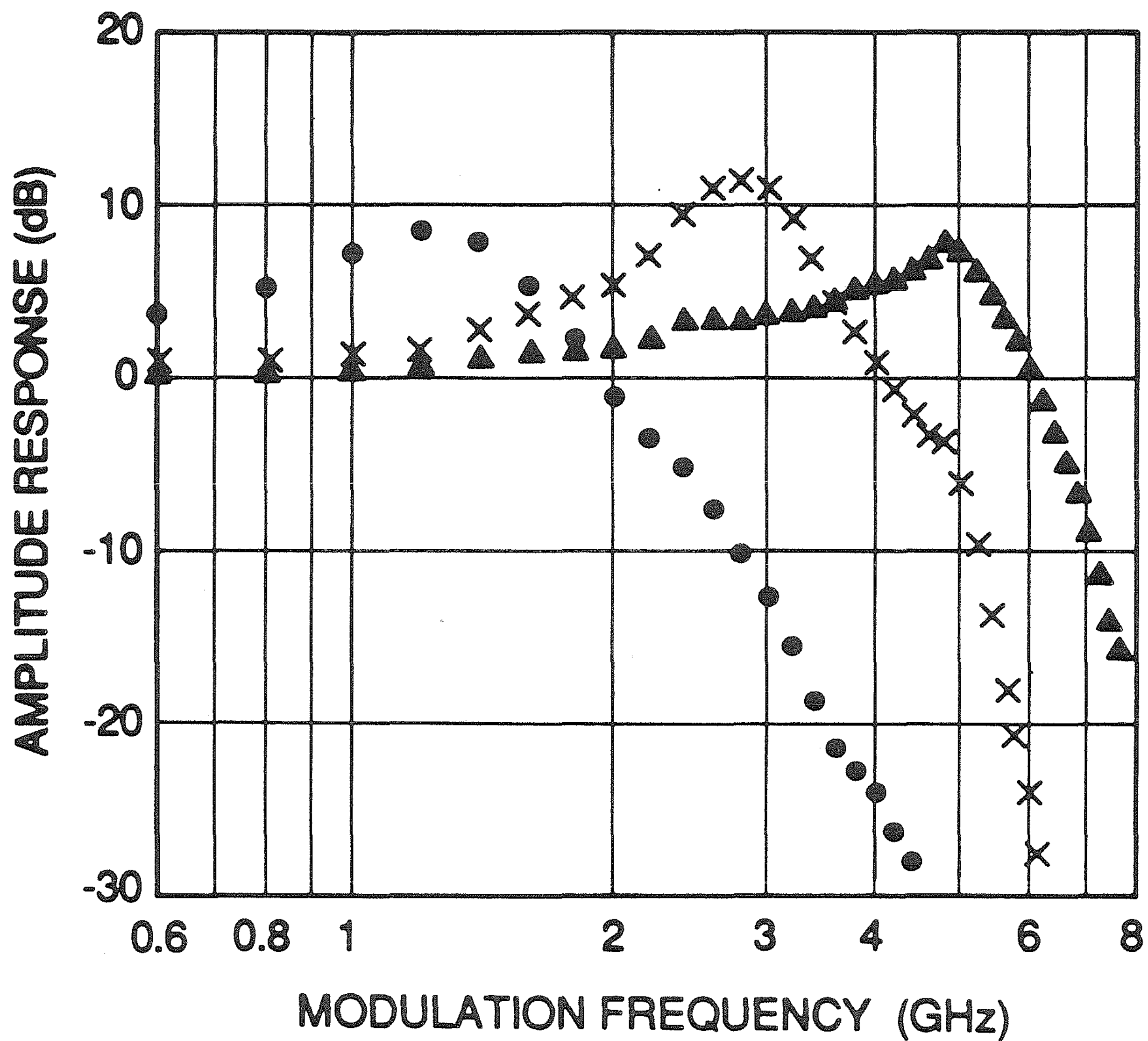

Figure 6.7: Modulation amplitude response of a 250 μm long 4 μm wide buried GRIN SCH 70 Å SQW laser at DC bias levels (current, power output at one facet) of ● 10.0 mA, 0.8 mW, × 14.0 mA, 2.5 mW, and ▲ 25.0 mA, 7.3 mW.

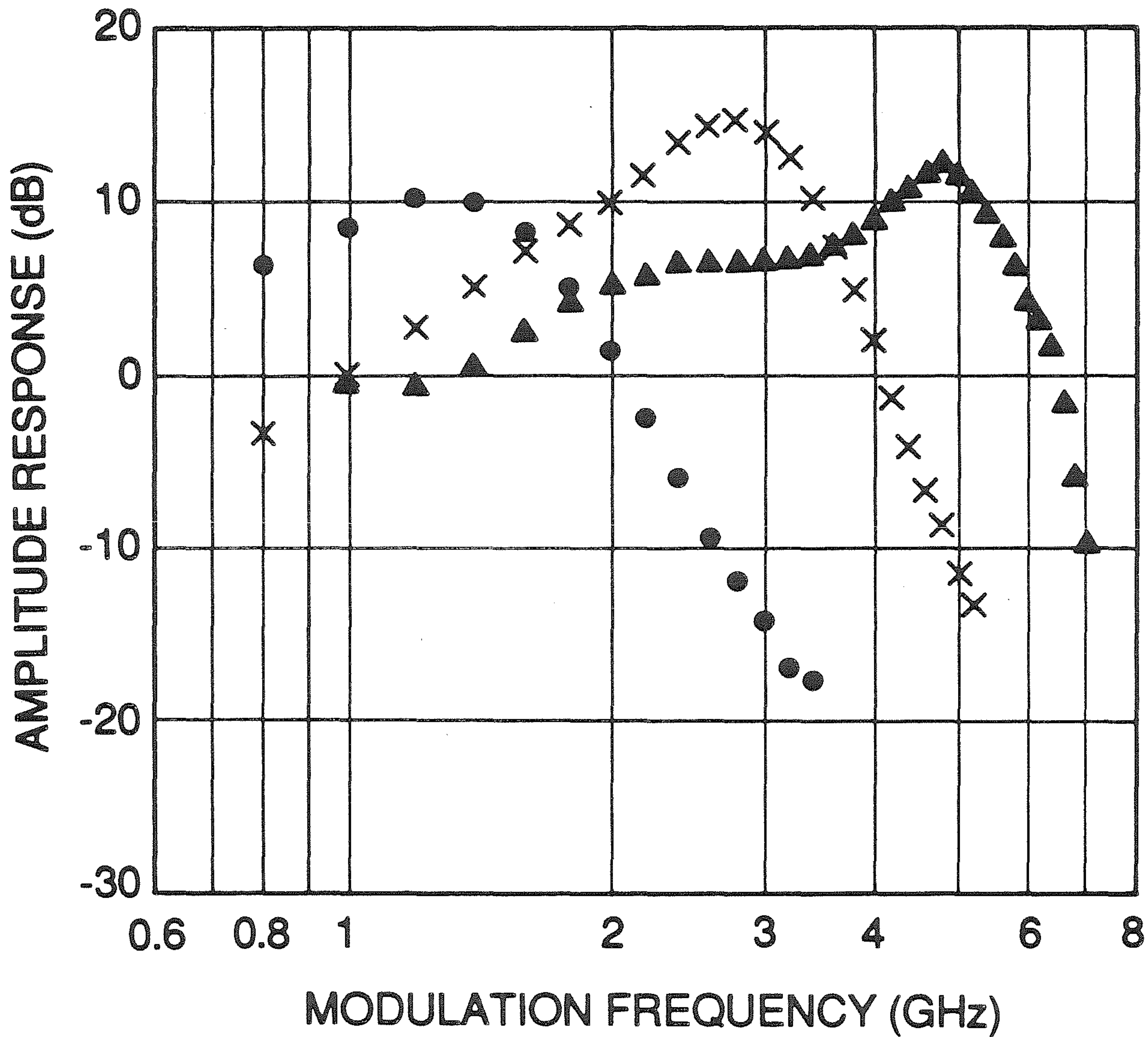

Figure 6.8: Modulation amplitude response of a 250 μm long 4 μm wide buried GRIN SCH 70 Å SQW laser with facet reflectivities of 57% and 89% at DC bias levels (current, power output at facet with 57% reflectivity) of ● 4.5 mA, 0.7 mW, × 6.5 mA, 1.9 mW, and ▲ 12.0 mA, 5.3 mW.

(Al,Ga)As lasers.[9] In the device with R_1= 57% and R_2 = 89% A increased to 6.2×10^{-6} cm^3 sec^{-1}.

While the experimental values of A fit the theoretical prediction of higher differential gain in a QW when the threshold gain is decreased, the actual numbers are roughly twice what was predicted by the calculations. There are several potential sources of error in the calculation of A. As discussed in Section 4.6, the most likely of the possible causes of the observed inaccuracy is the use of a Lorentzian lineshape function to account for intraband relaxations. Recent theoretical work by Yamanishi and Lee[14] has shown that the use of a Lorentzian lineshape function may cause the gain to be underestimated. As discussed in Section 4.6, adjusting the value of the intraband relaxation time does not improve the results obtained. The problem appears to result from the width of the Lorentzian lineshape; it causes transitions far away from the lasing energy to contribute to the gain. The work of Yamanishi and Lee shows that a narrower lineshape function results in a higher gain peak. A higher gain peak would mean that the gain saturates at a higher value than calculated (see Figure 2.2). If this were true the slope of the gain versus carrier density curve would be larger in the region of interest, which would result in higher values of A as observed experimentally.

The Lorentzian lineshape function has become the established method of accounting for intraband relaxations for calculations of the gain of QW semiconductor lasers.[15,16,17,18,19] The comparison of such calculations with experimental results reported here suggests that their theoretical basis should be examined further. These calculations are, however, accurate enough to explain the observed experimental trends.

While the measured values of f_r were not changed greatly by the application of high reflectivity end facet coatings, the amplitude of the resonance peak was

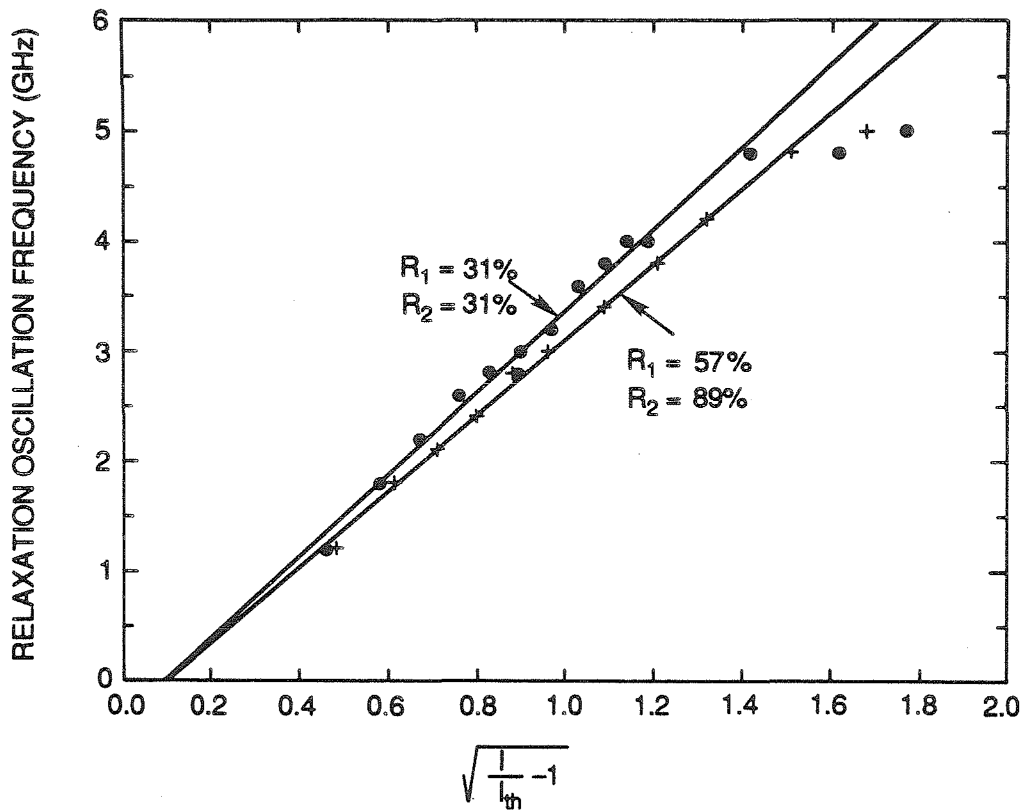

Figure 6.9: Relaxation oscillation frequency as a function of $\sqrt{I/I_{th} - 1}$ for an uncoated 250 μm long 4 μm wide buried GRIN SCH 70 Å SQW (Al,Ga)As laser and one with R_1 = 57% and R_2 =89%.

increased by coatings (compare Figures 6.7 and 6.8). It has previously been observed that anti-reflection coatings decrease the resonance peak height.[20] This result was predicted by considering the nonuniform distribution of photons and carriers along the length of a laser cavity with low end facet reflectivity.[21] Consideration of these effects, which are larger with low reflectivity end facets and are neglected by the simple rate Equations (6.1) and (6.2), shows that they produce damping which reduces the resonance peak. This effect might be the cause of the observed increase in resonance with the application of high reflectivity coatings.

For both the uncoated and coated lasers, the slope of the decreasing amplitude response at frequencies above f_r was steeper for high values of f_r around 5 GHz. For values of f_r below ~5 GHz, a change in the slope of the amplitude response as a function of frequency occurred at ~5 GHz. These effects are not predicted by the rate equations. The slope of a line asymptotic to the the amplitude of the frequency response of a second order system should be -40 dB per decade for frequencies above f_r regardless of the value of f_r or the amount of damping.[8] As noted in Section 6.4, the frequency response of the parasitics affecting a semiconductor laser has a sharp decay because the damping is strong enough to supress the resonance. Parasitics could, therefore, cause the the steeper decays observed above 5 GHz. The strong damping associated with the parasitics could also cause reduced amplitudes for resonance peaks. Reduced resonance peaks were observed for both coated and uncoated lasers at large values of f_r around 5 GHz. It has recently been shown experimentally that when the effect of parasitics on a transverse junction stripe laser is eliminated, the amplitude of the resonance peak increases with increasing f_r (for values of f_r in the range measured) and the slope of the amplitude response at frequencies above f_r does not depend on the value of f_r.[22,23] (For very high values of f_r, which have a large amount of damping, the resonant peak would be

expected to decrease even without parasitics.)

The theory that parasitics begin to affect the laser response around 5 GHz is also supported by the plot of f_r versus $\sqrt{I/I_{th}-1}$ in Figure 6.9. Around 5 GHz the linear dependence of f_r on $\sqrt{I/I_{th}-1}$ begins to disappear. The intrinsic properties of a semiconductor laser would not produce this effect. As discussed in Section 6.4, the parasitics affecting the laser could produce this result. 5 GHz is a reasonable estimate of the frequency at which the effect of parasitics would be significant for a buried heterostructure laser fabricated on a conducting substrate. Therefore strong evidence exists that the nonlinear dependence of f_r on $\sqrt{I/I_{th}-1}$ and the changes in the shape of the laser response curve around 5 GHz are due to parasitics.

6.6 Steps for Improvement

The experimental results described in the previous section suggest that if parasitics, especially parasitic capacitance, could be reduced, higher values of f_r could be reached at high bias levels for both coated and uncoated GRIN SCH SQW stripe lasers. A way to reduce the parasitic capacitance of a buried heterostructure laser is to fabricate the laser on a semi-insulating substrate.[2,12,13,24] A reasonable value for C for a BH on a semi-insulating substrate is 4 pF.[2] Since both contacts are on the top of this structure, the distance between them is shorter than that with a conducting substrate, so the resistance between them will be smaller. A reasonable value is $R_c \approx 4\ \Omega$.[2] Using these values of C and R_c and $L = 0.5$ nH Equation (6.32) gives a resonant frequency f_o of ~13 GHz for the equivalent circuit describing the parasitics. With a short bond wire L could be reduced to approximately 0.2 nH giving an upper limit of ~21 GHz for f_o. Since the 250 μm long 4 μm wide buried GRIN SCH SQW lasers could be operated at bias levels higher than that required to reach $f_r \approx 5$ GHz, it is likely that with semi-insulating substrates higher values

of f_r could be achieved. The lasers described here could be operated with values of $\sqrt{I/I_{th}-1}$ as large as 3.6. Assuming approximately the same operating range and slope for f_r as a function of $\sqrt{I/I_{th}-1}$, buried GRIN SCH SQW lasers on semi-insulating substrates would have values of f_r as high as 12 GHz. These values are similar to the best values achieved for conventional DH (Al,Ga)As lasers at room temperature.[24]

For conventional DH lasers the best lasers for modulation have short cavities[2,12,13,24] since τ_p is reduced with a short cavity and A is approximately constant for bulk DH lasers. For QW lasers, calculations indicate that the advantage would not be significant. Due to gain saturation, the increased threshold gain of a short cavity QW laser would result in a decrease in A, which would offset the reduction of τ_p.

Another structure modification that improves f_r for conventional DH lasers is the incorporation of (Al,Ga)As windows.[2,12,13,24] In an (Al,Ga)As window laser the GaAs active region does not extend the entire length of the laser cavity; at each end there is a short section of AlGaAs.[25,26] The window sections are for protecting the laser from catastrophic failure. Catastrophic failure occurs when local heating due to optical absorption in the active region near the end facets results in catastrophic facet damage at high output powers. Catastrophic failure therefore limits the photon density attainable in a semiconductor laser. Limiting the photon density of course limits f_r. Window lasers can be operated at output powers approximately three times that which would cause catastrophic failure in an otherwise identical laser without windows.[26] With careful fabrication, the increase in threshold current due to the windows is very small.

For QW lasers, the window structure could not be expected to be as advantageous for high frequency modulation as it is for bulk DH lasers. Catastrophic

failure is not as significant a problem for QW lasers as it is for conventional DH lasers. The uncoated 4 μm wide buried GRIN SCH SQW lasers described here could be operated at currents of more than $10I_{th}$ without catastrophic failure. This can be understood by realizing how small the QW active region is compared to the surrounding (Al,Ga)As layers. Most of the lasing mode is not in the QW active region; the facet of the QW laser is almost like that of a window laser. Heating in the QW due to optical absorption should therefore be small compared to that in a conventional DH laser and more easily dissipated in the surrounding layers. If QW window lasers were fabricated, great care would be required in the fabrication. Poor fabrication would result in an increase in internal loss, which would lead to a decrease in A which would reduce the suitability of the laser for achieving high values of f_r.

SQW stripe lasers can be fabricated in structures other than a buried heterostructure. How the high frequency modulation characteristics of these structures differs from those of BH SQWs should depend primarily on the parasitics. SQW lasers fabricated on patterned substrates by MBE or MO-CVD[27,28,29,30] (discussed in Chapter 4) should have parasitics similar to those of channeled-substrate lasers fabricated on patterned substrates by LPE (see Figure 5.2). The parasitic capacitance of a channeled-substrate laser is approximately ten times that of a BH laser[2,13] (although the contact resistance is lower). These laser structures could not, therefore, be expected to improve the high frequency modulation characteristics of QW lasers. Whether QW lasers formed by impurity induced disordering[31] have parasitic capacitance similar to or higher than that of a BH laser would depend on their exact structure, but there is no reason to believe that the parasitic capacitance would be significantly reduced.

Better high frequency modulation characteristics could be achieved with higher

values of A. A is proportional to $dg(E_L, N_{th})/dN$. As demonstrated by Figure 2.4 $dg(E_L, N_{th})/dN$ is calculated[15] to be higher for MQWs than for SQWs for values of N_{th} above a certain value. This suggests that higher values of f_r could be achieved with a MQW laser; higher values have in fact been observed experimentally for MQWs.[32] As discussed in Section 2.3, MQW lasers generally have higher threshold currents than SQW lasers, so this improvement in f_r is achieved at the expense of some increase in threshold current.

6.7 Conclusion

In conclusion, it has been demonstrated that narrow stripe buried GRIN SCH SQW (Al,Ga)As lasers with high reflectivity end facet coatings can be modulated directly at high speed with logic-level drives without the need for current prebias. The lasers exhibited truly ON-OFF switching with switch-on delays of <50 ps; the pattern effect was eliminated.

The relaxation oscillation frequency, which limits the useful bandwidth of a semiconductor laser, was examined. 250 μm long 4 μm wide buried GRIN SCH 70 Å SQW (Al,Ga)As lasers with and without high reflectivity end facet coatings had relaxation oscillation frequencies of up to 5 GHz. As expected, the results for uncoated and coated lasers were very similar. High reflectivity coatings increase the photon lifetime of the laser cavity, but also increase the optical gain parameter. Values of the optical gain parameter inferred from the measurements of relaxation oscillation frequencies were larger than predicted theoretically. The discrepancy is attributed to inaccuracy in the the calculations, which may be caused by the use of a Lorentzian lineshape function to account for intraband relaxations.

It is believed that the maximum relaxation oscillation frequency measured was limited by parasitic capacitance. It is expected that if the parasitic capacitance was

reduced through the use of a semi-insulating substrate, values as high as 12 GHz would be possible.

6.8 References

[1] H. Kressel and J. K. Butler, *Semiconductor Lasers and Heterojunction LEDs*, pp. 555-580, Academic Press, New York (1977).

[2] K. Y. Lau and A. Yariv, in *Semiconductors and Semimetals Volume 22: Lightwave Communications Technology* edited by W. T. Tsang, pp. 69-151, Academic Press, New York (1985).

[3] K. Petermann, *IEEE J. Quantum Electron.* **QE-15**(7), pp. 566-570 (1979).

[4] T. P. Lee and R. M. Derosier, *Proc. IEEE* **62**(8), pp. 1176-1177 (1974).

[5] K. Y. Lau, N. Bar-Chaim, P. L. Derry, and A. Yariv, *Appl. Phys. Lett.* **51**(2), pp. 69-71 (1987).

[6] K. Y. Lau, P. L. Derry, and A. Yariv, *Appl. Phys. Lett.* **52**(2), pp. 88-90 (1988).

[7] P. M. Boers, M. T. Vlaardingerbroek, and M. Danielsen, *Electron. Lett.* **11**(10), pp. 206-208 (1975).

[8] G. F. Franklin, J. D. Powell, and A. Emami-Naeini, *Feedback Control of Dynamic Systems*, pp. 222-234, Addison-Wesley Publishing Company, Reading (1986).

[9] K. Y. Lau, C. Harder, and A. Yariv, *Optics Commum.* **36**(6), pp. 472-474 (1981).

[10] K. Furuya, Y. Suematsu, and T. Hong, *Appl.Optics* **17**(12), pp. 1949-1952 (1978).

[11] D. Wilt, K. Y. Lau, and A. Yariv, *J. Appl. Phys.* **52**(8), pp. 4970-4974 (1981).

[12] K. Y. Lau, and A. Yariv, *IEEE J. Quantum Electron.* **QE-21**(2), pp. 121-138 (1985).

[13] C. S. Harder, thesis, *Bistability, High Speed Modulation, Noise, and Pulsations in GaAlAs Semiconductor Lasers*, pp. 26-62, California Institute of Technology,

Pasadena (1983).

[14] M. Yamanishi and Y. Lee, *IEEE J. Quantum Electron.* **QE-23**(4), pp. 367-370 (1987).

[15] A. Arakawa and A. Yariv, *IEEE J. Quantum Electron.* **QE-21**(10), pp. 1666-1674 (1985).

[16] M. Asada, A. Kameyama, and Y. Suematsu, *IEEE J. Quantum Electron.* **QE-20**(7), pp. 745-753 (1984).

[17] P. T. Landsberg, M. S. Abrahams, and M. Osiński, *IEEE J. Quantum Electron.* **QE-21**(1), pp. 24-27 (1985).

[18] P. W. A. McIlroy, A. Kurobe, and Y. Uematsu, *IEEE J. Quantum Electron.* **QE-21**(12), pp. 1958-1963 (1985).

[19] A. Arakawa and A. Yariv, *IEEE J. Quantum Electron.* **QE-22**(9), pp. 1887-1899 (1987).

[20] K. Y. Lau, I. Ury, N. Bar-Chaim, C. Harder, and A. Yariv, *Appl. Phys. Lett.* **43**(4), pp. 329-331 (1983).

[21] K. Y. Lau and A. Yariv, *Appl. Phys. Lett.* **40**(6), pp. 452-454 (1982).

[22] M. Newkirk and K. Vahala, *Appl. Phys. Lett.* **52**(10), pp. 770-772 (1988).

[23] K. Vahala and M. Newkirk *Conference on Lasers and Electro-Optics*, Anaheim (1988).

[24] K. Y. Lau, N. Bar-Chaim, I. Ury, and A. Yariv, *Appl. Phys. Lett.* **45**(4), pp. 316-318 (1984).

[25] S. Takahashi, T. Kobayashi, H. Saito, and Y. Furukawa, *Jpn. J. Appl. Phys.* **17**(5), pp. 865-870 (1978).

[26] H. Blauvelt, S. Margalit, and A. Yariv, *Appl. Phys. Lett.* **40**(12), pp. 1029-1031 (1982).

[27] Y.-H. Wu, M. Werner, K.-L. Chen, and S. Wang, *Appl. Phys. Lett.* **44**(9), pp. 834-846 (1984).

[28] E. Kapon, J. P. Harbison, C. P. Yun, and N. G. Stoffel, *Appl. Phys. Lett.* **52**(8), pp. 607-609 (1988).

[29] E. Kapon, J. P. Harbison, C. P. Yun, and N. G. Stoffel, *Conference on Lasers and Electro-Optics*, Anaheim (1988).

[30] D. Fekete, D. Bour, J. M. Ballantyne, and L. F. Eastman, *Appl. Phys. Lett.* **50**(11), pp. 635-637 (1987).

[31] K. Meehan, P. Gavrilović, N. Holonyak, Jr., R. D. Burnham, and R. L. Thornton, *Appl. Phys. Lett.* **46**(1), pp. 75-77 (1985).

[32] K. Uomi, T. Mishima, and N. Chinone, *Appl. Phys. Lett.* **51**(2), pp. 78-80 (1987).